2
2006

LIBRARY
Michigan State
University

This is to certify that the
dissertation entitled

ADSORPTION AND INTERACTIONS OF BIOMACROMOLECULES
AT FLUID-LIKE INTERFACES

presented by

Sachin Shashikant Vaidya

has been accepted towards fulfillment
of the requirements for the

Ph.D. degree in Chemical Engineering

Robert J. Ofoli
Major Professor's Signature

7/1/05
Date

MSU is an Affirmative Action/Equal Opportunity Institution

PLACE IN RETURN BOX to remove this checkout from your record.
TO AVOID FINES return on or before date due.
MAY BE RECALLED with earlier due date if requested.

DATE DUE	DATE DUE	DATE DUE
AUG 0 3 2008		
0 5 0 4 1 0		

2/05 c:/CIRC/DateDue.indd-p.15

ADSORPTION AND INTERACTIONS OF BIOMACROMOLECULES AT FLUID-LIKE INTERFACES

By

Sachin Shashikant Vaidya

A DISSERTATION

Submitted to
Michigan State University
in partial fulfillment of the requirements
for the degree of

DOCTOR OF PHILOSOPHY

Department of Chemical Engineering and Materials Science

2005

ABSTRACT

ADSORPTION AND INTERACTIONS OF BIOMACROMOLECULES AT FLUID-LIKE INTERFACES

By

Sachin Shashikant Vaidya

The adsorption and interactions of biomacromolecules at biologically relevant interfaces have been characterized in this study. While each chapter addresses a unique issue, they all share an underlying common theme of increasing our understanding of the behavior of biomolecules at fluid-like interfaces. The primary tool for all three studies was total internal reflection fluorescence microscopy (TIRFM).

The first study addressed sequential and competitive adsorption and interactions of human plasma fibronectin (HFN) and human serum albumin (HSA) at the oil-water interface. Among key results, fibronectin adsorption is rapid and essentially irreversible, even over short time scales. This is probably due to the highly flexible nature of the protein, which allows its domains to quickly attain energetically favorable conformations. In contrast, HSA adsorption is relatively reversible at short times, and the protein is readily displaced by fibronectin even after incubation at the interface for as long as two hours. HSA more effectively resists displacement by fibronectin at longer time scales, although significant fibronectin adsorption occurred even under those conditions. Displacement of fibronectin by HSA was essentially negligible under all conditions. This study is relevant to emerging research thrusts such as the development of biomimetic interfaces, where effects of interfacial competition, adsorption time scales, and extent of adsorption irreversibility on interfacial dynamics are important.

The second study addressed the adsorption of bovine serum albumin at a model oil-water interface. Estimates of protein interfacial coverages were obtained using a protocol based on a fluorescence recovery after photobleaching (FRAP) technique previously proposed by Zimmerman et al. (1990). Protein coverages ranged from 0.02-0.3 mg/m^2 for bulk concentrations of 0.2 mg/ml to 3.5 mg/ml. These values are an order of magnitude lower than typical estimates reported in the literature for the solid-liquid interface. It is likely that coverages at the oil-water interface are lower because more rapid protein relaxations at this interface result in greater interfacial area per molecule, thus inhibiting adsorption of later-arriving proteins. Fluorescence lifetime measurements of BSA-FITC in solution and at the interface (obtained by two-photon time correlated single photon counting spectroscopy) yielded similar results, suggesting that the quantum yield of BSA-FITC at the interface and in the bulk solution are identical.

The final study was on the adsorption of liposomes composed of 1,2-Dioleoyl-sn-Glycero-3-Phosphocholine (DOPC) and 1,2-Dioleoyl-sn-Glycero-3-Phosphate (Monosodium Salt) (DOPA) to poly(dimethyldiallylammonium chloride) (PDAC) and poly(allylamine hydrochloride) (PAH). The liposomes adsorbed preferentially on PDAC, but in much smaller amounts on sulfonated poly(styrene) (SPS) due to electrostatic repulsion between the negatively charged liposomes and the SPS coated surface. Poly(ethylene glycol) (m-dPEG acid) coated surfaces also resisted liposome adsorption. These results were exploited to create arrays of lipid bilayers by exposing PDAC, PAH and m-dPEG patterned substrates to DOPA/DOPC vesicles of various compositions. Such arrays may be useful for high-throughput screening of compounds that interact with cell membranes.

Dedicated to my mother, father and sister,
and to Salil for all that he missed

ACKNOWLEDGEMENTS

I would like to thank my advisor Dr. Robert Y. Ofoli for his invaluable guidance and for his friendship during these long years. I am grateful to him for recruiting me and giving me the opportunity to advance my studies at Michigan State. His open-door policy has always encouraged me to speak freely with him and he has taught me to be an independent thinker. I would like to thank my committee members for agreeing to mentor me and for their advice and support during the course of my dissertation. I would like to thank Dr. Melissa Baumann for her inputs and for her careful critique of this dissertation, Dr. Gary Blanchard for his assistance with the two-photon spectroscopy measurements and for his patience when I was incessantly bugging him about experiments and Dr. Ilsoon Lee and Dr. Mark Worden for their mentorship, fruitful collaborations during these past years, and for providing me with generous use of their laboratory facilities.

During my years at MSU, I developed friendships that I will never forget and it remains the single most valuable possession that I carry forward. Sunder and Bhaskar are my earliest friends here, right from the Shaw Hall days and although everyone has gone their separate ways, we share the best of memories. I would like to thank the A-24 gang, Arun, Vinay, Pradeep, Mandar, Srini and Akshay for being the best roommates. Arun has been my closest friend over the last 12 years and his friendship has meant a lot to me. I would also like to thank Tejas, Soumya, Abhi, Kiran, Amit, Prajakt, Giri, and Prerna for being great friends.

I would like to thank Lavanya Parthasarathy for been a great friend and colleague Without her, it would have been impossible to navigate the treacherous TIRFM waters.

We started our PhDs together and have learned far more than this dissertation will ever tell. Ari Gajraj was a great mentor in the early years and I would like to thank him for his guidance, and for the music. I would also like to thank Neeraj Kohli for endless scientific discussions and for all our collaborations and wonderful research ideas and goals that Nobel prize winners always seemed to beat us to (by at least a couple of years!). I would also like to thank Nancy Albright and JoAnn Peterson for all their help during these past six years.

I have been most influenced in my life, by my parents and sister who have sacrificed a lot for me. They have always encouraged me to seek higher goals and have never doubted me. This dissertation would not have been possible if not for their love and support. This dissertation is dedicated to the memory of my brother, who I wish, could be here. Finally I would like to thank my wife Mukta for her support during the final years of this dissertation. She has always been there for me, especially at the worst times when the end seemed just as far away as the beginning. Her constant love and encouragement has been the beacon that has guided me to the end.

TABLE OF CONTENTS

LIST OF FIGURES

LIST OF TABLES

NOMENCLATURE

pre-exponential factor (or amplitude) of exponential decay

^{2} index for estimating goodness of fit

wall-shear rate

wavelength of incident light in free space

incident angle of light

critical angle for total internal reflection

fluorescence lifetime of excited molecules

absorbance

bulk concentration of proteins

two-dimensional interfacial concentration of proteins

penetration depth of evanescent wave

diffusion coefficient of species i

unbleached fluorescence emission after pattern photobleaching step

total fluorescence as a function of time, prior to photobleaching

$_k(t)$ bulk contribution to the total fluorescence

depth of channel

incident light intensity at depth z=0

evanescent wave intensity at depth z

radiative decay rate

k_{nr} non-radiative decay rate

l aqueous depth of flow cell

L molar labeling ratio of proteins (dye/protein)

m_i fraction of total population that is mobile with diffusion coefficient D_i

n_1 refractive index of denser medium

n_2 refractive index of rarer medium

q quantum yield of fluorophore

q_I instrument constant

q_b quantum yield of fluorophores in solution

q_s quantum yield of adsorbed fluorophores

Q volumetric flow rate in flow cell

s thickness of adsorbed protein layer

t time

w width of flow channel

z depth coordinate into the flow cell

Abbreviations

AFM atomic force microscopy

BLM bilayer lipid membrane

BSA bovine serum albumin

DOPA 1,2-Dioleoyl-sn-Glycero-3-Phosphate (Monosodium Salt)

DOPC 1,2-Dioleoyl-sn-Glycero-3-Phosphocholine

FITC fluorescein isothiocyanate

FRAP Fluorescence recovery after photobleaching

FRAPP fluorescence recovery after pattern photobleaching

HFN human plasma fibronectin

HSA human serum albumin

HTS hexadecyltrichlorosilane

OTS octadecyltrichlorosilane

PEG polyethylene glycol

PEO polyethylene oxide

PEM polyelectrolyte multilayers

PAH poly(allylamine hydrochloride)

PDAC poly(diallyldimethyl ammonium chloride)

PMT photomultiplier tube

QCM quartz crystal microbalance

SAM self-assembled monolayer

SPS sulfonated polystyrene

2p-TCSPC 2-photon time-correlated single photon counting

TIRFM total internal reflection fluorescence microscopy

VA-TIRFM variable angle of incidence total internal reflection fluorescence microscopy

1 INTRODUCTION

1.1 Background

The term adsorption, coined in the 19th century, is defined as the preferential partitioning of a molecule along the boundary of two phases. This partitioning occurs due to the affinity of regions in the molecule for one phase or the other. Though classical adsorption has its roots in catalysis, the study of adsorption of molecules at biologically relevant interfaces (bio-adsorption) is now important to a large number of applications. For example, protein adsorption at cellular interfaces is among the first and most important events that take place before the initiation of processes such as cell differentiation, proliferation and growth, and considerable effort has been expended in the literature to characterize the adhesion of proteins to surfaces.

In addition to examining the process of biomolecular adsorption, it is also important to investigate the behavior of these molecules following adsorption at the interface. For example, proteins are flexible molecules that are known to undergo relaxation after adsorption. The relaxation occurs as the protein tries to minimize its free energy, and leads to protein denaturation that may make the adsorption irreversible. There is considerable focus on studying the conformational changes that such molecules undergo, during and after the adsorption process. Another area where protein adsorption is important is in the field of tissue engineering, particularly in the design of implants and scaffolds. The liquid-liquid interface is an important emerging interface in the field of tissue engineering as it presents a "soft interface" which can be used for culturing cells.

In the area of biosensor development, current research thrusts lie in developing sustainable biomimetic interfaces. The interfaces feature lipid bilayers deposited on them, using vesicular adsorption or Langmuir Blodgett methods, which allows them to mimic the cellular membrane. When liposomes adsorb to the interface, they typically tend to fuse and rupture, thus forming lipid bilayers. The lipid bilayers have varying properties depending on characteristics of the interface such as heterogeneity, surface charge and roughness. Understanding the mechanisms and controlling the parameters that govern liposome adsorption and rupture to form lipid bilayers is critical to the design of viable biosensor systems.

This dissertation examines biomolecular adsorption and interactions using a collage of studies. While each chapter addresses a unique issue, they all share the underlying common theme of increasing the basic understanding of the behavior of biomacromolecules at different types of biologically-relevant interfaces. In Chapter 2, sequential and competitive interactions between human plasma fibronectin and human serum albumin are examined at a model oil-water interface. Chapter 3 addresses the development and evaluation of a protocol for quantifying protein interfacial coverages at the liquid-liquid interface. Finally, Chapter 4 examines the adsorption of liposomes to 3-dimensional polyelectrolyte multilayers, and characterization of the resulting interfaces using fluorescence recovery after pattern photobleaching (FRAPP) measurements to determine the lateral diffusion coefficients of bilayers assembled on the biomimetic interface.

1.2 Sequential and competitive adsorption between human serum albumin and human plasma fibronectin at the oil-water interface

The liquid-liquid interface is of vital importance in key areas such as biomedical engineering and food processing. The hydrocarbon-water interface is a crude first order approximation of a biological cell membrane[1]. Drug-ion transfer has been studied across the oil-water interface as a gauge of pharmacological activity[2]. An examination of the literature reveals that a majority of the existing studies on protein adsorption have concentrated on the solid-liquid interface, with relatively few studies targeting the liquid-liquid interface. However, a number of techniques have been used to probe the oil-water interface. These include atomic force microscopy to probe orogenic displacement of proteins from the oil-water interface[3], neutron reflectivity to probe buried oil-water interfaces[4], total internal reflection fluorescence microscopy to study protein adsorption[5,6], optical second harmonic generation studies[7], quasi-elastic surface light scattering to study interfacial tensions at the heptane-water interface[8] and radiolabeling to study surfactant adsorption to the oil-water interface[9].

Recently, the use of perfluorcarbon liquids as oxygen carriers and as soft interfaces for cell-growth has come into focus[10]. Proteins play a major role in cell attachment, differentiation and growth at these interfaces. With recent advances in tissue engineering, there is a need for better understanding of several aspects of protein adsorption in order to better design such biomimetic interfaces. In particular, effects of adsorption time scales, interfacial competition, and extent of adsorption irreversibility are among some issues of key interest. Hence studies of protein adsorption at such fluid interfaces can aid in better

designs for tissue engineering at the liquid-liquid interface as well as shed light on the underlying mechanisms of protein unfolding.

Chapter 2 of this dissertation presents a study of sequential and competitive interactions between human plasma fibronectin and human serum albumin at a model oil-water interface. Protein adsorption experiments were conducted under transport-limited conditions, characterizing both sequential adsorption and competitive adsorption. These studies of the interactions between human plasma fibronectin and human serum albumin have revealed trends consistent with those predicted for protein adsorption in other works reported in the literature. This study is unique in that it is among the first studies of its kind that uses TIRFM to probe such interactions at the liquid-liquid interface.

1.3 Estimating protein interfacial coverage at the liquid-liquid interface

Quantifying the amounts of protein adsorbed to the solid-liquid interface is accomplished easily using techniques such as ellipsometry, radiolabeling, neutron reflectivity, quartz crystal microbalance, total internal reflection fluorescence microscopy, surface plasmon resonance, and optical waveguide lightmode spectroscopy. The interfacial signals detected using these methods can be converted into surface coverages with models that rely on the evolving refractive index of the adsorbing film, by monitoring changes in the oscillation frequency or by using other internal or external calibration methods. Protein adsorption to interfaces is governed by several factors that influence interfacial saturation coverages. For example, electrostatic interactions between the protein and the surface play a critical role in determining how much protein is

deposited at the interface. These electrostatic interactions can also influence other factors such as conformation and structure of the evolving adsorbate layer.

Proteins undergo lateral relaxations during denaturation at interfaces that eventually increase the total area occupied per molecule. The rate of transport of proteins to the interface is another important factor that can significantly influence interfacial coverages. Surface heterogeneity and roughness can also influence protein adsorption, though a recent research article has shown that nanoscale roughness has little influence on the amount or structure of protein adsorption[11]. The amount of protein adsorbed at an interface also depends on the type of the protein adsorbing. For example, typical values for interfacial coverages for albumin are in the range of 0.3-3 mg/m^2 at the solid-liquid interface, depending on the bulk protein concentration and surface properties[12-14].

Estimates of protein interfacial coverages at the liquid-liquid interface have been done primarily using radiolabeling[15]. It is also possible to estimate interfacial coverages from tensiometry data by using the Gibbs isotherm. In an article published by Graham et al. in 1975[9], the authors commented on the fact that one of the outstanding problems with respect to liquid-liquid interfaces was the direct determination of interfacial coverages. Indeed, with the exception of radio-labeling, there does not appear to be an easy, non-invasive technique that can produce reliable estimates of interfacial coverages at the oil-water interface to date.

Chapter 3 of this dissertation presents a protocol to quantify adsorbed amounts of proteins at the liquid-liquid interface using a method that has been previously applied to making these estimates at the solid liquid interface[16]. Included in these studies are

examinations of the lifetimes of the dye-labeled proteins at the liquid-liquid interface. The fluorescence lifetime of a molecule is a measure of the amount of time a molecule spends in the excited state before its eventual decay to the ground state. Lifetimes of fluorescent molecules are strongly dependent on the surrounding environment, and can be related to the quantum yield of the dye. Lifetime studies can, therefore, provide us with information about the quantum yields of bulk and interface-associated fluorophores. The influence of mobile interfaces on interfacial coverages is also discussed.

1.4 Fabrication and characterization of 3D arrays of lipid-bilayers on polyelectrolyte multilayers

In the last decade, a considerable amount of research has been conducted on the development of biosensors. Biosensors are molecular devices that combine a biological recognition mechanism with a physical transduction technique[17], and are used for detection of compounds that may be present in small concentrations. They have been used for the detection of analytes such as glucose[18] and fructose[19], among others. Biosensors use a variety of methods for detecting the analyte of interest, including electrochemical, optical and colorimetric methods. Biosensors are engineered for detection of signals based on their ability to respond to different molecular mechanisms such as ion-channel activation (sensing of current)[17], fluorescence resonance energy transfer (FRET)[20] and redox phenomena (cyclic voltammetry).[21] These represent only a small sampling of the available mechanisms on which biosensors can be based.

Biosensors that rely on ion-channel activity and/or use membrane bound proteins or enzymes, incorporate lipid bilayers in their design. The lipid-bilayers are necessary in

order to preserve the functional characteristics of the proteins that are bound to them. For biosensors based on activation of ion-channels, the channel proteins are typically reconstituted into liposomes which are then deposited on the sensing substrate. Lipid bilayers are generally deposited on the biosensor substrate using Langmuir-Blodgett deposition methods or liposome adsorption. The choice of lipids used to construct supported lipid bilayers is important as the characteristics of the resulting bilayer have a very strong influence on the activity of the subsequently reconstituted transmembrane protein/enzyme or ion-channel. Properties such as membrane fluidity, which is an indicator of the ability of lipid molecules to diffuse freely through the bilayer, play important roles in maintaining the correct conformation of the biomolecules embedded within them. It is also important to have bilayers that are highly insulating, since the presence of large defects will render such sensors ineffective[22].

There is considerable research on biomimetic interfaces, where the ultimate goal is to develop viable, sustainable bilayer interfaces with the smallest number of defects. In recent years, developments have been made in the area of polymeric cushions upon which lipid bilayers can be deposited[23]. In addition to being able to provide ionic reservoirs, polymeric cushions allow transmembrane proteins to attain their necessary conformation and to retain biological activity, which would otherwise be impeded by proximity of the protein to the substrate surface. The use of polyelectrolyte multilayers has been proposed as one such viable method for a polymeric cushion.

Chapter 4 of this dissertation presents a study to fabricate and characterize biomimetic interfaces that are based on polyelectrolyte multilayers. This work was done in collaboration with Neeraj Kohli (co-advised by Dr. R. Mark Worden and Dr. Ilsoon

Lee) in the Department of Chemical Engineering and Materials Science. The work consists of equal contributions from Neeraj Kohli and the author of this dissertation. The biomimetic interfaces employed in this study consist of arrays of lipid bilayers that have been deposited on polyelectrolyte multilayer (PEM) substrates composed of positively and negatively charged polyelectrolyte layers. The bilayers were deposited on the substrate by preferential adsorption of charged liposomes on oppositely charged polyelectrolytes. Such arrays can be used in applications that may require high throughout screening. The deposition of liposomes on the PEMs was monitored using total internal reflection fluorescence microscopy, fluorescence microscopy and quartz crystal microbalance. The resulting bilayers were characterized using FRAPP. Bilayer formation on two different kinds of PEM substrates was studied. Possible interactions between the lipid bilayer and the PEM surface are discussed, based on the diffusion coefficients obtained in the two cases.

2 ADSORPTION AND INTERACTION OF FIBRONECTIN AND ALBUMIN AT THE LIQUID-LIQUID INTERFACE

2.1 ABSTRACT

The goal of this work was to investigate the dynamics of human plasma fibronectin (HFN) at the oil-water interface and to characterize its interactions with human serum albumin (HSA), using total internal reflection fluorescence microscopy (TIRFM), along with measurements of interfacial tension. Among key results, fibronectin adsorption at the oil-water interface was observed to be rapid and essentially irreversible, even over short time scales. For example, after washout experiments with protein-free buffer over a 3-hour rinse cycle, fibronectin desorption from the interface was found to be negligible. This may be due to the highly flexible nature of the protein, which allows the various domains to quickly attain energetically favorable conformations. On the other hand, HSA adsorption at the oil-water interface is relatively reversible at short times, and the protein is readily displaced by fibronectin even after HSA has been adsorbed at the interface for as long as two hours. At longer adsorption times, HSA is able to more effectively resist complete displacement by fibronectin, although significant fibronectin adsorption was observed even under those conditions. Displacement of adsorbed fibronectin by HSA was found to be essentially negligible under all conditions. Fibronectin also adsorbs preferentially from a mixture of HFN and HSA, even when the concentration of HSA is substantially higher. This study is relevant to such emerging research thrusts as the development of biomimetic interfaces for a variety of applications,

where there is a clear need for better understanding of the effects of interfacial competition, adsorption time scales, and extent of adsorption irreversibility on interfacial dynamics.

2.2 INTRODUCTION

Adsorption of plasma proteins to surfaces is one of the first and most important events before the initiation of key cellular activities such as cell attachment, migration, differentiation and proliferation. With recent advances in tissue engineering and the development of synthetic bio-interfaces, there is a need for better understanding of several aspects of protein adsorption in order to better design such biomimetic interfaces. In particular, effects of adsorption time scales, interfacial competition, and extent of adsorption irreversibility are among some issues of key interest. Vitronectin, laminin and fibronectin are among the more important proteins involved in cell attachment processes, and several studies have been published on their adsorption and interactions on a variety of substrates[24-27]. The present study focuses on the sequential and competitive adsorption of fibronectin and human serum albumin at a model interface.

Fibronectin belongs to the family of high molecular weight glycoproteins that are found in the extracellular matrix and in serum, and which are responsible for key functions including provision of a structural framework for cell attachment, migration and differentiation, as well as cell-cell and cell-substrate adhesion through integrin receptors[28]. With a molecular weight of 440-500kDa, fibronectin is a relatively large molecule in comparison to other well characterized proteins such as lysozyme (14kDa),

serum albumin (67 kDa) and beta-casein (24kDa). Its diffusion coefficient has been reported to be 2.1 x 10^{-7} cm^2 /s[28]. Fibronectin has been reported to have globular and filamentous forms depending on solution conditions[29], and dimensions varying from an average length of 15 nm[30,31] to 60nm[32,33]. It is a flexible protein that can adopt a number of conformations depending on the morphology of the surface. It can adsorb in both an extended and a globular configuration[34], and has been shown to undergo conformational changes upon binding to dextran, as the molecule goes from a compact to an elongated conformation[35,36]. Bergkvist et al.[37] reported end to end distances of greater than 100nm for fibronectin adsorbed onto mica and silica surfaces.

The adsorption characteristics of fibronectin also depend on the hydrophobicity of the surface to which it is adsorbing. Atomic force microscopy studies of adsorption of HFN-coated microspheres onto hydrophobic and hydrophilic surfaces have shown that fibronectin has a strong interaction with both surfaces[38]. Ellipsometric measurements of HFN adsorption on modified silica show greater HFN surface coverages and irreversiblility on hydrophobic surfaces than on hydrophilic surfaces, which demonstrate a slightly lower HFN coverage and some degree of reversibility[39]. Studies of HFN adsorption on titanium indicate that surfaces appear more hydrophobic in the presence of the protein[27]. It has been recently reported that fibronectin exhibits history-dependent adsorption behavior, i.e., the rate of adsorption depends on the structure of the evolving adsorbed layer[13].

Several techniques have been used for measuring protein adsorption, including total internal reflection fluorescence (TIRF)[40], optical wave-guide light spectroscopy[13], ellipsometry[41], radiolabeling[42] and, more recently, atomic force microscopy[43]. Most of

these studies have focused on adsorption of biomacromolecules at the solid-liquid interface, with relatively few studies concentrating on adsorption dynamics at the liquid-liquid interface[5,6,15,42,44,45]. Yet, there is general agreement that the liquid-liquid interface is of considerable importance in biological systems, particularly in biomedical engineering[10,46,47], pharmaceutical sciences, and food processing. The liquid-liquid interface also serves as an excellent model for interactions of biomacromolecules at relatively mobile interfaces.

In an earlier article[5], our laboratory reported studies of protein adsorption at a model oil-water interface using total internal reflection fluorescence microscopy (TIRFM). The present study reports on dynamic interactions between fibronectin and human serum albumin (a protein present in substantial concentrations in blood) under both competitive and sequential adsorption scenarios. In particular, information is presented on the influence of timescales on adsorption irreversibility, and on subsequent replacement by a competing protein at the liquid-liquid interface. Recent studies of competitive adsorption between albumin and fibronectin have shown that albumin co-adsorption significantly influences the availability of fibronectin on polymeric hydrophobic substrates[48]. Since human serum albumin is typically used as a blocking agent for elimination of non-specific adsorption, its competitive interaction with fibronectin is of considerable biological interest.

2.3 Theory

Total internal reflection occurs when light propagating through an optical dense medium of refractive index n_1, arrives at the interface between the denser medium and an optical rarer medium n_2, at angle exceeding the critical angle,

$$\theta_c = \sin^{-1}\left(\frac{n_2}{n_1}\right) \tag{2.1}$$

Upon total internal reflection, an electromagnetic field is induced in the rarer medium at the interface. This electromagnetic field is known as the evanescent wave. The intensity of this field decays exponentially with distance z, away from the interface. This distance-dependent intensity is given by

$$I(z) = I_o \exp(-\frac{z}{d_p}) \tag{2.2}$$

where $I(z)$ is the intensity at any depth z, and I_o is the intensity of the light at z=0.

The penetration depth d_p represents the characteristic depth at which the light intensity approaches 1/e of its maximum magnitude I_o, and is given by

$$d_p = \frac{\lambda_o}{4\pi n_1 \sqrt{\sin^2\theta - (n_2/n_1)^2}} \tag{2.3}$$

where λ_o is the wavelength of the incident radiation in vacuum, and θ is the angle of incidence. The penetration depth in our apparatus lies within 100nm of the interface, depending on the geometry and the properties of the denser and the rarer medium. Thus,

this is an interfacially selective technique as only molecules within the proximity of the interface are illuminated.

2.4 Experimental Protocol

2.4.1 Materials:

Human plasma fibronectin (HFN), at a purity greater than 95% as determined by SDS-PAGE[49], was purchased from Chemicon International (FC-010, Temecula, CA). Human serum albumin (HSA) was purchased from Sigma (A8763, Sigma-Aldrich Corp. St. Louis, MO). Both proteins were used without further purification. The proteins were labeled with fluorescein-5-isothiocyanate (FITC), purchased from Molecular Probes (Catalog # F-1907, Eugene, OR). The labeling reaction was carried out in the dark, as described in the literature[50] in 0.1 M carbonate buffer at a pH of 9.2 for a period of 6 hours. The unbound labels were removed by a 2-stage dialysis process performed over a period of 36 hours. This procedure was determined to be sufficient to remove all unreacted FITC. The reaction mixture was dialyzed against 0.05 M phosphate buffer at a pH of 7.4, using a molecular porous regenerated cellulose dialysis membrane (Spectra/Por 1, MWCO 6000, The Spectrum Companies, Gardena, CA). The solutions were either divided into aliquots and frozen for later use, or stored at 4°C and used within one week of preparation.

In the case of samples containing fibronectin, no vigorous stirring or vortexing was used; instead all mixing was done using gentle swirling, to avoid precipitation of the protein[49]. Absorbance spectroscopy was used to measure the protein concentrations and labeling ratios at 280nm and 496nm, respectively, using a diode array spectrophotometer

(8452 A, Hewlett-Packard, Brielle, NJ). After subtracting the corresponding absorbance contribution from FITC at 280 nm, protein concentrations were computed using optical densities $\left(A_{1cm}^{1mg/ml}\right)$ of 1.3[49] and 0.53[51] for fibronectin and albumin, respectively. It was observed that conjugation of FITC to human serum albumin causes an increase in absorbance of the protein at A_{280} to an extent greater than the contribution from fluorescein's computed concentration dependent absorbance. We believe that this is because the extinction coefficient for human serum albumin at 280 nm is influenced by FITC conjugation, which may result in an overstatement of labeled protein concentrations. For the purpose of this study, no correction was made to account for this and further studies are continuing in our laboratory to understand this effect. Dilutions from protein stock solutions were made just prior to infusion into the flow cell, to eliminate or minimize the tendency of fibronectin to rapidly adsorb to the sides of the storage container. The oil used in this study was an immersion oil with a refractive index of 1.46 at 589.3nm, largely comprising long chain aliphatic hydrocarbons (Cargille Laboratories, Cedar Grove NJ Cat. # 19572; code 06350).

Quartz slides (n=1.46, Heraeus Quarzglas) were used as substrates onto which the oil was deposited to form layers of film thicknesses typically ranging from 20 to 50 μm, as estimated using a microbalance. All slides were cleaned using the protocol described by Cheng et al.[40]. The oil was deposited in a smooth film on the quartz slides using previously described protocols[5,6]. Prior to assembling the flow cell, the bottom slide was coated with polyethylene oxide (Sigma, St. Louis, MO) by immersion in 600 ppm solution to reduce or eliminate protein adsorption on that surface[52-54].

2.4.2 TIRFM Setup

The experimental setup has been described previously[5,55]. The experimental layout and a diagram of the flow cell is depicted in Figure 2.1a and Figure 2.1b. Briefly, the apparatus consists of an inverted microscope (Zeiss Axiovert 135M, Carl Zeiss Inc. Thornwood, NY)), the 488 nm line of a 5W continuous wave argon ion laser (Lexel Lasers Model 95, Fremont, CA), a side–on photo-multiplier tube (PMT) (Hamamatsu R4632, Bridgewater, NJ) jacketed in a thermoelectrically cooled housing (TE 177-TSRF, Products for Research, Danvers, MA), a CCD camera (NTI, VE1000, Dage-MTI, Michigan City, IN), and a modular automation controller (MAC 2000, Ludl Electronic Products, Hawthorne, NY) that regulates the voltage supply to the photo-multiplier tube. A double syringe pump system (Model 551382, Harvard Apparatus South Natick, MA) was used to infuse and withdraw sample solutions at precisely controlled rates from a custom-designed flow cell. The photo-multiplier tube can be operated in both analog and digital (photon counting) mode; however, several experiments were conducted in strictly analog mode prior to adding a photon counter to the system. In photon counting mode, an SR400 photon counter (Stanford Research Systems, Sunnyvale, CA) is used for recording fluorescence emission, and the output signal is amplified by a fast preamplifier (SR445, Stanford Research Systems, Sunnyvale, CA). Fluorescence intensities were recorded using software written in Labview 6.0 (National Instruments, Austin, TX)[1].

---

[1] Labview flowsheets are located in Appendix A: Labview flowsheets. Sample Labview templates for photon counting using the SR400 were obtained from http://www.ni.com and modified accordingly for our application.

An optical chopper (OC) (SR 540, Stanford Research Systems, Sunnyvale CA) was used to prevent unintended photobleaching of fluorophores during all experiments. Analog measurements were filtered using a program written in Matlab[2] (Release 12, The Mathworks Inc., Natick, MA) to eliminate dark current measurements during the dark phases of the chopper cycle. For digital measurements, the photon counter is triggered by an output reference voltage from the chopper, so that data collection only occurs during periods when the sample is illuminated by the laser beam, thereby enhancing the signal to noise ratio.

An optical chopper was used to significantly reduce the possibility of photobleaching by the monitoring beam during long experiments. This is because photobleaching can occur even at the low monitoring beam intensity of 4 μW used in these experiments, and makes the accurate interpretation of experimental results difficult. The optical chopper reduces the exposure time of the sample to the laser beam; typically, in a 17-second data collection cycle, the total time the sample cell is exposed to the laser beam amounts to less than two seconds. Since the illumination of fluorophores only occurs during data sampling periods, this ensures that no unintended photobleaching occurs. The intensity of the monitoring beam was carefully controlled in all experiments. As a general protocol, no experiments were conducted with a monitoring beam intensity exceeding 13.5 μW, even over short periods of data collection.

A system of optical flats[5] (F1 and F2) enables us to easily switch between a low intensity monitoring beam for observation of adsorption dynamics and a high intensity

---

[2] Matlab programs listed in Appendix B: Matlab programs for filtering and averaging analog measurements

beam for conducting fluorescence recovery after photobleaching (FRAP) experiments. The laser beam passes through the first optical flat and is split into a high intensity photobleaching beam and a low intensity monitoring beam. An adjustable shutter (D122, Uniblitz, Vincent Associates, Rochester, NY) placed between the optical flats, blocks the high intensity beam in the "closed" mode while allowing the low intensity monitoring beam to pass through. Upon triggering, the shutter allows the passage of the high intensity beam for a controlled amount of time. The optical flats are aligned so that the high intensity and low intensity beams are recombined after passing through the second flat. A second shutter placed below the PMT is synchronized with the first shutter in order to prevent the photomultiplier from being exposed to high intensity light during the photobleaching step. This is done to prevent damage to the photomultiplier tube in addition to avoiding light induced hysteresis in the PMT signal.

The flow-cell where adsorption experiments are monitored is depicted in Figure Figure 2.1b. The flow cell is formed using two microscope slides separated from one another by a 900 μm aluminium spacer with an oval cut into it. An o-ring (Parker, Lexington, KY) inside the oval spacer between the top and bottom slide prevents leakage of sample solution. The underside of the top microscope slide is coated with a thin layer of oil. The bottom slide is ground to a thickness of 0.75 mm and has two holes drilled into it (1.60 mm diameter, separated by 42.3 mm, centered) to allow for the infusion and withdrawal of solutions. The entire assembly is coupled to a prism and is firmly screwed on to an anodized aluminium shell that sits on top of an inverted microscope stage.

All TIRFM experiments were conducted under conditions of gentle shearing flow. In most experiments, measurements were made under continuous flow conditions to

eliminate the possibility of bulk depletion of proteins, which is a possibility at the very low protein concentrations used in this study. In experiments conducted over long timescales, flow was allowed into the sample cell until apparent saturation of the interface has been achieved, which typically took approximately one hour. After that, flow was terminated, and experiments were conducted under static conditions. This was done to prevent destabilization of the interface by continuous flow over long periods.

Interfacial tension measurements: To provide comparative data for the TIRFM experiments, static and dynamic interfacial tension experiments were also conducted at the liquid-liquid interface, using a Kruss K12 tensiometer (Kruss USA, Charlotte, NC).

2.5 Results and Discussion

All the experimental data are presented in terms of fluorescence emission intensity profiles normalized by the maximum fluorescence value in each data set. It is also possible to convert fluorescence emission data to interfacial surface densities using a transport-limited model[12,56]. It is difficult to use this model for these data because, to avoid inducing instabilities at the liquid-liquid interface, there are limitations on the range of shear rates over which the TIRFM apparatus can be operated, which prevents model validation. For the experiments discussed in this paper, no external calibrations were used to standardize the fluorescence emission profiles. Also, variability in the thickness of the oil layers formed on quartz substrates, along with potential instabilities in the oil layer during the course of an experiment, results in variations from one experiment to another, thus complicating comparative data analyses. The uneven nature of the oil-water interface can introduce artifacts in the fluorescence data due to light scattering. While every

precaution is taken to minimize scattering effects, it cannot be fully eliminated. A typical oil-water interface can be visualized as a wavy interface filled with undulations where one phase protrudes into the other. This makes such interfaces less reproducible than a solid-liquid interface such as a hexadecyltrichlorosilane self assembled monolayer (HTS-SAM) - water interface .

As a result, we have refrained from assigning undue physical significance to small observed variations in interfacial dynamics, and have concentrated instead on characterizing general trends. This limitation made it necessary to develop an internal calibration procedure that would allow precise determination of absolute interfacial concentrations from fluorescence emission intensity measurements at the liquid-liquid interface. This protocol will enable more rigorous comparisons to be made between data sets and will be discussed in the next chapter.

2.5.1 Sequential adsorption of HSA and HFN

Data on the sequential adsorption of unlabeled HFN following the pre-adsorption of labeled human serum albumin (HSA-FITC) are shown in Figure 2.2. In this experiment, HSA-FITC was introduced into the flow cell alone at a flow rate of 0.05 ml/min, and adsorption was allowed to proceed for approximately 70 min. At t=74 min., a mixture of HSA-FITC (at the same bulk concentration as before) and unlabeled HFN was infused into the flow cell, and the subsequent emission intensity of HSA was monitored. All experiments were conducted under continuous flow conditions to ensure that bulk depletion of protein did not occur. It should also be noted that HSA was infused

into the flow cell along with HFN to ensure that any observed changes in fluorescence emission intensity would not be the result of the depletion of HSA in the bulk.

The introduction of the binary protein mixture significantly reduced the fluorescence emission intensity from its near plateau value to a level near the baseline, indicating that unlabeled HFN is displacing HSA-FITC from the interface in substantial amounts, even though the bulk concentration of HSA-FITC is greater than that of HFN. Since the bulk concentration of HSA-FITC was the same before and after HFN was introduced, its disappearance from the interface cannot be attributed to concentration-induced mass transfer of the protein from the interface into the bulk.

Figure 2.3a and Figure 2.3b represent data from experiments complimentary to the one above, with the modification that HFN was labeled with FITC (HFN-FITC), while HSA was unlabeled. In the experiment depicted in Figure 2.3a, HFN-FITC at a concentration of 0.1mg/ml is allowed to adsorb for 60 minutes, followed by infusion of a solution containing unlabeled HSA at 0.1mg/ml and HFN-FITC (at the same bulk concentration as before). As the data show, there is negligible change in the magnitude of the fluorescence emission intensity following introduction of the mixture of proteins into the flow cell. Even when the experiment was repeated with a 10-fold increase in the bulk concentration of HSA (1mg/ml), there is no discernible change in the fluorescence emission intensity (Figure 2.3b).

The steady fluorescence emission levels in the two experiments following introduction of the protein mixture indicate that adsorbed HFN was not displaced from the interface by HSA, even at the much higher bulk albumin concentration. Since the

adsorption of non-labeled species at the interface cannot be detected, we cannot completely rule out HSA adsorption into empty pockets due to incomplete HFN adsorption at the interface. However, there is little discernible increase or decrease in the HFN-FITC fluorescence emission intensity, suggesting that while there may be adsorption/desorption occurring between molecules of the same species, there is no visible change in the total quantity of HFN at the oil-water interface. Comparison of these results with those obtained in the experiments described earlier using HSA indicate that, while HFN easily displaces adsorbed HSA from the interface, HSA demonstrates little tendency to displace HFN from the interface, even at substantially higher bulk concentrations.

These results are not surprising. Data from long term wash-out experiments indicate that HFN adsorbs essentially irreversibly at the oil-water interface (Figure 2.3c). In the first experiment (represented by the upper curve in Figure 2.3c), a pure buffer solution was circulated in the flow cell as HFN-FITC adsorption approached equilibrium; in the second experiment (lower curve in Figure 2.3c), a protein solution containing only unlabeled HSA was circulated through the system, beginning at about the same time as the buffer wash in the previous case. These experiments were conducted to determine whether the introduction of the HFN-free solutions would cause the protein to detach from the interface. Both sets of data reveal very little HFN desorption and/or removal from the interface over the period of the attempted washout, with only a small reduction in the fluorescence emission intensity over the duration of the rinse. We believe the small reduction in fluorescence emission is the result of the elimination of the bulk fluorescence contribution to the overall signal as the flow cell is flushed free of labeled

bulk proteins, rather than an indication of the removal of interface-bound species. Thus adsorption of HFN at the oil-water interface appears to be practically irreversible. Other researchers have also reported fibronectin adsorption irreversibility on hydrophobic surfaces and partial reversibility at hydrophilic surfaces[39].

The results of the sequential adsorption experiments above were confirmed in two additional experiments: (i) adsorption of HSA-FITC following pre-adsorption of unlabeled HFN at the interface, and (ii) adsorption of HFN-FITC following pre-adsorption of unlabeled HSA. The differences between these experiments and the ones presented earlier are that a) the protein initially introduced into the flow cell is unlabeled; and b) only the competing protein of interest (rather than a mixture of the two proteins) is introduced into the flow cell following adsorption of the first. Therefore, diffusion due to concentration gradients can conceivably induce a depletion in the interfacial concentration of the protein that was adsorbed at the interface.

The profile in Figure 2.4a is an example of a sequential adsorption experiment of type (i). In a typical experiment, unlabeled HFN was pre-adsorbed at the indicated concentration for an hour, a duration long enough to obtain adsorption levels near pseudo-equilibrium coverage in the experimental apparatus. The fluorescence emission intensity at the interface was periodically measured, with the results essentially giving the dark current or background noise. HSA-FITC was then introduced into the flow cell after 60 minutes of pre-adsorption of HFN (0.1 mg/ml), and its adsorption profile was monitored. As Figure 2.4a shows, the introduction of HSA-FITC (0.130 mg/ml) induces a negligible change in the fluorescence emission intensity, which remains very close to the background level. After about 40 minutes of apparently negligible HSA-FITC

adsorption, a higher concentration of labeled HSA was introduced into the flow cell. Twenty minutes after the introduction of the more concentrated mixture, a small increase in the fluorescence emission intensity was observed, although this was significantly lower than what would be observed for HSA adsorption in the absence of HFN.

The experiment was repeated, with the only modification being a five-fold reduction in the bulk concentration of pre-adsorbed HFN from 0.1 to 0.02 mg/ml. The lower curve (open circles in Figure 2.4b) represents the HSA-FITC adsorption profile after pre-adsorption of HFN at this lower bulk concentration. In this case, a small increase in fluorescence emission intensity due to HSA adsorption can be observed. However, the maximum signal reached a plateau at a level just slightly above the background noise. For comparison, the adsorption profile of HSA-FITC at the same concentration (0.140 mg/ml) at a bare oil-water interface (solid circles) has been included. The resulting fluorescence emission intensities for this control experiment is more than an order of magnitude higher than for the case where a low concentration of unlabeled HFN was pre-adsorbed at the interface.

In Figure 2.4a, the increase in fluorescence upon introduction of the higher concentration of HSA-FITC is to be expected, since the increased bulk concentration of labeled proteins contributes additional, albeit small, amount of fluorescence emission to the observed signal. It is likely that, upon continuation of the experiment beyond 125 minutes, the signal would have increased, though it would have been significantly below the levels that would be expected in the absence of HFN. Even upon decreasing the HFN bulk concentration to 0.02 mg/ml (Figure 2.4b), little increase is observed in the fluorescence emission intensity, suggesting that even at this low fibronectin

concentration, albumin is effectively unable to displace adsorbed HFN molecules from the interface. It also appears that even fibronectin concentrations as low as 0.02 mg/ml are sufficient to preclude HSA adsorption. Thus, we conclude that prior adsorption of HFN at the oil-water interface effectively inhibits subsequent albumin adsorption, even at short adsorption timescales. The data in Figure 2.4 also confirm that the previous observations were not due to labeling effects.

It is important to note that all the above experiments were conducted at a low shear rate of approximately 0.5 s^{-1}, and at flow rates that did not exceed 0.05 ml/min. This is because, unlike the solid-liquid interface, the liquid-liquid interface may become unstable at high shear. By comparison, these types of experiments have been conducted at the solid-liquid interface at shear rates of 1.5 s^{-1} or higher[12]. The low shear rates and low flow rates used in the experiments can reduce the speed at which proteins arrive at the interface. Thus, once a protein arrives at the interface, it can have a significant amount of time to adsorb, unfold and undergo conformational changes before a second protein arrives, all of which can contribute to greater adsorption irreversibility. The adsorption of early arriving molecules can therefore be less reversible than that of later arriving molecules. In addition, the low shear rates and resulting expanded relaxation time can lead to a lower availability of open surface locations at which later arriving molecules can adsorb. The effect is that the overall surface coverage may be lower than expected. The results of the sequential adsorption experiments above suggest that HFN adsorbs rapidly and uniformly at the interface, leaving few or no empty interfacial spaces that HSA can adsorb to.

2.5.2 Effect of adsorption timescales

The three profiles in Figure 2.5 are from complimentary experiments conducted over longer adsorption timescales. The first fluorescence emission intensity profile is for the adsorption of HFN-FITC at time t=0 onto a clean oil-water interface from a solution containing only labeled HFN (curve 1). The second profile is of fibronectin adsorption onto an adsorbed HSA layer that has been at the interface for two hours (curve 2). The third profile is of fibronectin adsorption initiated at t=6 hrs onto an adsorbed albumin layer which has been at the interface for six hours (curve 3). As the data show, adsorption of HFN onto a 2-hour old layer of HSA results in an apparently and unexpectedly higher surface coverage than for the case when HFN-FITC adsorbs to a clean oil-water interface. This higher surface coverage after two hours of HSA residence time was initially surprising, because one would expect that the presence of a pre-adsorbed layer of albumin would at least partially inhibit fibronectin adsorption, and that the extent of inhibition would increase with the age of the adsorbed layer. In fact, Wertz and Santore[12] reported nearly complete suppression of fibrinogen adsorption after 4 hours of albumin adsorption on to a hexadecyltrichlorosilane monolayer on quartz.

However, recent reports on fibronectin adsorption to hydrophobic (methylated) substrates[37] suggest that fibronectin adsorbs in both extended and compact conformations, but that most of the adsorbed layer is in the compact conformation. Indeed, the ability of the molecule to undergo transitions from one conformation to the other is made possible by its flexibility in domain-connecting segments and ionic interactions. It is known that the compact conformation of fibronectin is stabilized by intramolecular ionic interactions[57]. A recent report by Michael and coworkers[58] proposes

a mass action model comprising two states to describe fibronectin adsorption to surfaces. They speculated that fibronectin initially adsorbs reversibly and then a fraction of the reversibly bound molecules undergo a transition to the irreversibly adsorbed state, occupying a larger area in the process.

The cartoon in Figure 2.6 depicts a possible sequence of events that provides a plausible physical model for the observation at t=0 and t=2 hours in this study. In the case of fibronectin adsorption onto a bare oil-water interface, early arriving HFN molecules undergo the transition from the reversibly bound state to the irreversibly bound state, which allows them to occupy more of the interfacial area. This results in inefficient packing and hence a fewer number of molecules at the interface. The slow flow rate used in the experiments probably further enhances this effect. We speculate that, in the experiments involving 2 hours of albumin pre-adsorption (curve 2 in Figure 2.5), HFN, displaces loosely bound HSA from the interface upon introduction into the flow cell, and occupies the area in the spread conformation (occupying larger area). In areas where it is unable to displace albumin that has been irreversibly bound, it adsorbs in a compact configuration into the spaces between existing albumin molecules but, due to spatial constraints, it is unable to transition into the relaxed state. However, the compact state results in more efficient packing, thereby increasing the effective interfacial coverage.

In the third experiment (curve 3 in Figure 2.5), HSA is essentially irreversibly adsorbed after 6 hrs[12], resulting in significantly reduced fibronectin adsorption. We believe this is due to the occurrence of two simultaneous processes: a) as albumin unfolds and undergoes molecular relaxation, it reduces the ability of HFN to displace it; b) at the

same time, it also occupies more area per molecule, thereby decreasing the size of the interfacial area where direct attachment of HFN can occur.

This hypothesis appears to be supported by the results of experiments conducted to assess displacement of labeled HSA by unlabeled HFN. HSA-FITC (0.130 mg/ml) was adsorbed at the oil-water interface for periods of one (1) and three (3) hours in separate experiments (Figure 2.7). After each adsorption profile approached pseudo-steady state, a solution of unlabeled HFN at a concentration of 0.1 mg/ml was infused into the flow cell and the HSA fluorescence emission intensity was monitored for a period one (1) hour. In the case of albumin that had adsorbed at the oil-water interface for one (1) hour (solid circles), a significant portion of the adsorbed protein was removed by the HFN wash. In contrast, albumin that had adsorbed to the oil-water interface for three (3) hours (open triangles) appeared to more effectively resist desorption by HFN. Therefore, while significant amounts of HSA was displaced from the interface by HFN in both cases, the longer HSA residence time at the interface significantly mitigated HFN adsorption.

It was also observed that pre-adsorption of higher concentrations of albumin (0.5 mg /ml) at the bare interface followed by introduction of 0.05 mg/ml HFN-FITC still resulted in significant adsorption of fibronectin (Figure 2.8). A subsequent wash with buffer also resulted in little desorption of fibronectin. Sagvolden and others[38] measured interaction forces between fibronectin-coated microspheres and bovine serum albumin-covered substrates and found low interaction forces between the two surfaces, indicating no direct binding between fibronectin and albumin. Their experiments also suggested that fibronectin displaced albumin on hydrophilic polystyrene but was unable to do so on

hydrophobic polystyrene. These observations of fibronectin adsorption at the oil-water interface suggest that, even in the presence of pre-adsorbed albumin, fibronectin still adsorbs in significant amounts. This indicates that fibronectin may either displace the adsorbed albumin or adsorb onto the albumin film as a second layer. If the latter case were true then, since fibronectin does not directly bind to albumin[38], flushing of the flow cell with protein-free buffer should result in significant quantities of fibronectin being desorbed, as such a layer would at best be only loosely bound to the prior adsorbed layer. However, the desorption of HFN-FITC after introduction of protein-free buffer is not very significant (at a flow rate of 0.05 ml/min) as has shown in Figure 2.8. Based on these observations, it is likely that albumin has limited affinity for the oil-water interface, even though the interface is essentially hydrophobic.

2.5.3 Competitive adsorption of HFN and HSA

The lower curve (open triangles) in Figure 2.9 represents the adsorption profile of a mixture of labeled HSA (0.125 mg/ml) and unlabeled HFN (0.05 mg/ml) adsorbing onto a bare oil-water interface. For comparison, the closed circles show HSA alone at the same concentration adsorbing to a bare oil-water interface (solid circles). It is clear that albumin has very limited affinity for the interface in the presence of HFN. While no overshoots were observed in the adsorption profiles in any of these experiments, it appears that, over the time scale of the experiments, fibronectin preferentially adsorbs and effectively limits HSA adsorption. HSA adsorption is visible but very low over the entire duration of the experiment. One other group has reported similar results. Malmsten and Lassen[59] reported preferential adsorption of fibrinogen (a protein similar to fibronectin) from a binary mixture of albumin/fibrinogen onto methylated surfaces. They

observed that albumin was unable to frustrate fibrinogen adsorption, in comparison to the ease with which it inhibited gamma-globulin adsorption.

To assess the observations of fibronectin's strong interaction with the oil-water interface in the TIRFM apparatus, some long duration experiments were conducted at the oil-water interface, using a K12 Kruss Interfacial Tensiometer. Figure 2.10 depicts the interfacial tension profiles at the oil-water interface for different compositions of a mixture of fibronectin and albumin. In Figure 2.10a, adsorption from a solution of HFN (0.1 mg/ml) and HSA (0.125 mg/ml) is monitored. For comparison, the curves above and below are the interfacial tensions of the pure proteins at their respective concentrations. The strong interaction of fibronectin with the surface and its tendency to easily displace albumin from the interface is apparent. At short times (t<5000 seconds), the interfacial tension profile of the mixture follows that of pure albumin adsorbing to the interface due to the higher diffusion coefficient of albumin (6.1×10^{-7} cm^2/s[60]) . At longer times, however, the adsorption profile rapidly approaches that of pure fibronectin. Figure 2.10b depicts the a similar experiment with a higher concentration of HSA (1mg/ml).

In general, it has been shown that smaller molecular weight proteins arrive earlier at the interface (due to their higher diffusion coefficients). The smaller proteins are then preferentially displaced by the higher molecular weight (hence, later arriving) proteins, in a sequence commonly known as the Vroman sequence[61,62]. Recent modeling work on competitive adsorption between proteins has shown that, for the Vroman sequence to occur, the bulk solution must have an excess composition of the small protein, and a stronger interaction between the larger protein and the surface[63]. This study clearly provides strong experimental evidence of the Vroman effect.

2.6 Conclusions

The principal aim of this work was to study the competitive interaction of fibronectin and human serum albumin at a model oil-water interface, using TIRFM. All the experiments reported here were conducted under low shear conditions, to prevent destabilization of the oil-water interface. Under these conditions, it has been demonstrated that it is possible to use TIRFM to study competitive and sequential adsorption interactions at the liquid-liquid interface. The results of this work have revealed adsorption dynamics of the two proteins consistent with previous reports in the literature for solid-liquid interfaces. These results are among the first TIRF measurements describing the sequential and competitive interactions between competing proteins at a model oil-water interface.

It was observed that adsorbed albumin at the oil-water interface is readily displaced by fibronectin, even when albumin is present at much higher bulk concentrations. It was also observed that albumin demonstrated no tendency to displace adsorbed fibronectin at the interface, even when it is present in much higher concentrations in the bulk. Albumin adsorption at short time scales is also reversible at the oil-water interface. However, at longer adsorption time scales, albumin adsorption is somewhat less reversible, and the protein is able to prevent subsequent fibronectin adsorption to some extent, although significant amounts of HFN still adsorbs at the interface. On the other hand, fibronectin adsorption appears to be irreversible over all timescales examined, and albumin adsorption is almost completely frustrated by pre-adsorption of even small quantities of fibronectin at the interface.

This work addresses some key issues on adsorption dynamics between two proteins of much biological interest. The work was also accomplished at an interface that has received relatively little attention, but is clearly relevant to biological systems. The careful measurements of protein dynamics presented in this work were all obtained within 85 nm of the oil-water interface. Therefore, the data represent some of the most interfacially sensitive measurements of protein dynamics accomplished by total internal reflection fluorescence microscopy at a liquid-liquid interface.

2.7 Recommendations for future work

Since albumin adsorption is almost completely frustrated by pre-adsorption of small quantities of fibronectin, it would be interesting to examine this sequential adsorption behavior under conditions where very low concentrations of fibronectin are used to pre-treat the oil-water interface. It would also be interesting to conduct fluorescence recovery after photobleaching experiments on adsorbed layers of proteins, when a mixture of the two competing proteins is present in the solution. Some preliminary FRAP experiments have been initiated with HFN at the oil-water interface and further investigations are in progress to fully characterize the bulk and lateral diffusion coefficients of this fibrous protein at the oil-water interface. Ongoing work in our laboratory is targeted at investigating the influence of the oil-layer thickness on the reversibility of HSA and HFN adsorption to the liquid-liquid interface[64].

Atomic force microscopy is another useful technique for observing the adsorbed state conformation of proteins and other bio-macromolecules. Adsorbed fibronectin has already been characterized by AFM on silica and mica surfaces[37]. Cluster formation

during the adsorption of vitronectin, another glycoprotein similar to fibronectin, has also been reported using AFM[65]. HFN and HSA molecules adsorbed to HTS coated surfaces have already been imaged. It would be interesting to image a similar surface after sequential adsorption of HSA and HFN is complete, to visualize the conformation of the adsorbed proteins. Finally, direct visualization of protein adsorption using AFM at the oil-water interface can give us much insight into the topography of such interfaces. Mackie et al.[3] used an indirect method of AFM imaging to study orogenic displacement of protein films adsorbed at the oil-water interface by transferring the protein films from the oil-water interface to a mica surface using Langmuir-Blodgett methods. Given the 'roughness' of the oil-water interface, studies involving AFM imaging are very challenging and, to date, direct imaging of protein adsorption at liquid-liquid interfaces has not been reported in the literature.

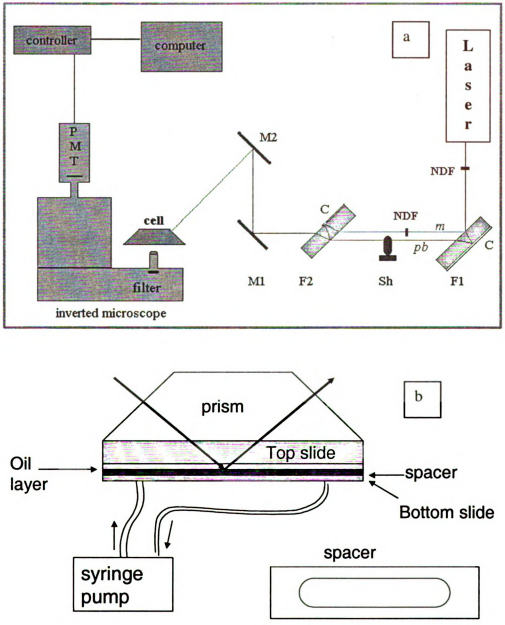

Figure 2.1: a) Experimental layout for TIRFM set-up: NDF: Neutral density filter, OC: optical chopper, F1,F2: optical flats, Sh: shutter, M1,M2: Mirrors, C: coatings b) Layout of flow cell for TIRF experiments.

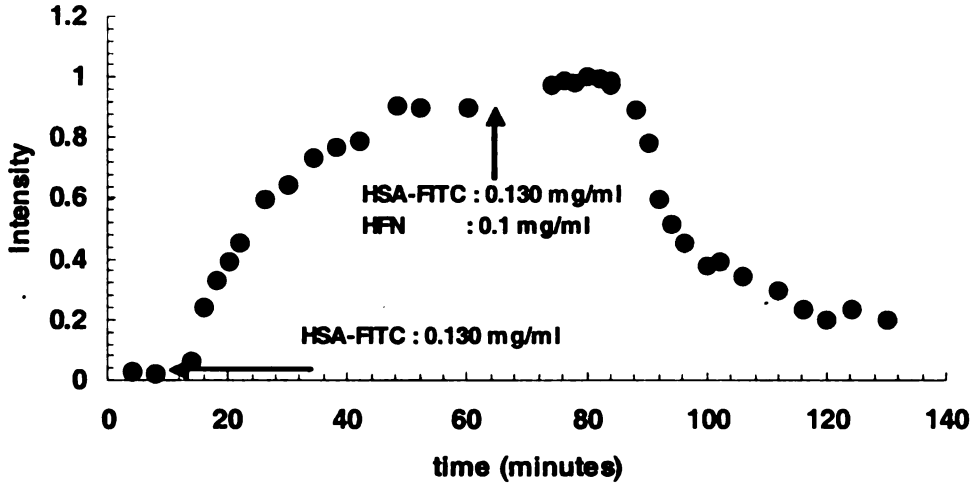

Figure 2.2: Sequential adsorption of unlabeled HFN (0.1 mg/ml) at the oil-water interface, following adsorption of labeled HSA (0.130 mg/ml) to near interfacial equilibrium. In this experiment, a mixture of labeled HSA and unlabeled HFN was introduced into the flow cell approximately 75 minutes after the adsorption of labeled HSA had been initiated. The plot gives strong evidence of displacement of adsorbed HSA at the interface.

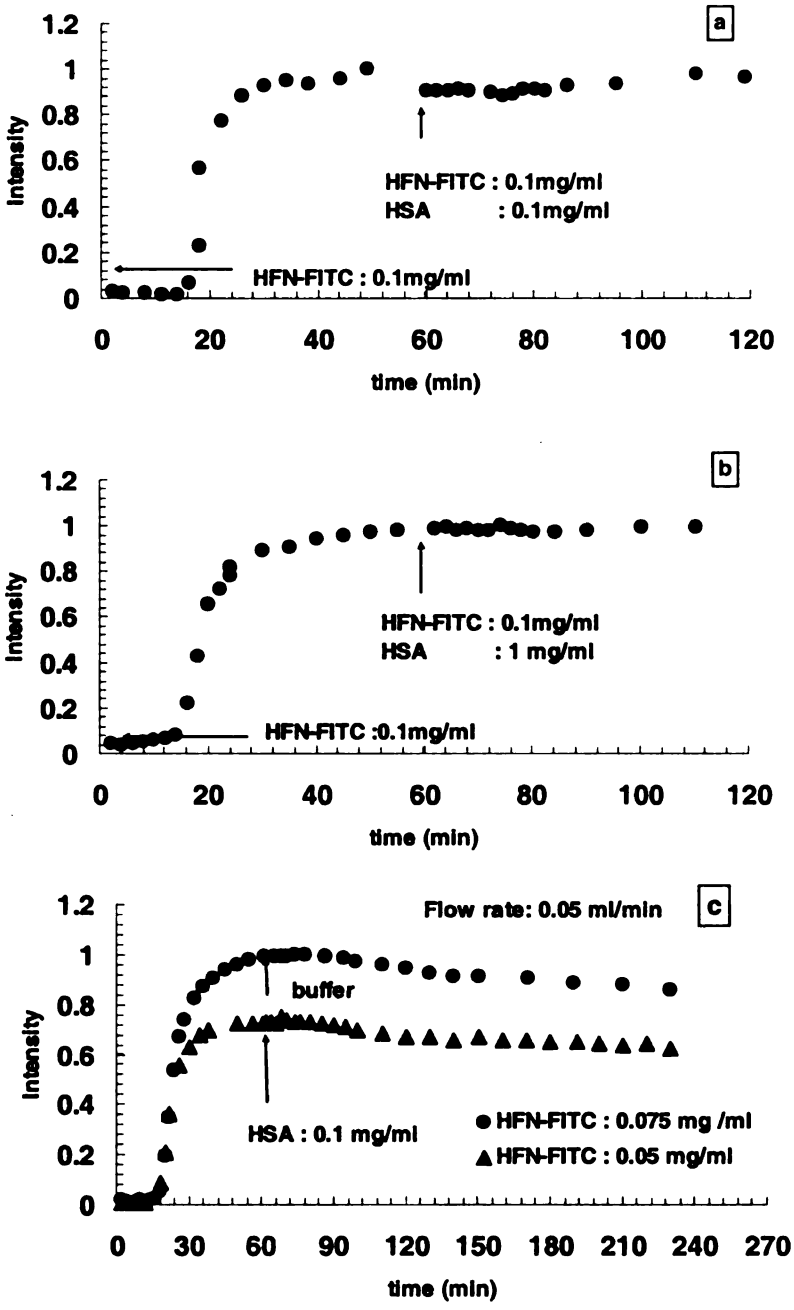

Figure 2.3: Sequential adsorption of HFN/HSA at the oil-water interface. In this experiment, a mixture of labeled HFN and unlabeled HSA was introduced into the flow cell approximately 60 minutes after adsorption of labeled HFN had been initiated. The profiles show that HSA had no apparent effect on HFN adsorption. In the top graph (a), HSA and HFN are at the same bulk concentration (0.1 mg/ml); in the bottom graph (b), the concentration of HSA is an order of magnitude higher (1 mg/ml). (c) Desorption of HFN from the interface by interfacial rinsing. Based on this data, adsorption of HFN at the oil-water interface is essentially irreversible. Little reduction in HFN fluorescence emission intensity is observed upon introduction of a protein-free rinse (solid circles) or circulation of unlabeled HSA (solid triangles) after 60 minutes of HFN at the interface.

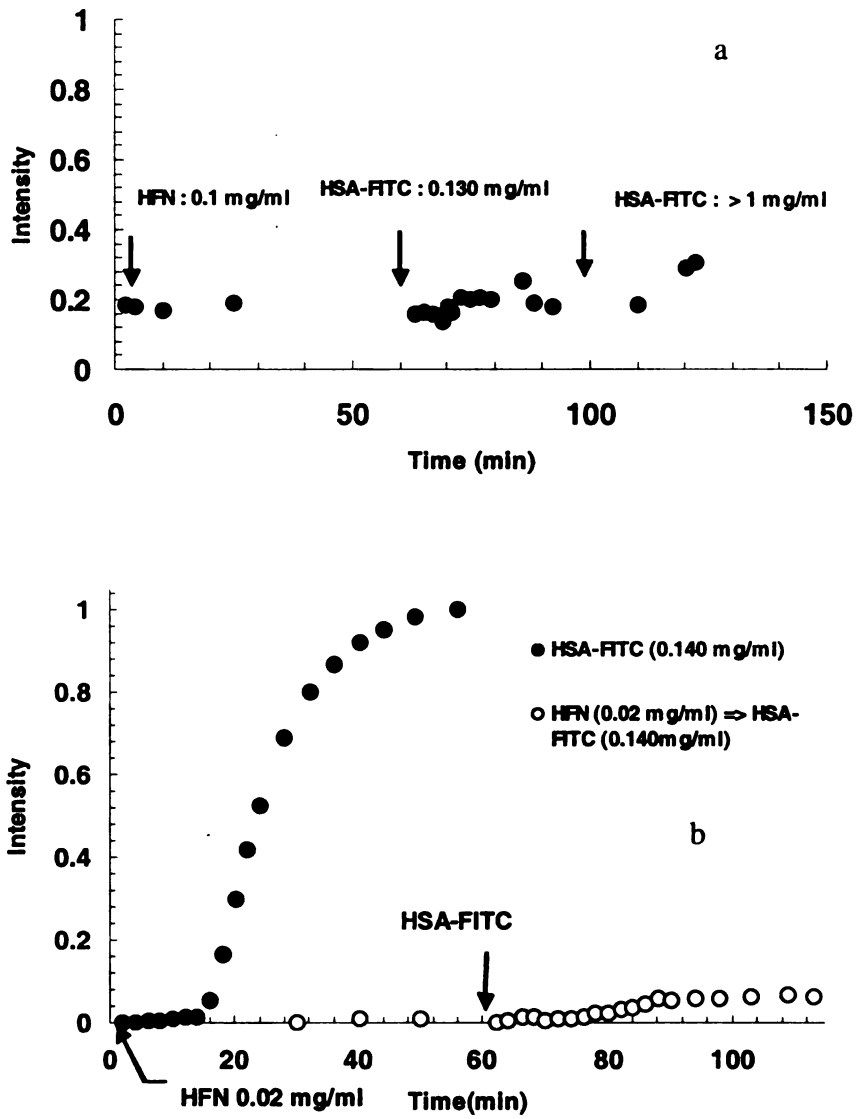

Figure 2.4: Sequential adsorption of HSA and HFN at the oil-water interface. Figure 2.4a shows that pre-adsorption of HFN completely frustrates subsequent HSA adsorption. In this experiment, unlabeled HFN was adsorbed for 60 minutes. Subsequently, labeled HSA was introduced into the flow cell. In the top graph (a) HFN is present in the bulk solution at a concentration of 0.1 mg/ml; in the bottom graph (b), the concentration of HFN is at a much lower bulk concentration of 0.02 mg/ml. Curve 2 in this plot (solid circles) is for HSA adsorbing by itself at the same bulk concentration, and is given for comparison.

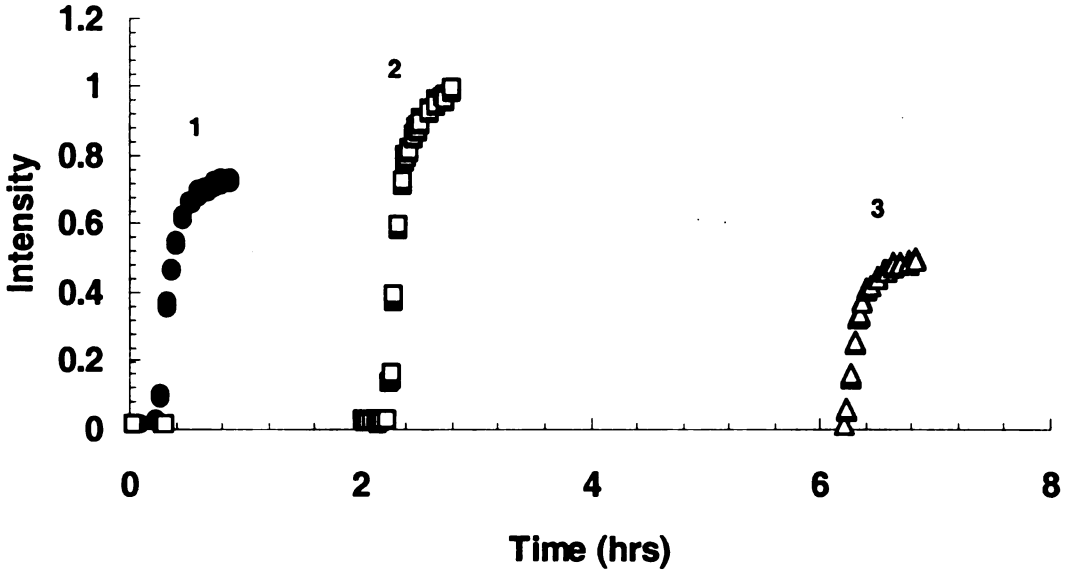

Figure 2.5: Effect of pre-adsorption of HSA on HFN adsorption at the oil-water interface: Curve (1) (solid circles) shows adsorption of labeled HFN to a bare oil-water interface. Curve (2) (open squares) shows adsorption of labeled HFN to an oil-water interface at which unlabeled HSA had been pre-adsorbed for 2 hrs. Curve (3) (open triangles) shows labeled HFN adsorption at an oil-water interface at which unlabeled HSA had been pre-adsorbed for a period of 6 hrs. Bulk concentrations of HSA and HFN are 0.1 mg/ml and 0.05 mg/ml, respectively.

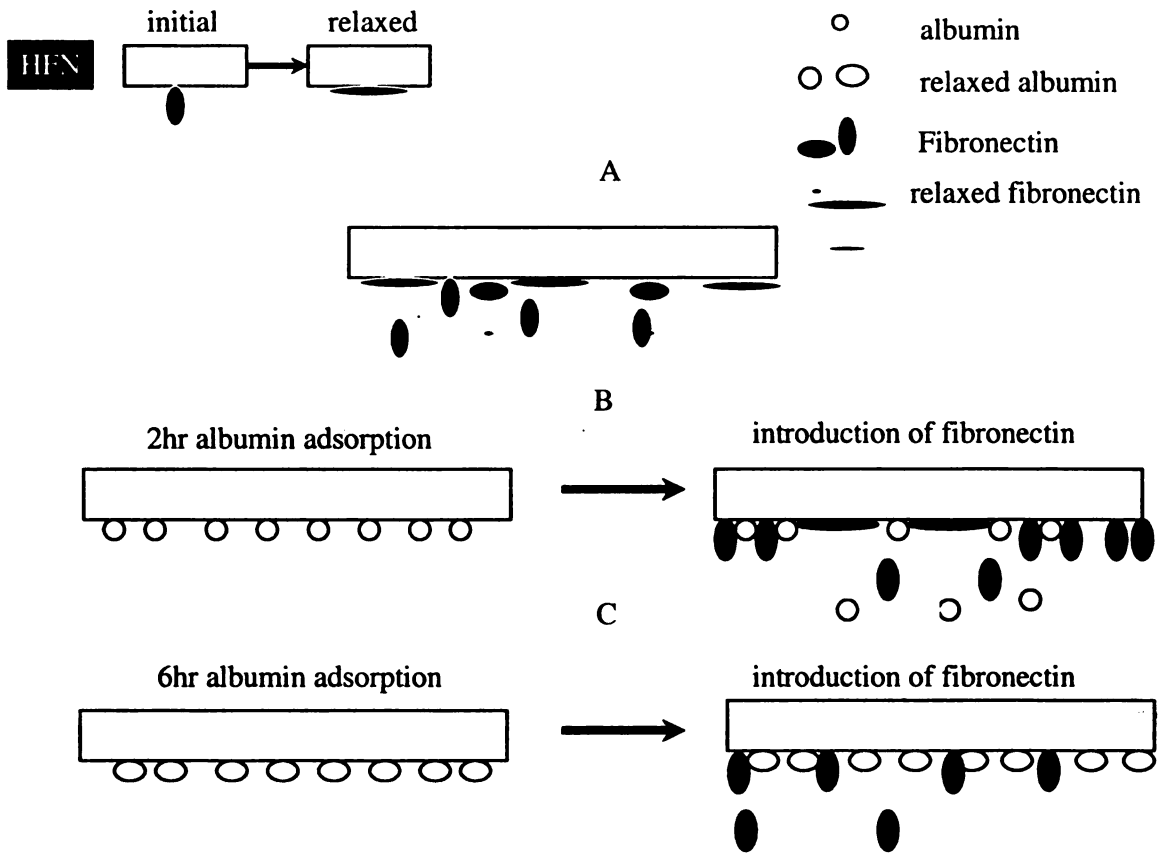

Figure 2.6: Cartoon of a model proposed for adsorption of HFN at an oil-water interface at which HSA has been pre-adsorbed. Curves A, B and C represent models for proposed interfacial organization, under conditions corresponding to curves 1, 2 and 3 in Figure 5.

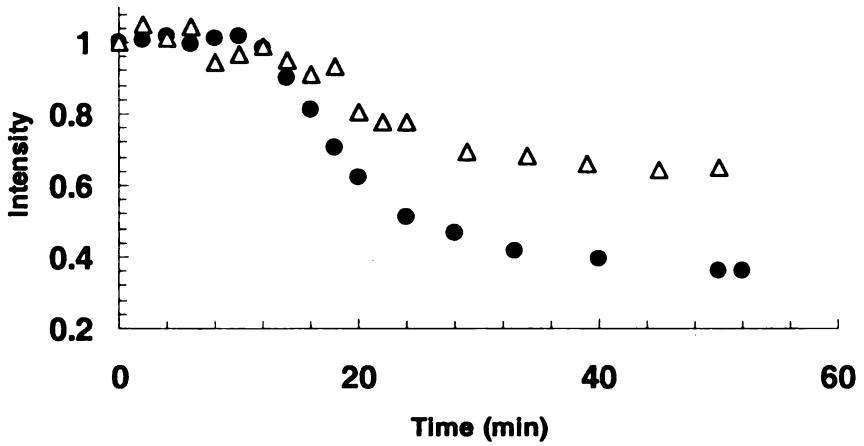

Figure 2.7: Displacement of labeled HSA by unlabeled HFN at the oil-water interface. In each experiment, unlabeled HFN (0.1 mg/ml) is introduced into the flow cell after HSA-FITC (0.130 mg/ml) adsorption for 1 hour (solid circles) and 3 hours (open triangles), respectively (t=0 minutes). In each set, the data has been normalized by the pseudo-saturation intensity obtained prior to the buffer wash. Clearly, HSA is more effective at mitigating displacement by HFN after three hours at the interface than after one hour.

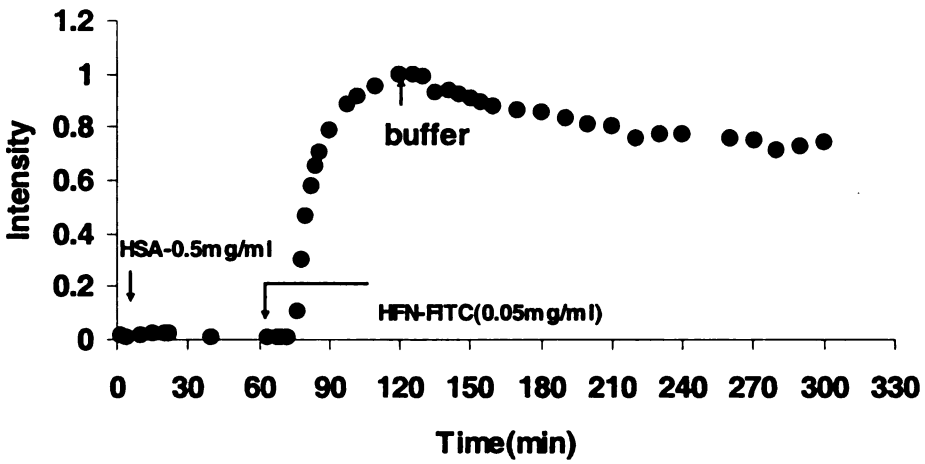

Figure 2.8: Effect of pre-adsorbed HSA concentration on subsequent HFN adsorption. Clearly, pre-adsorption of a higher bulk concentration of albumin (0.5 mg/ml) does not significantly inhibit subsequent HFN (0.05 mg/ml) adsorption at the interface.

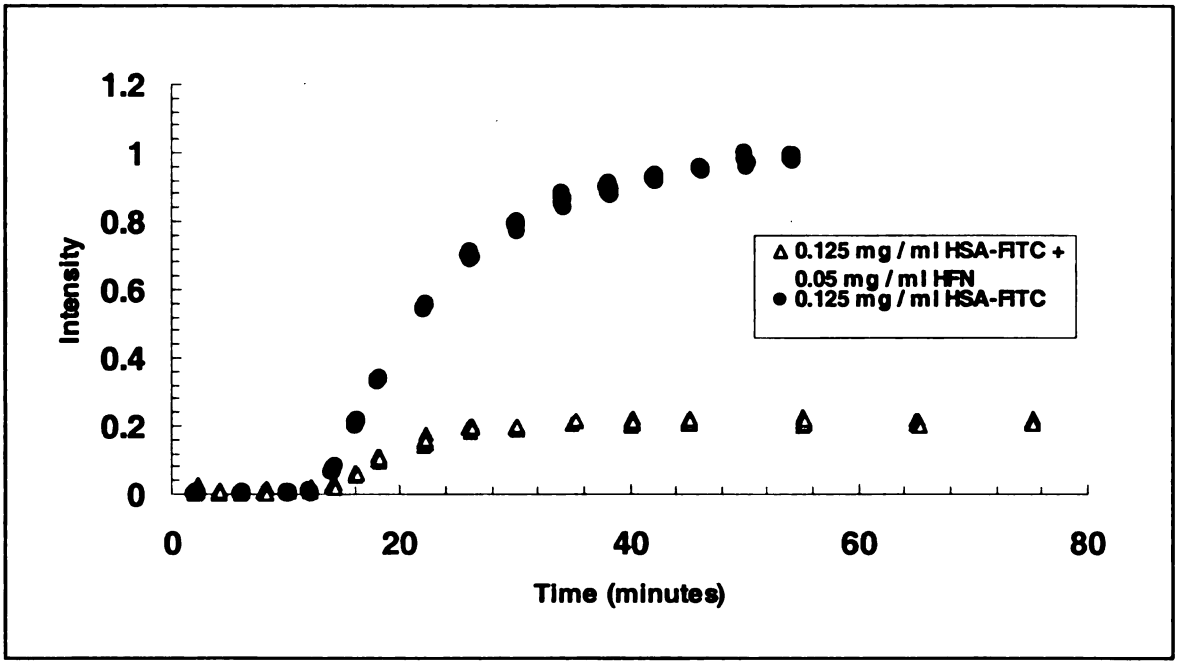

Figure 2.9: Competitive adsorption of HSA and HFN at the oil-water interface: This plot shows preferential adsorption of HFN from a mixture of HFN (0.05 mg/ml) and HSA (0.125 mg/ml) to a bare oil-water interface. The bottom curve (open triangles) is adsorption of a mixture of unlabeled HFN and labeled HSA to a bare oil-water water interface, and is shown for comparison.

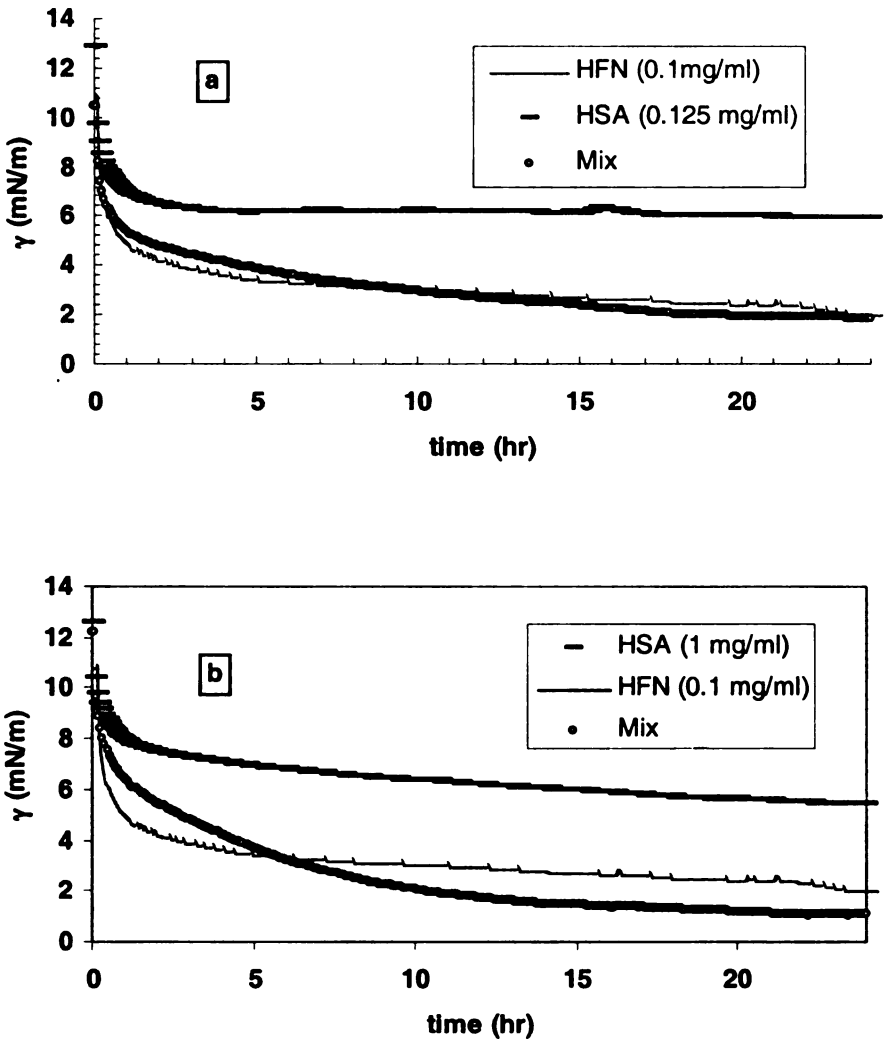

Figure 2.10: Interfacial tension measurements of a mixture of HFN (0.1 mg/ml) and HSA (0.125 mg/ml) adsorbing to an oil-water interface (middle curve) are shown in Figure 10a. For comparison, interfacial tension measurements of pure HSA (top curve) and pure HFN (bottom curve) are also presented. In Figure 10b, the concentration of HSA is increased to 1mg/ml. Over long times, the interfacial tension of the mixture approaches that of pure fibronectin.

3 ESTIMATING PROTEIN INTERFACIAL COVERAGE AT THE LIQUID-LIQUID INTERFACE: A TIRF - FRAP STUDY

3.1 ABSTRACT

The adsorption of bovine serum albumin labeled with FITC (BSA-FITC) to a model oil-water interface has been studied, using total internal reflection fluorescence microscopy (TIRFM). Estimates of the interfacial coverage of proteins at the oil-water interface were obtained using a protocol based on TIRFM–FRAP, previously proposed by Zimmerman and Gaub (1990). Protein coverages ranged from 0.02-0.3 mg/m^2 for bulk concentrations in the range of 0.2 mg/ml to 3.5 mg/ml. These values are an order of magnitude lower than typical estimates reported in the literature for the solid-liquid interface. It is speculated that the lower coverages at the oil-water interface may be due to more rapid protein relaxations at this fluid interface, which would tend to inhibit late arriving protein molecules by occupying a greater interfacial area per molecule. Measurements of fluorescence lifetimes of BSA-FITC were also made to examine if there were differences in the lifetimes between molecules at the interface and those in the bulk using two-photon excitation spectroscopy. No differences were found between these two lifetimes, suggesting that the quantum yield of BSA-FITC at the interface is the same as its quantum yield in the bulk solution.

3.2 Introduction

Proteins are among the most important molecules involved in key biological processes. Protein adsorption is one of the first and most important steps that must occur before key cellular processes such as cell attachment and differentiation can occur. They function as enzymes, which are responsible for catalyzing several important reactions. Proteins also play important roles in the storage and transport of biologically important molecules such as oxygen[66].

Protein adsorption to interfaces has been monitored using several methods. Techniques such as radio-labeling[15,42], tensiometry[67], optical reflectometry[68], neutron reflectometry[69,70], ellipsometry[59,71] and TIRFM[5,6,12] have been commonly used to characterize interfacial adsorption behavior. More recently, methods such as quartz crystal microbalance (QCM)[72], surface plasmon resonance (SPR)[61], optical wave guide light mode spectroscopy (OWLS)[13] and AFM[43,73,74] are becoming increasingly popular. It is important to be able to accurately estimate the quantity of adsorbed protein because this allows us to make quantitative and qualitative predictions about the structure and characteristics of the adsorbed protein film, including predictions on whether the adsorption is limited to a single monolayer.

Techniques such as reflectometry and ellipsometry rely on the evolving refractive index of the protein film to estimate the surface coverage. Research groups that use TIRFM for observation of protein adsorption conduct their experiments in regimes where adsorption is strictly transport-limited, so that surface coverages are calculated by direct application of the Leveque solution[12,40]. This results in conversion of fluorescence

intensities to surface coverages by application of a simple conversion factor. Other TIRFM-based calibrations use angle scanning methods where the penetration depth of the evanescent wave is varied[75], or use external and internal standards to calibrate the fluorescence signal[14]. Adsorbed amounts can also be computed by a visual count of individual protein molecules, from AFM images of adsorbed protein layers[43].

In contrast with the considerable literature on protein adsorption at the solid-liquid interface, there are relatively few reports on estimating interfacial coverages at the liquid-liquid interface. Estimates of surfactant and protein interfacial coverages at the liquid-liquid interface have been obtained by radiolabeling[9,15] and neutron reflectivity[4] Because of the instability of the interface boundary, estimating coverages at liquid-liquid interfaces is a challenging problem. For example, quantitative interfacial concentrations of proteins at the interface can be easily obtained by scraping the adsorbed protein off the surface. For obvious reasons, this cannot be done at liquid-liquid interfaces. Also, the curvature of the interface presents additional problems for optical experiments.

In the experiments on sequential and competitive adsorption between human plasma fibronectin and human serum albumin at the oil-water interface, it was observed that HFN preferentially adsorbs over HSA. It was also observed that HFN displaces pre-adsorbed albumin over nearly all adsorption time scales. However fluorescence studies at the oil-water interface are subject to greater amounts of "noise" induced by light scattering than at the solid-liquid interface, due to the uneven interface. Such scatter can also occur due to contaminants such as dust particles which can stick to the oil, even after taking the utmost experimental precautions. Electromagnetic energy from the increased light scattering can further excite both bulk and surface associated molecules, inducing a

level of fluorescence emission beyond what is induced by the direct laser beam. This can result in artificial elevations in the level of fluorescence emission that is collected by the objective, which complicates direct comparison of fluorescence emission data between different experiments. Thus, a calibration technique that allows us to directly convert fluorescence emission intensities into interfacial mass coverages will eliminate such artifacts. This will also allow us to make more rigorous comparisons between data sets obtained under different experimental conditions.

Gajraj[55] in our laboratory had previously adapted a technique for estimation of coverages at the liquid-liquid interface, using the technique first proposed by Zimmerman et al[16] and is based on a combination of total internal reflection fluorescence microscopy (TIRFM) and fluorescence recovery after photobleaching (FRAP). The technique relies on the ability to discriminate between fluorescence recovery from bulk species and that from surface-associated molecules. Gajraj reported interfacial coverages that were greater than an order of magnitude lower than similar values reported in the literature.

In the present study, a calibration protocol has been developed to obtain an adsorption isotherm for BSA at the oil-water interface. One of the important assumptions of this internal-standard technique was that the quantum yield of a fluorophore in the bulk solution remains unchanged upon its adsorption at the interface. The validity of this assumption was examined by conducting two-photon excitation spectroscopy studies of fluorescence lifetimes of BSA-FITC adsorbed at the oil-water interface and in the free solution. The influence of shear rate (flow rates) on the ultimate interfacial coverage of BSA at the liquid-liquid interface was also assessed, along with shear rate studies of

protein adsorption at a hydrophobic solid-liquid interface (Octadecyltrichlorosilane (OTS) self assembled monolayers on glass) and compared.

3.3 Theory

3.3.1 Total internal reflection

A detailed derivation of Maxwell's equations governing the theory of total internal reflection is available elsewhere (see Reichert et al.[76], for example). In brief, when a light beam traveling through an optically dense medium of refractive index n_1 approaches the interface between the dense medium and a rarer medium or refractive index n_2 ($n_2<n_1$) at an angle of incidence exceeding the critical angle θ_c, it undergoes total internal reflection. The critical angle at which this occurs is given by Equation (2.1). When the beam undergoes total internal reflection, the reflected ray travels through the same medium as the incident ray. However, an electromagnetic field is generated in the rarer medium beyond the interface. The intensity of this field (called the evanescent wave) decays exponentially with perpendicular distance z from the interface as given by Equation (2.2). The characteristic penetration depth of this wave, d_p, is given by Equation (2.3) and indicates the distance at which its intensity has reduced to 1/e of its maximum value at the interface. Typical values for d_p vary from 50 to a few hundred nanometers. Thus, only fluorophores located in the vicinity of the interface are excited by this energy field. This interfacial selectivity makes this optical technique ideal for studying surface and interfacial phenomena.

3.3.2 The calibration protocol

The theory for estimating protein interfacial coverages using TIRFM and FRAP was developed by Zimmerman et al[16]. A complete discussion of this technique can be found in Gajraj[55] and the key steps towards developing this theory has been outlined below for completeness .The fluorescence emitted by an excited fluorophore is given by

$$F(t) = \int_0^\infty q_I I(z) q(z) C(z) dz \tag{3.1}$$

Here, $I(z)$ is the intensity of light striking fluorophores of concentration $C(z)$ located at a distance z from the interface, $q(z)$ is the quantum yield of the fluorophore at z, and q_I is an instrument constant. The total fluorescence collected by the objective is a function of contributions from surface-bound proteins and fluorescently labeled proteins present in the bulk that are illuminated by the tail of the evanescent wave:

$$F(t) = F_{surface}(t) + F_{bulk}(t) \tag{3.2}$$

Incorporating the expression for the decaying evanescent wave given by Equation (2.2) gives

$$F(t) = q_I I_o \int_0^l \exp\left[-\frac{z}{d_p}\right] C(z) q(z) dz \tag{3.3}$$

where l is the depth of the flow cell. This integral can be deconvoluted into bulk and surface contributions and represented as

$$F(t) = F_{surface} + F_{bulk} = q_l q_s I_o C_s + q_l q_b C_b I_o \int_s^l \exp\left(-\frac{z-s}{d_p}\right) dz \quad (3.4)$$

where q_s and q_b are the quantum yields of fluorophores at the interface and in the bulk, respectively.

In developing Equation (3.4), Zimmerman et al.[16] assumed a model where a layer of adsorbed proteins of thickness s and two-dimensional concentration C_s is in equilibrium with fluorescently labeled proteins in the bulk solution at a three-dimensional concentration C_b. This equation also assumes that that plane of total internal reflection occurs at the interface between the protein film of thickness s and the bulk solution. This interface can facilitate total internal reflection as the refractive index of the protein film is assumed to be close to that of the oil (n=1.51). It is important to note that the presence of an intermediate film of arbitrary refractive index and nanometer scale thickness between the dense medium and the rare medium will not prevent total internal reflection from occuring. For proteins such as serum albumin, a typical value of film thickness estimated using ellipsometry is approximately 5 nm[16,55]. This value of s is considerably smaller than the thickness of the flow cell (l). Therefore, the definite integral in Equation (3.4) can be solved after noting that $s<<l$. Thus the term corresponding to F_{bulk} can be rewriten as follows:

$$\begin{aligned} F_{bulk} &= q_l I_o C_b q_b \int_s^l e^{-\left(\frac{z-s}{d_p}\right)} dz = q_l I_o q_b C_b (-d_p) \left[e^{-\left(\frac{z-s}{d_p}\right)} \right]_s^l \\ &= q_l I_o q_b C_b d_p \end{aligned} \quad (3.5)$$

Combining this with Equation (3.7) leads to the following relationship for the total fluorescence emission from the sample:

$$F(t) = I_o q_I (q_s C_s + q_b C_b d_p) \tag{3.6}$$

The assumption that the quantum yields of surface and bulk associated fluorophores are equal (q_o) (an assumption that would be discussed in detail later) leads to,

$$F(t) = q_I I_o q_o (C_s + C_b d_p) \tag{3.7}$$

The bulk contribution to the total intensity is simply

$$F_{bulk}(t) = q_I q_o I_o C_b d_p \tag{3.8}$$

Thus the unknown constants can be factored out and Equations (3.7) and (3.8) can be combined and rearranged to give

$$C_s = C_b d_p \left(\frac{F(t)}{F_{bulk}(t)} - 1 \right) \tag{3.9}$$

The variables in the above equation can be easily estimated as shown in Figure 3.1. *F(t)* represents the total fluorescence measured prior to initiation of the bleaching pulse, and is obtained at the end of a typical adsorption experiment at the oil-water interface. $F_{bulk}(t)$ is the fluorescence after a series of bleach pulses are applied. Both values are corrected for background fluorescence before incorporation into Equation (3.9)

.

This technique relies on the ability of the evanescent wave to selectively and primarily excite surface fluorophores, along with only a small number of bulk associated fluorophores. It also relies on the fact that the diffusion coefficient of proteins in the bulk is significantly higher than that of proteins bound at the interface. As a result, surface bound fluorophores can be considered irreversibly bleached within the time scale of observation, while bleached bulk fluorophores would be instantaneously replaced by unbleached fluorophores, thus resulting in an apparently unbleachable bulk fraction. The diffusion coefficient of proteins such as albumin and fibronectin is in the range of 10^{-7} cm^2/s. For a freely diffusing molecule undergoing Brownian motion, the time required to travel through a bleached region of depth d_p, based on the Stokes-Einstein equation is

$$t = \frac{d_p^{\,2}}{2D} \tag{3.10}$$

For a penetration depth of approximately 80 nm, this results in a characteristic time of diffusion on the order of approximately 1 to 10 milliseconds. As a result, fluorophores in the bulk that are bleached by the evanescent wave are quickly replaced by unbleached fluorophores that essentially instantaneously diffuse into the bleached zone. Hence, bulk species can be treated as an unbleachable fraction that maintains a constant contribution to the total fluorescence emitted. A cartoon showing the sequence of photobleaching and bulk recovery is shown in Figure 3.2. This cartoon shows a region near the interface that is filled with fluorophores that are adsorbing to the interface. The open circles represent unbleached fluorophores while the closed circles represent bleached fluorophores.

Prior to application of the bleach pulse, all the fluorophores are unbleached and contribute to the total emission $F(t)$. Immediately after the application of the bleach pulse, all the fluorophores in the illuminated region would be bleached. However, after a few milliseconds have elapsed, the bulk fluorescence would recover due to the rapid replacement of bleached fluorophores in the bulk with unbleached fluorophores by diffusion as predicted by Equation (3.10). Since the immobilized fluorophores at the interface would remain bleached, the fluorescence emission at this point is represented by $F_{bulk}(t)$. This procedure is an elegant method of separating bulk and surface contributions to the total fluorescence emission intensity. In the current experimental configuration, the typical dwell time between measurements is 100 milliseconds, thus providing sufficient time for bleached bulk molecules to be replaced by unbleached ones.

The bulk and surface fluorescence contributions can also be separated by rinsing the flow-cell with a protein-free buffer, which would presumably deplete the bulk of labeled protein species, while leaving interface-associated species in place. However there are several disadvantages to using this method at the oil-water interface.

(i) Since the interface is mobile, it is necessary to conduct such a wash at very low flow rates to prevent inducing interfacial destabilization. As a result, ensuring that all the labeled protein present in the bulk solution has been eliminated requires a thorough wash-out that would take approximately three hours (this corresponds to the time required to exchange about 10 volumes of the flow cell). In such an extended wash-out period, there is no reliable method of preventing adsorbed species and the oil film from being entrained and removed from the interface.

(ii) The quantum yield of fluorophores is dependent on the local environment. Thus, eliminating labeled proteins from the bulk would change the local environment around the surface-bound fluorophores. This may result in changes in their quantum yield, thereby introducing artifacts in the data.

Equation (3.9) was developed on the underlying assumption that the quantum yields of the surface and bulk associated fluorophores are equal. However, as noted above, the quantum yield of fluorophores is a very sensitive function of the environment surrounding it. Thus the proximity of a tagged protein to other fluorophores (which results in quenching) or its location in a highly viscous or hydrophobic environment can affect the quantum yield. Hence, if $q_s < q_b$, this can result in significant underprediction of interfacial coverages by Equation (3.9). It is, therefore, necessary to test the validity of this assumption at the oil-water interface. While the estimation of absolute quantum yields is a challenging problem, it can be related to the fluorescence lifetime τ, a variable that describes the length of time a molecule resides in the excited state before eventually transitioning to the ground state. The fluorescence lifetime is more readily measurable, and comparison of the lifetimes of molecules at the surface and in the bulk can provide us with insight into the relationship between q_s and q_b. This approach is discussed in greater detail below.

3.3.3 Two-photon fluorescence lifetime spectroscopy and the quantum yield problem

3.3.3.1 Rationale

In the development of the calibration protocol outlined in the preceding section, it was assumed that the quantum yield of surface-associated and bulk-associated

fluorophores are identical. Although this assumption has been made to simplify the mathematical analysis, it is a well known fact that the quantum yield of a fluorophore is highly sensitive to the surrounding environment. As noted above, direct measurement of fluorescence quantum yields is difficult. In fact, the estimation of the relative quantum yield of fluorophores to within 5% precision is extremely difficult and the values against which the relative yields are standardized are themselves subject to greater than 5% variation[77,78]. Estimation of the absolute quantum yield is considerably more difficult and requires sophisticated instrumentation. The two most common methods used for measuring quantum yields are calorimetry[79] and by comparison with known standards. Therefore, estimating the quantum yield of a fluorophore adsorbed to (or in the proximity of) an interface is obviously very difficult.

The quantum yield of a fluorophore is defined as the ratio of the number of photons emitted to the number of photons absorbed, and is given by[80]

$$q = \frac{k_r}{k_r + k_{nr}} \tag{3.11}$$

where k_r and k_{nr} are the rates of radiative and non-radiative decay, respectively. The lifetime τ of the fluorophore is given by:

$$\tau = \frac{1}{k_r + k_{nr}} \tag{3.12}$$

The variables k_r and k_{nr} can be calculated as

$$k_r = \frac{q}{\tau} \tag{3.13}$$

$$k_{nr} = \left(\frac{1-q}{\tau}\right) \tag{3.14}$$

Thus fluorophores with a large radiative decay rates have high quantum yields and short lifetimes. In fact, the radiative decay rate k_r is a function of the oscillator strength of the electronic transition[81], which is only slightly sensitive to the environment around the fluorophore. Thus k_r can be treated as a constant for a given fluorophore. Variations in fluorescence lifetimes and quantum yields of fluorophores resulting from changes in non-radiative decay rates are due to events such as collisional quenching and fluorescence resonance energy transfer[82]. Thus, in principle, the quantum yield and the fluorescence lifetime are directly proportional to each other, assuming that there are no changes in the radiative decay rate. Then, the lifetime and quantum yield of a fluorophore will increase or decrease together[82]. Thus, the quantum yield of a given fluorophore can be indirectly probed by measuring its associated lifetimes.

It is relatively easy to obtain estimates of the fluorescence lifetimes of fluorophores. The lifetime of the fluorophore is the length of time a molecule spends in the excited state, prior to its eventual transition to the ground state. It is related to the quantum yield (please see Equation (3.13)). To estimate the quantum yield, the time interval between the application of the input pulse and the arrival of the first emitted photon was measured, using time correlated single photon counting (TCSPC). Since

fluorescence emission is a random event, the distribution of these arrival times represents the fluorescence decay for a large number of photons.

Estimating the lifetime (τ) for BSA-FITC molecules in the bulk solution using conventional TCPSPC spectroscopy is relatively easy. However, estimating the parameter for BSA-FITC molecules adsorbed at the oil-water interface is a much more challenging problem. In addition to the constraints imposed by the geometry of the experimental set-up and detection equipment, there is the serious challenge of isolating the interfacial signal from the background bulk fluorescence signal. Since the beam excites a large region around the interface, a significant portion of the emission signal can be considered to originate from bulk contributions. This results in "noise" that is difficult to deconvolute. Finally, the oil-water interface is not a "smooth" interface when compared to the solid-liquid interface. There are "ridges and bumps" at the boundary of the two phases due to the juxtaposition of one phase into another at various points along the interface. In addition, the relative affinity of the aqueous phase for quartz causes water to creep around the oil phase at the cuvette walls, producing a curved interface. All these factors combine to produce a more complicated optical path. Thus, using the conventional set-up for exciting the fluorophores does not produce reliable estimates of the dynamics at the interface. Therefore, to obtain more reliable estimates of the fluorescence lifetimes of the adsorbed protein molecules, two-photon time correlated single photon counting spectroscopy was used.

3.3.3.2 Theory

Two-photon fluorescence occurs when a fluorophore simultaneously absorbs two photons of wavelength 2λ and then undergoes an electronic transition at a wavelength

λ[83]. The number of photons absorbed in two-photon spectroscopy is directly proportional to the square of the incident light intensity. The fluorescence emission from a sample undergoing a two-photon transition can be described as,

$$F = \alpha \iiint C(r,z) I^2(r,z) dV \tag{3.15}$$

where $C(r,z)$ is the concentration profile of the fluorophore undergoing the electronic transition, $I(r,z)$ is the intensity of the incident light, and the integration is computed over a volume in space.

The non-linear dependence of the absorption on the square of the incident light intensity is responsible for the spatial selectivity of this technique. Since the amount of light absorbed is proportional to the square of the number of incident photons, very high intensities are required in order to obtain a measurable amount of 2-photon excitation[84]. This excitation occurs at the focal point of a laser beam that has been focused through a converging lens (or an objective). As a result, fluorescence is emitted only from regions illuminated by the focal volume occupied by the beam at its waist, thereby affording excellent spatial selectivity. An additional advantage of 2-photon spectroscopy is that the excitation and emission wavelengths are widely separated, so there is little possibility of data contamination due to spectral overlap. For example, for experiments discussed in this chapter, the excitation wavelength was 700 nm while the emission wavelength was set near the emission maximum of FITC at about 530 nm.

Two-photon excitation has primarily been used to study the excited states of molecules, because it follows different selection rules for electronic transitions as

compared to single photon absorption processes[84,85]. However, in the last decade, it has been used extensively for studying biological samples because of its excellent spatial selectivity and low background fluorescence[86-89]. In most cases, the emission spectra for 1-photon and 2-photon excitation are the same. This is an important point because, in this study, lifetimes were measured using 2-photon spectroscopy. These results are then extrapolated to speculate on possible changes in quantum yield that occur during the TIRFM experiments, which use single-photon excitation. All TIRFM studies in this dissertation were conducted with excitation at 488nm, whereas the two-photon studies were conducted at an excitation of 700 nm. It has been previously demonstrated that emission spectra for most dyes such as fluorescein or Cascade Blue is independent of the excitation wavelength, which would indicate that the fluorescence quantum efficiency is independent of the excitation wavelength[85].

3.3.3.3 Measurement of Fluorescent Lifetimes

Fluorescence emission curves can typically be described by single or multi-exponential decay. For a fluorophore undergoing exponential decay[80],

$$F(t) = F_o e^{-t/\tau} \tag{3.16}$$

where F_o is the fluorescence intensity at t=0, and τ is the lifetime. For decays that are not adequately described by a single exponential, the decay profiles are typically fitted to a sum of exponentials,

$$F(t) = \sum_i \alpha_i e^{-t/\tau_i} \tag{3.17}$$

where α_i is the pre-exponential factor representing the fractional contribution to decay of the fluorophore with a lifetime τ_i.

Decay profiles that are best fit to multi-exponential models can suggest the presence of multiple fluorophore populations, or the presence of a single fluorophore in different environments. For example, the presence of two lifetime components for BSA-FITC can be attributed to FITC being present in two different kinds of regions on the protein. Multi-exponential fits can also be merely statistical in nature and may not imply any underlying physical phenomenon. These decay profiles are usually analyzed using the method of least squares which minimizes the sum of the weighted squares of residuals defined as

$$\chi^2 = \frac{1}{n-p}\sum_{i=1}^{n} w_i \left[y_i - f(t_i : \alpha_i, \tau_i) \right]^2 \tag{3.18}$$

where n is the total number of data points, p is the number of fittable parameters and the factor w_i is the weight associated with each square residual.

This weight is related to the standard deviation associated with each count interval. For photon counting applications, it is reasonable to assume that the error follows Poisson counting statistics[90]. Thus the variance at each interval is directly proportional to the number of counts at that interval.

$$\sigma_i^2 = y_i \tag{3.19}$$

Thus, the decay curves can be weighted as,

$$w_i = \frac{1}{\sigma_i^2} = \frac{1}{y(t_i)} \tag{3.20}$$

3.4 Experimental Methods

3.4.1 Materials and Methods

BSA was purchased from Sigma Aldrich (St. Louis, MO). Fluorescein isothiocyanate (F-1907) was obtained from Molecular Probes (Eugene, OR). The oil used for the experiments was an immersion oil (Type A) obtained from Cargille (Cedar Grove NJ). This oil had a refractive index of approximately 1.515. Octadecyltrichlorosilane (OTS) was obtained from Sigma Aldrich (St. Louis, MO)

3.4.2 Protein labeling

BSA was labeled with FITC in 0.1M carbonate buffer at pH 9.2 for 4-6 hours. The solution was then passed through a PD-10 column (Amersham Biosciences, Piscataway, NJ) that had been pre-equilibrated with 0.05M phosphate buffer (pH 7.4). The column was then eluted with 0.05M phosphate buffer to recover the protein conjugate. This was followed by overnight dialysis against phosphate buffer to completely remove unbound labels from the solution and to ensure complete buffer exchange. Labeling ratios were determined by measuring the absorbance of the conjugate at 496nm and 280nm. In all experiments, the labeling ratio was kept below 1.3. All protein solutions were stored at 4°C and used within a week. All adsorption experiments were conducted in 0.05M phosphate buffer.

3.4.3 Preparation of surfaces

The microscope slides (Fisher Premium slides) used for TIRFM experiments were purchased from Fisher Scientific (Pittsburgh, PA). Slides on which oil films were deposited were cleaned by ultrasonication in RBS-35 detergent solution. The slides were rinsed thoroughly in deionized water and then immersed in concentrated nitric acid for 30 minutes. The slides were stored in deionized water to prevent dust accumulation on the surface. Microscope slides on which OTS monolayers were deposited were cleaned by ultrasonication in RBS-35 detergent solution. After rinsing the slides thoroughly with deionized water, they were immersed for 30 minutes in piranha solution (70% sulfuric acid and 30% hydrogen peroxide)[3]. The slides were subsequently rinsed with deionized water and dried thoroughly under nitrogen. They were then immersed in 1% (vol/vol) solution of OTS in hexadecane for approximately 15 minutes, after which they were thoroughly rinsed with methylene chloride and chloroform[69]. The contact angle of the self assembled OTS monolayers was measured using a home-built contact angle instrument and was found to be greater than 110 degrees in all cases[4].

3.4.4 TIRFM instrumentation and experimental set-up:

The TIRFM instrumentation, flow cell design and optical configurations for FRAP were described in detail in Chapter 2. The oil layer was deposited on a clean glass slide by rolling a clean glass rod through a drop of oil placed at one end of the glass slide.

---

[3] Piranha solution is extremely corrosive. Face mask, acid-resistant gloves and protective clothing must be used while handling piranha. Use extreme caution.

[4] Static contact angle measurements were made using a homemade contact angle instrument in Dr. Michael Mackay's laboratory at Michigan State University.

For adsorption and FRAP experiments, monitoring beam intensities ranged from 1-4 μW and photobleaching beam intensities were at least 10mW or higher. The duration of each photobleaching pulse varied from 350ms to 1 s. Typically, bleaching was carried out for a total duration of 5 to 10 seconds till no further recovery was observed from the sample. It was found that longer bleaching times are required to completely bleach fluorophores at the oil-water interface as compared to the OTS-water interface. This may be due to a higher fraction of reversibly associated protein at the oil-water interface than at the OTS-water interface. In some experiments, the observation area was reduced by placing an aperture before the photomultiplier tube. This was done to ensure that fluorescence emission was collected from only a small portion in the center of the bleached region to counter the effects of lateral diffusion. No significant difference in computed interfacial coverage was observed in the presence of the aperture.

Experiments were initiated by introducing the buffer solution into the flow cell using an infusion/withdrawal syringe pump. After beam alignments and fine-focusing were completed, BSA-FITC was introduced into the flow cell at a controlled flow rate and adsorption was allowed to proceed until the fluorescence emission intensity reached a stable value. A series of rapid bleach pulses were then applied to completely bleach the interfacial fluorophores. The residual fluorescence emission corresponded to the contribution of bulk-illuminated fluorophores to the pre-bleach emission intensity. Typically, three to four different sites on each interface were bleached to determine the degree of variation in surface coverage across the interface, and to ensure that the data are statistically relevant.

3.4.5 Two photon lifetime spectroscopy: Experimental set-up.

Estimates of the fluorescence lifetime of FITC and BSA-FITC were obtained using a two-photon time correlated single photon counting spectrometer (2P-TCSPC). The experimental layout of the 2P-TCSPC spectrometer is shown in Figure 3.3. A description of the experimental set-up can be found in DeWitt et al.[68], although the system has been modified slightly from its original implementation. Briefly, the output from a 30 W CW mode-locked Nd:YAG laser (Coherent Antares 76 S) at 1064 nm was frequency doubled using a temperature tuned Type I LBO crystal to produce a 532 nm beam. This light was used to excite a cavity dumped dye laser (Coherent 702-2). For these experiments, pulses at 700nm were generated using LDS-698 laser dye (Exciton). In all experiments, the fluorescence light is collected at 90° with respect to the incident light. The emitted light was polarization-selected using a Glan-Taylor prism. The polarization of this light was then scrambled and wavelength selection is carried out using a subtractive double monochromator (CVI Digikrom 112). The collected light was focused on to a cooled two-stage microchannel plate photomultiplier tube (MCP-PMT, Hamamatsu R3809U). The PMT signal was sent to one channel of the quad constant fraction discriminator (CFD Tennelec TC454), where it is processed for input to the time-to-amplitude converter (TAC, Tennelec TC 864). This system can measure lifetimes from several microseconds to the instrument response function of 35 picoseconds FWHM. The experiments were conducted in quartz cuvettes, and the oil-water interface was assembled by depositing an oil-layer over the protein solution. After adsorption had been initiated, the laser beam was carefully focused at the oil-water interface and the collection lens was

adjusted to maximize the collected signal. The excitation beam was at 700nm, while emission was monitored near the emission maximum for FITC (530nm).

3.4.5.1 Data analyses for TIRFM and calibration protocol

Interfacial coverages were computed using Equation (3.9). The prebleach fluorescence was estimated by averaging a few data points before the bleaching pulse. Typically, the interface was bleached with a series of pulses for approximately 5-10 seconds, in order to eliminate fluorescence emission from interfacially-bound molecules. An arithmetic average of the first few points after the completion of bleaching was used to calculate F_{bulk}. Typically, the first point right after the bleach pulse is applied is ignored because this may be influenced by a partial opening of the shutter while the photon counter is sampling data. Each data point consisted of the photon count rate collected for 50 milliseconds. A dwell time of 200 milliseconds was used between each reading. Since the repeated photobleaching of interfacial species may also induce some photobleaching of bulk associated fluorophores outside the evanescent wave area, the longer dwell times provide sufficient time for complete recovery of the bulk fluorescence emission. The background counts were subtracted from both F and F_{bulk} prior to applying Equation (3.9). This subtraction is important, because the background contribution cannot be ignored due to a slight fluorescence emission from the oil.

3.4.5.2 2-pTCSPC lifetime measurements

Fluorescence lifetimes were estimated by fitting the decay to Equations (3.16) and (3.17), using OriginPro 7.5 (OriginLab Corporation, Northampton, MA). The data used for fitting were not normalized against the maximum value (at t=0). Also, no constraints

(such as $\sum_i \alpha_i = 1$) were imposed on the fit. Although normalization and constraints are routinely used in fitting lifetime data, we chose not to implement this because relatively low fluorescence emission intensities (counts) were obtained using 2p-TCSPC for the protein sample. To avoid making a biased estimate of the maximum count at t=0 (there is considerable scatter around this value), the program was allowed to fit all parameters with no imposed constraints.

3.5 Results and Discussion

3.5.1 Adsorption isotherm for BSA-FITC at the oil-water interface

The adsorption isotherm for BSA-FITC at the oil-water interface is shown in Figure 3.4. Experiments were conducted for BSA-FITC bulk concentrations of 0.2, 0.5, 1.0, 2.0 and 3.5 mg/ml. Interfacial coverages obtained were in the range of 0.02 to 0.3 mg/m^2. The values obtained are much improved in comparison to the results of earlier work done in our laboratory[55] primarily due to (i) improved detection equipment, and (ii) the modified bleaching protocol, where longer bleaches were utilized to ensure that all interfacial fluorophores were adequately bleached. However, the values obtained are an order of magnitude lower than typical values that have been reported in the literature for the solid-liquid interface.

There are very few reports in the literature on the adsorption of BSA at the liquid-liquid interface to provide comparative data. Beaglehole et al.[91] studied BSA adsorption to the oleyl alcohol-water interface using ellipsometry. They reported interfacial coverages of 0.45 mg/m^2 for BSA at a bulk concentration of 3.5 mg/ml, with no apparent signs of saturation. In contrast, Sengupta and Damodaran reported much higher

equilibrium saturation values of 4.1 mg/m^2 for BSA at the triolein-water interface using radiolabeling[42]. This value appears abnormally high.

Estimates of adsorbed amounts of BSA at the solid-liquid interface vary, depending on surface properties and the technique used for making the measurements. Hlady and co-workers reported BSA interfacial coverages ranging from 0.4 mg/m^2 to 1.2 mg/m^2 on hydrophilic silica using TIRFM[14]. Malmsten and Lassen reported HSA coverages of 4±2 mg/m^2 on hydrophobic surfaces using ellipsometry[59]. Calonder and co-workers[13] reported interfacial coverages of 1.25 mg/m^2 for HSA on Si-Ti-O_x surfaces using OWLS. Wertz and Santore used TIRFM to study BSA adsorption to HTS-SAMs and obtained interfacial coverages in the range of 1 to 3 mg/m^2 by modeling the initial adsorption rate under transport-limited conditions[12]. Finally, Choi et al.[69] reported interfacial coverages ranging from 0.4 to 1 mg/m^2 for HSA adsorption to HTS SAMs depending on the transport conditions, and the density of the SAMs, using optical reflectometry.

We believe that some of the lower interfacial coverages obtained at the oil-water interface can be attributed to competition between slow arriving molecules and quick relaxation of already adsorbed molecules (because relaxed molecules occupy more area per molecule), and the slow transport of new albumin molecules to the interface. Evaluation of this hypothesis and supporting experiments/arguments are summarized in a later section.

3.5.2 Molecular relaxations and its influence on ultimate coverages at the oil-water interface

The interfacial coverage reported above at the oil-water interface is an order of magnitude lower than typical values reported in the literature, which are on the order of 1 mg/m^2, and points to the fact that the total adsorption at this oil-water interface is limited by other processes. A plausible hypothesis is that the reduced interfacial estimates reflect the competition for interfacial space between adsorbed molecules quickly undergoing interfacial relaxations and protein molecules arriving at the interface. As discussed earlier, proteins are extremely complex entities that contain several hydrophobic and hydrophilic regions. All proteins exist in energetically favorable conformations that minimize the free energy of the system. Upon adsorption, they undergo conformational changes (or re-orientations) to minimize the free energy in the changed environment around them. This can amount to relaxation, by which the molecule undergoes denaturation and typically expands, thus occupying a larger surface area in the process. The rate of this process is significantly influenced by the properties of the surface/interface to which the protein is adsorbing, and the conditions of the experiment.

In these experiments, the flow rate is held constant at 0.047 ml/min. This low flow rate was chosen to minimize the possibility of generating destabilizing forces that can sweep away the oil-film. The wall shear rate is given by

$$\gamma = \frac{6Q}{wh^2} \tag{3.21}$$

where Q is the flow rate and w and h are the width and height of the flow channel.

For the geometry of the flow cell, γ has an approximate value of 0.27 s^{-1}. Thus, transport of proteins to the interface occurs at a very slow rate under these experimental conditions. Figure 3.5 depicts a plausible model for the reduced interfacial coverages. This model is similar to that proposed in Chapter 2, at short adsorption time scales. Initially, the albumin molecules that arrive first at the oil-water interface adsorb and occupy a small area. However, with time, protein unfolding and relaxations cause the adsorbed molecules to occupy a greater surface area per molecule, thereby limiting the space available for adsorption of later arriving molecules. It is conceivable that if this rate of relaxation is high enough in comparison to the rate of transport of protein to the interface, it can result in reduced interfacial coverages.

For example, Wertz and Santore have proposed that albumin can increase its molecular area by a factor of at least five as it undergoes relaxations[12]. Thus the protein molecule expands from an initial molecular area of 25 nm^2/molecule to approximately 140 nm^2/molecule during the relaxation process. In the same paper, the authors have shown that albumin interfacial coverages are influenced by protein concentration and wall shear rate. They further reported that the ultimate coverage is more strongly influenced by molecular relaxations than by a fundamental isotherm shape[12].

The profiles in Figure 3.6 depict BSA-FITC adsorption (0.2 mg/ml) to the oil-water interface at three different flow rates: (i) 0.024 ml/min (γ=0.13 s^{-1}), (ii) 0.048 ml/min (γ=0.27 s^{-1}), and (iii) 0.096 ml/min (γ=0.54 s^{-1}). The profiles indicate a significant increase in albumin interfacial coverage at 0.048 ml/min and 0.096 ml/min, in comparison to the coverage at a flow rate of 0.024 ml/min. An interfacial coverage of

approximately 0.040 mg/m^2 was obtained at flow rates of 0.048 ml/min and 0.096 ml/min. On the other hand, the surface coverage at 0.024 ml/min was 0.016 mg/m^2. There are two possible reasons for the lower coverage at 0.024 ml/min[12].

(i) If the adsorption follows the convective-diffusion model for gentle shearing flow, then the initial adsorption rate is proportional to the third power of the shear rate ($\gamma^{1/3}$). Thus a reduction in the shear rates (or flow rate) will reduce the interfacial coverage. However, it should be noted that, at the above flow rate, the initial adsorption rates probably do not strictly follow the transport-limited adsorption kinetics predicted by the Leveque equation, because of the higher bulk protein concentrations (0.2 mg/ml)[12].

(ii) With reference to the model proposed in Figure 3.5 along with the arguments made in the preceding paragraph, we hypothesize that interfacial relaxation of the adsorbed albumin molecules are primarily responsible for the apparently low interfacial coverage obtained at the lowest flow rate. Due to slowly arriving molecules at this flow rate, the adsorption proceeds very slowly and continues for almost 90 minutes after the first increase in fluorescence is detected. Thus, there is sufficient time for molecules arriving earlier to undergo the molecular relaxations that reduce the interfacial area available for the adsorption of later arriving molecules.

The difference between the interfacial coverage for adsorption at the two flow rates of 0.048 ml/min and 0.096 ml/min are not significant. While this is initially surprising, it should be noted that the oil film in contact with the glass is likely to become

unstable at a flow rate of 0.096 ml/min, and hydrodynamic shear may be sweeping some of the oil and adsorbed proteins from the interface.

It is worthwhile to conduct a modeling exercise to compare the coverage obtained above with that predicted by models for transport-limited adsorption from a solution in fully developed laminar slit flow[56]. The Leveque solution to the convective diffusion equation is given by

$$\frac{d\Gamma}{dt} = 0.538\left(\frac{\gamma}{x}\right)^{1/3} D^{2/3}C \tag{3.22}$$

where Γ is the two-dimensional interfacial concentration and x is the distance along the flow channel.

The Leveque equation only applies when a steady-state concentration near the interface is established at times well before the surface coverage reaches the point where it starts decreasing the adsorption rate. Thus, this equation applies when the adsorption rate does not decrease before a characteristic time given by

$$t_c = \left(\frac{x^2}{\gamma^2 D}\right)^{1/3} \tag{3.23}$$

where t_c is the time required to establish the steady-state concentration profile.

This corresponds to 940 seconds for γ=0.13 s^{-1}, 580 seconds for γ=0.27 s^{-1}, and 360 seconds for γ=0.54 s^{-1}. Assuming no errors in the experimental model, if the experimental adsorption rate is lower than that predicted by Equation (3.22), then the

experimental adsorption rate is considered to be limited by some property of the interface[69,92]. The profiles in Figure 3.6 were analyzed to compare the initial adsorption rates obtained using this model with those predicted by Equation (3.22). Table 3.1 shows these comparisons. The fact that the experimental adsorption rate is orders of magnitude lower than that predicted by the Leveque solution is indicative of surface effects that lower the initial adsorption rate. The parameter *R*, which is the ratio of the initial adsorption rate for any shear rate to that obtained at the shear rate of 0.27 s^{-1} (which we arbitrarily chose as a standard), was also calculated. If it is assumed that there is a calibration error in our protocol that causes underestimation of the surface coverage (due to light scattering artifacts) by a constant factor, the ratio *R* will account for this. When comparing experiments conducted at γ=0.13 s^{-1} with those at γ=0.27 s^{-1}, we obtained a value of R_{12}= 0.17, which is much lower than the corresponding theoretical value of 0.8 predicted by the Leveque solution. This is an indicator that factors other than transport rates are strongly influencing the interfacial coverage. Rapid molecular relaxations that reduce the available interfacial area or lower binding affinities to the surface are possible factors.

The data presented in Figure 3.6 has been re-plotted in Figure 3.7 for the cases of γ=0.13 s^{-1} and γ=0.27 s^{-1}. A closer examination of this data indicates that in each case protein adsorption proceeds linearly until surface crowding causes the profile to deviate from its linear profile. During the initial stages of protein adsorption, the only limiting factor controlling protein adsorption is the rate of protein transport to the interface. However, in later stages, interfacial crowding causes the amount of available space to limit the adsorption kinetics. The departure of the adsorption behavior from the linear

profile as predicted by Equation (3.22) due to crowding effects is further complicated by protein relaxations, which serves to enhance this effect. Thus, in Figure 3.7 the departure of the adsorption profile from the solid line occurs at 0.027 mg/m^2 and 0.014 mg/m^2 for γ=0.27 s^{-1} and γ=0.13 s^{-1} respectively. In the absence of protein relaxations, these departures would occur at the same interfacial level. The occurrence of these departures at different levels for shear-rates that differ by a magnitude of 2, is further confirmation of the presence of protein relaxations that effectively lower pseudo-saturation coverage.

3.5.3 Relaxations at the OTS-water interface

Preliminary investigations of albumin molecular relaxations at the OTS-water interface have been initiated, by using the TIRF-FRAP calibration protocol for quantifying interfacial coverage. Wertz and Santore have conducted detailed investigations of the influence of albumin molecular relaxations on ultimate coverages at the hexadecyltrichlorosilane (HTS) SAMs by modeling the adsorption process as transport-limited[12,56]. In their studies, they used shear rates ranging from 1.1 s^{-1} to 42 s^{-1}. A limited number of experiments at the OTS-water interface were run to compare the influence of shear rate on molecular relaxations at the solid-liquid interface and the oil-water interface. Figure 3.8 shows results of adsorption of BSA-FITC at a bulk concentration of 0.2 mg/ml to the OTS-water interface. The OTS SAM interface is hydrophobic. These studies were conducted at flow rates of 0.47 ml/min (γ=2.7 s^{-1}) (Figure 3.8, upper curve) and 0.047 ml/min (γ=0.27 s^{-1}) (Figure 3.8, lower curve). Interfacial coverages computed using the TIRF-FRAP protocol was approximately 0.25 mg/m^2 and 0.13 mg/m^2 at shear rates of 2.7 s^{-1} and 0.27 s^{-1}, respectively. Choi et al

reported similar HSA coverage at the HTS-water interface at shear rates of 1.1 s^{-1} [69]. The following observations were made:

(i) The BSA-FITC interfacial coverage at the OTS SAM is 4-5 times higher than the corresponding coverage for BSA-FITC at the oil-water interface at the same bulk concentration (0.2 mg/ml) and shear rate (0.27 s^{-1}).

(ii) While on the same order of magnitude, the ultimate coverage obtained is lower than the coverage reported by Zimmerman et al. for the same concentration, using the TIRF-FRAP technique (> 1mg/m^2).

(iii) Molecular relaxations do appear to influence BSA-FITC adsorption at the hydrophobic solid-liquid interface for the two shear rates chosen, even at the relatively high bulk concentration of 0.2 mg/ml. Wertz and Santore reported similar results at the HTS-water interface for a much lower bulk concentration of 0.01 mg/ml[12].

From the observations above, it is apparent that the interfacial coverage at this particular oil-water interface is much lower than that obtained at the OTS-water interface. Also, since molecular relaxations appear to reduce the interfacial coverage from 0.25 mg/m^2 (γ=2.7 s^{-1}) to 0.13 mg/m^2 (γ=0.27 s^{-1}) at the solid-liquid interface, it is certainly plausible that the relaxations could occur at a greater rate at the relatively more mobile oil-water interface, where the interconnecting segments of the protein are much freer to move, thereby reducing the coverage at the liquid-liquid interface. The slow transport rate to the interface possibly exacerbates the situation. Finally, the reason for the discrepancy between these results and those obtained by Zimmerman and co-workers is unclear.

However it should be noted that an exhaustive study at varying concentrations and shear-rates at the OTS-water interface have not been conducted. This is the focus of ongoing work in our laboratory. Therefore, the results at the solid-liquid interface are only preliminary.

3.5.4 Sequential adsorption experiments

In order to examine the influence of molecular relaxations of pre-adsorbed protein molecules on subsequent protein adsorption, sequential protein adsorption studies were conducted. In these experiments, adsorption of 0.2 mg/ml BSA-FITC was initiated and after 60 minutes of adsorption, the ultimate interfacial coverage was estimated by utilizing the calibration protocol. Subsequently, BSA-FITC at a concentration of 0.5 mg/ml (step 2) was introduced and the coverage upon 60 minutes of adsorption was estimated. This was then followed by the introduction of BSA-FITC at a concentration of 1 mg/ml (step 3).

In sequential adsorption experiments, molecular relaxations of the existing layer can affect the adsorption of proteins that are introduced later. This can happen in two principal ways: (i) Molecular relaxations of existing protein molecules result in reduction of the available space for later arriving molecules to adsorb and (ii) These relaxations change the structure of the adsorbate film, thus potentially influencing the interactions of later arriving molecules with the existing layer. Thus, it is expected that such sequential adsorption experiments will result in lower amounts of protein adsorption occurring in steps 2 and 3 as compared to single shot experiments, where initial protein adsorption is occurring at a bare oil-water interface. However Figure 3.9, shows little difference

between the coverages obtained in the sequential adsorption experiments and those obtained in the single-shot experiments shown in Figure 3.4. This is a surprising result, and suggests that transport rates have a more dominating influence on protein adsorption at the oil-water interface.

3.5.5 Fluorescence Lifetime measurements

Fluorescence decay curves obtained using 2p-TCSPC were fit to Equations (3.16) and (3.17). The results are summarized in Table 3.2 and Table 3.3. A typical fluorescence decay curve is shown in Figure 3.10. In all cases, the two-parameter exponential model provided a better fit than the single-exponential model as confirmed with hypothesis testing using the F-test statistic. The single-exponential model also provided a reasonably good fit. For the purpose of discussion, we have chosen to use the parameters obtained from the single-exponential model to facilitate easy comparison. Figure 3.11 and Figure 3.12 depict the profiles of the fluorescence decay and the fit to the single exponential model.

The lifetime of the interfacially bound molecules was approximately 3.37 ns, while the lifetimes of the proteins present in the bulk solution was approximately 3.31 ns. Since there is no significant difference in the two lifetimes, we conclude that the quantum yield of BSA-FITC immobilized at the interface is unchanged from its value in solution, thus justifying the simplifying assumption made during the development of the TIRFM-FRAP model. The similarity in fluorescence lifetimes indicates that the emission characteristics of the fluorophore are not influenced by the mobile interface.

The similarity in lifetimes also indicates that the dye molecules adsorbed to the interface are free of concentration quenching effects which would lower the quantum yield. In solution, Lakowicz et al[93] has reported mean decay times of 3.12 ns for HSA-FITC conjugated at a labeling ratio of 1. In the same study the authors reported a mean decay lifetime of 1.84 ns for HSA-FITC adsorbed to quartz surfaces. Since HSA is known to form a complete monolayer on glass, we speculate that the rigid interfacial properties are responsible for the decreased lifetimes.

Fluorescence decay curves were also measured for unbound FITC dissolved in phosphate buffer. The profiles and the single-exponential fit are shown in Figure 3.13, and the fitted parameters are given in Table 3.2 and Table 3.3. The fluorescence lifetime calculated was approximately 4.96 ns. The lifetime values obtained compare reasonably with typical values in the literature[78].

3.5.6 Other sources of error

The protocol utilized in this study is an excellent method of internally calibrating adsorbed amounts. While care has been taken to minimize all experimental errors, there are some sources of measurement errors that can cause influence the interfacial estimates. These are discussed below.

3.5.6.1 Possibility of incomplete bleaching of interfacial fluorophores

Bleaching experiments were conducted using a beam intensity of 15 mW. At this intensity, it takes 2-5 seconds of pulses to bleach the interface until no further recovery is apparent from the interface. It was observed that longer durations are required to bleach fluorophores at the oil-water interface than at the solid-liquid interface. Longer bleach

durations are generally not advisable, because this can result in unintended photobleaching of bulk fluorophores in a zone wider than the evanescent wave profile. The interfacial coverage calculated by Equation (3.9) is especially sensitive to the value of F_{bulk}. Thus, small reductions in F_{bulk} (due to over-bleaching) to near the background level can translate to large changes in the computed interfacial coverage.

Several experiments were conducted in an attempt to check for incomplete bleaching of fluorophores by conducting buffer wash-out experiments. In these experiments, the background fluorescence at the start of the experiment was noted. After the adsorption and photobleaching steps were completed, a buffer wash (with protein free buffer) was conducted to remove any fluorescently labeled proteins present in the bulk solution. In theory, if all the interfacial fluorophores have been bleached, the signal after the wash should return to the background signal. In these experiments, some residual fluorescence was found after the buffer wash. However, given the restriction on low flow rates in the experiment, a thorough wash to remove all fluorophores would take in excess of 240 minutes. Thus, we cannot rule out the possibility that this residual fluorescence is due to incomplete washout of the protein solution.

3.5.6.2 Elevation of the bulk-signal contribution by light scattering:

As discussed above, the background fluorescence which is the number of counts estimated at the bare oil-water interface prior to the start of the experiment, is subtracted from all fluorescence measurements. This background fluorescence is due to emission from the oil layer, which is slightly fluorescent. Due to considerable scattering of light at the oil-water interface, the background fluorescence can increase as (i) fluorophores fill the flow-cell, and (ii) as the protein film evolves at the interface. If this scattering is

significant, it artificially elevates the F_{bulk} signal by additionally exciting the labeled fluorophores outside the evanescent field. This can result in significant underestimation of the interfacial coverage. Consider, for example, the following analysis of the counts of fluorescence obtained in experiments conducted at the oil-water interface and at the solid-liquid interface.

In a typical experiment at the oil-water interface that was conducted using BSA-FITC at a bulk concentration of 1 mg/ml, 3595 counts per sample time were obtained prior to photobleaching (F). The number of counts obtained after photobleaching was 2135 (F_{bulk}). Prior to the start of the experiment, 1070 background counts per sample time were recorded. Thus, in theory, the fluorescence from the bulk due to evanescent wave excitation is presumed to be 1065 counts for this experiment, while the total background corrected fluorescence prior to bleaching is 2525 counts. The ratio F/F_{bulk} is calculated to be 2.37. However if the bulk fluorescence has a significant component arising from scattered light, it is clear that this can make a significant difference to computation of F/F_{bulk}. At a bulk concentration of 1mg/ml, the bulk solution is very fluorescent, even at a labeling ratio of 1.0, and it is likely that extraneous scatter from the oil-water interface is artificially elevating the bulk contribution by a significant amount. Thus, it is not inconceivable for computed interfacial coverage to double in the absence of significant scattering.

Similarly, in an experiment conducted at the OTS-water interface, for an albumin bulk concentration of 0.2 mg/ml, F was 5860 counts, F_{bulk} was 846 counts and $F_{background}$ was estimated to be 472. Thus, the background corrected bulk fluorescence is 373 counts and F/F_{bulk} is computed to be 14. If scattering effects are elevating the bulk fluorescence

count and the evanescent wave accounts for only half of the 373 counts, this ratio doubles to 28. Hlady and coworkers[14] used TIRFM to quantify protein adsorption, and used external calibrations to show that that scattering effects can cause a significant (up to a 6-fold) under-prediction of interfacial coverage.

It is our opinion that some of the protein coverages reported in the literature are excessively high. As a simple modeling exercise, one can consider a surface that has an interfacial coverage of 3 mg/m^2 (a value that has been reported in the literature) for a bulk concentration of 0.2 mg/ml. Based on Equation (3.9), the ratio F/F_{bulk} required to obtain a surface coverage of 3 mg/m^2 at a bulk concentration of 0.2 mg/ml is approximately 195. In other words, assuming a background-corrected total fluorescence count of 5380 counts, this ratio gives us a value of F_{bulk} of 27 counts, a value which is lower than the average noise in the system. It is thus very unlikely that the background counts could be as low as shown above.

Deviation in q_s/q_b from unity: Although it has been clearly demonstrated that the lifetime of the surface and bulk-associated fluorophores are similar, assuming that the quantum yields are also similar requires the reasonable assumption that the radiative rates are essentially unchanged. However any changes in the radiative rate k_r which offsets changes in the non-radiative decay rate could keep the lifetime constant, while reducing or increasing the quantum yield. Changes in k_r have been reported in the literature for fluorophores in the proximity of metal surfaces[82] and for fluorophores in different solvents[78].

3.6 Conclusions

Protein interfacial coverages at the oil-water interface have been estimated using TIRFM-FRAP. Values obtained at the interface ranged from 0.02 mg/m^2 to 0.3 mg/m^2. These values are a significant improvement over those reported previously from our laboratory, primarily due to improved protocols and more sophisticated detection equipment[55]. We propose that adsorbed molecules undergo relaxations that reduce the available area where molecules arriving later can adsorb, thereby restricting the interfacial coverage density. The interfacial coverages at the oil-water interface in this study are lower, in comparison to the coverage obtained by us at the same bulk concentration and shear rate at a hydrophobic solid-liquid interface. The values obtained for the hydrophobic solid-liquid interface using the TIRFM-FRAP methodology is consistent with values reported in the literature. Several scenarios have been presented to account for the differences between the results for the two interfaces. 2p-TCSPC studies indicate that the lifetime of adsorbed BSA-FITC molecules at the oil-water interface is similar to the corresponding value in solution, indicating that the quantum yields are not very different.

3.7 Recommendations for future work

It would be interesting to study the influence of objective working distance and depth of focus on the computed interfacial coverages, since objectives with higher numerical apertures will offer a shorter depth of focus, which will more accurately reject stray light contributions to the overall signal[55]. An alternative method would be to use variable angle of incidence TIRFM (VA-TIRFM), in which the penetration depth of the

evanescent wave is varied by controlling the angle of incidence. This method will allow us to obtain an estimate of scattering effects at the liquid-liquid interface. Finally, similar measurements at other oil-water interfaces, such as the perfluorocarbon-water interface (a biologically relevant interface), will help assess the validity of this method.

The use of 2-photon spectroscopy to study lifetimes of fluorescently conjugated biomolecules at the oil-water interface is among the first of its kind in the literature. It would be interesting to supplement the lifetime data with measurement of rotational diffusion and reorientation dynamics of molecules that are adsorbed at the oil-water interface. Such studies will also provide us with information about dye and protein partitioning at the oil-water interface. Additionally, probing the adsorbed layer using the intrinsic fluorescence of the protein (say, tryptophan) will allows us to examine the protein in its unaltered state. At the same time, this will make it possible to obtain information about reorientation dynamics of the adsorbed protein in presence of an extrinsic fluorophore and compare it against measurements obtained using the intrinsic fluorescence[94].

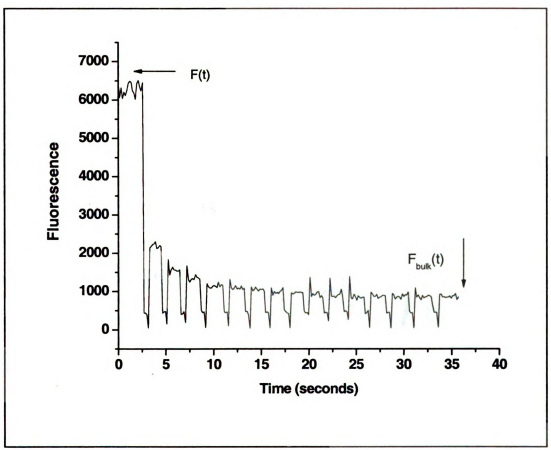

Figure 3.1: A typical photobleaching experiment for calibrating interfacial coverages. *F(t)* represents the total fluorescence prior to bleaching. F_{bulk} *(t)* is the total fluorescence measured after bleaching is terminated.

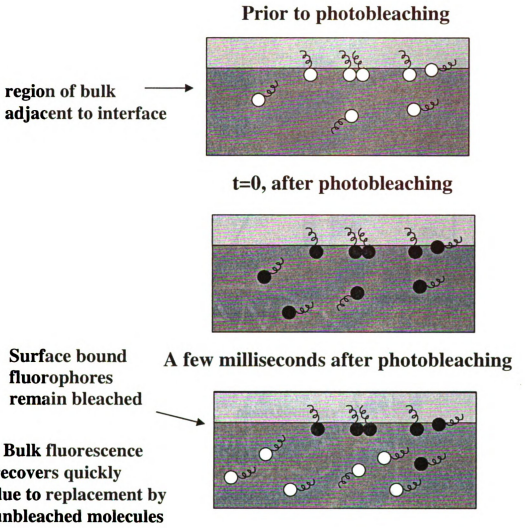

Figure 3.2: Schematic showing the photobleaching steps involved in the calibration protocol. The black circles represent bleached fluorophores while the white circles represent unbleached fluorophores. Due to the high diffusion coefficient of the bulk associated fluorophores, the bleached fluorophores in the bulk are rapidly replaced by unbleached fluorophores thereby resulting in an "unbleachable bulk fraction", while the surface bound fluorophores remain bleached.

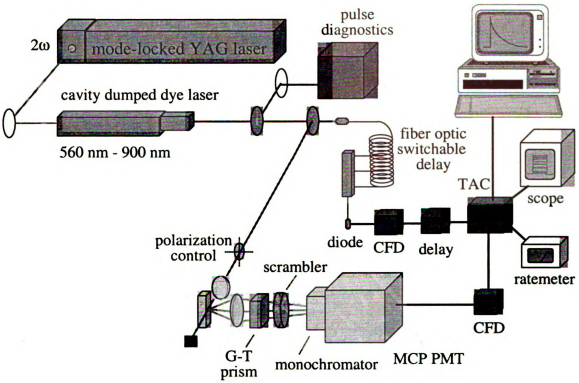

Figure 3.3: Experimental layout for 2-photon time correlated single photon counting. G-T: Glan-Taylor prism; MCP-PMT: microchannel-plate photomultiplier tube; CFD: constant fraction discriminator; TAC: Time to amplitude converter

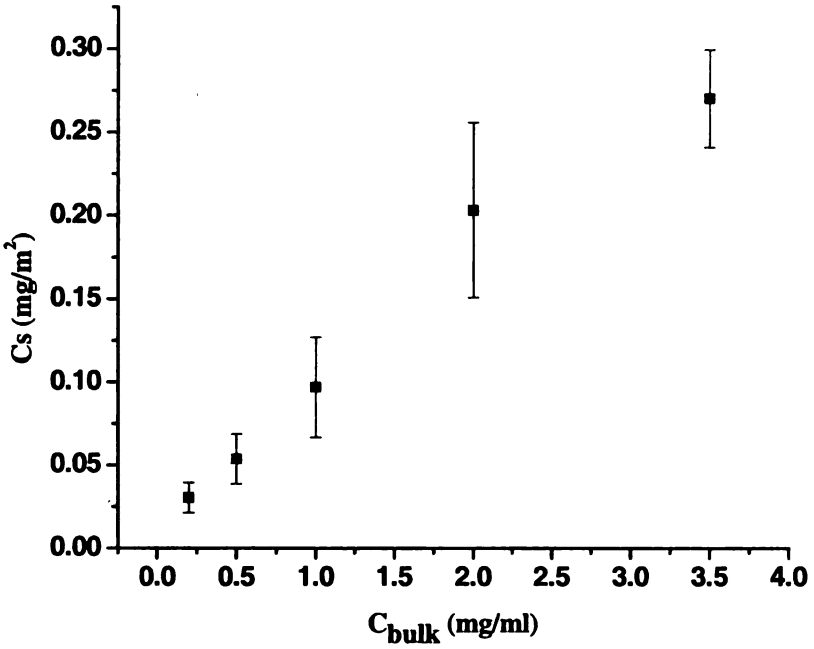

Figure 3.4: Adsorption isotherm of BSA-FITC at the oil-water interface using TIRFM-FRAP protocol.

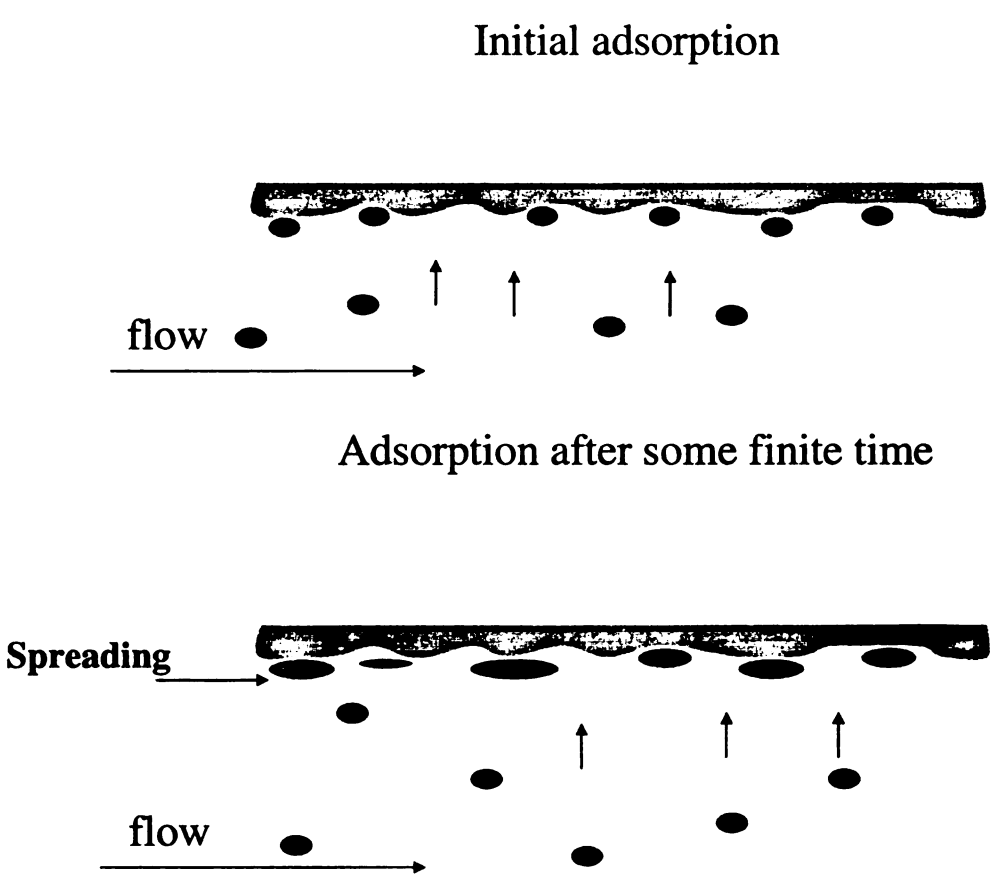

Figure 3.5: Proposed model of interfacial relaxations for albumin at an oil-water interface. Molecules that arrive early, occupy a small area per molecule. However with time, they spread and occupy larger areas, thereby restricting available area for molecules that arrive much later, due to slow transport rates.

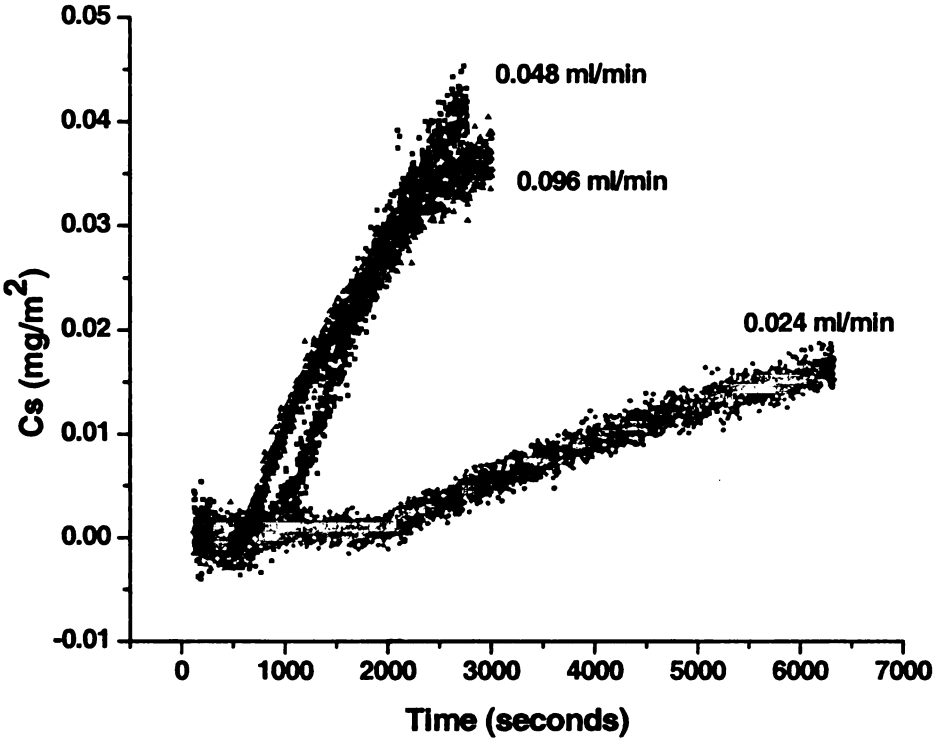

Figure 3.6: Adsorption of BSA-FITC (0.2 mg/ml) at the oil-water interface as a function of flow rate. Three flow rates were used in this experiment: (1) 0.024 ml/min (γ=0.13 s^{-1}); 0.048 ml/min (γ=0.27 s^{-1}) and (3) 0.096 ml/min (γ=0.54 s^{-1}) At a flow rate of 0.024 ml/min, considerably less protein adsorbs to the oil-water interface presumably due to molecular relaxations of adsorbed protein that reduce the available interfacial area.

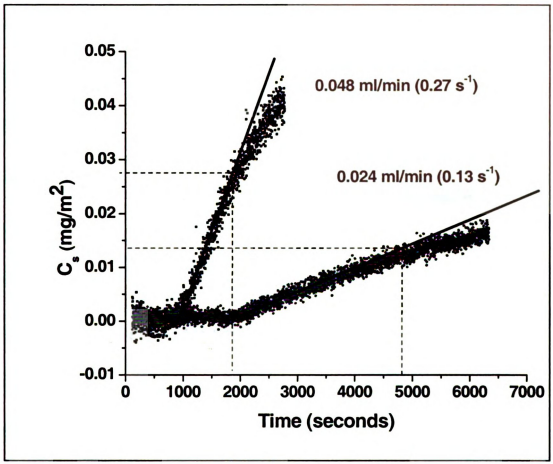

Figure 3.7: Influence of molecular relaxations on the adsorption of BSA-FITC (0.2 mg/ml) to the oil-water interface:. The data shown above has been re-plotted from Figure 3.6 for γ=0.27 s^{-1} and γ=0.13 s^{-1}. The departure of the adsorption profile from the straight line, at different interfacial levels for different transport conditions suggests the presence of relaxations.

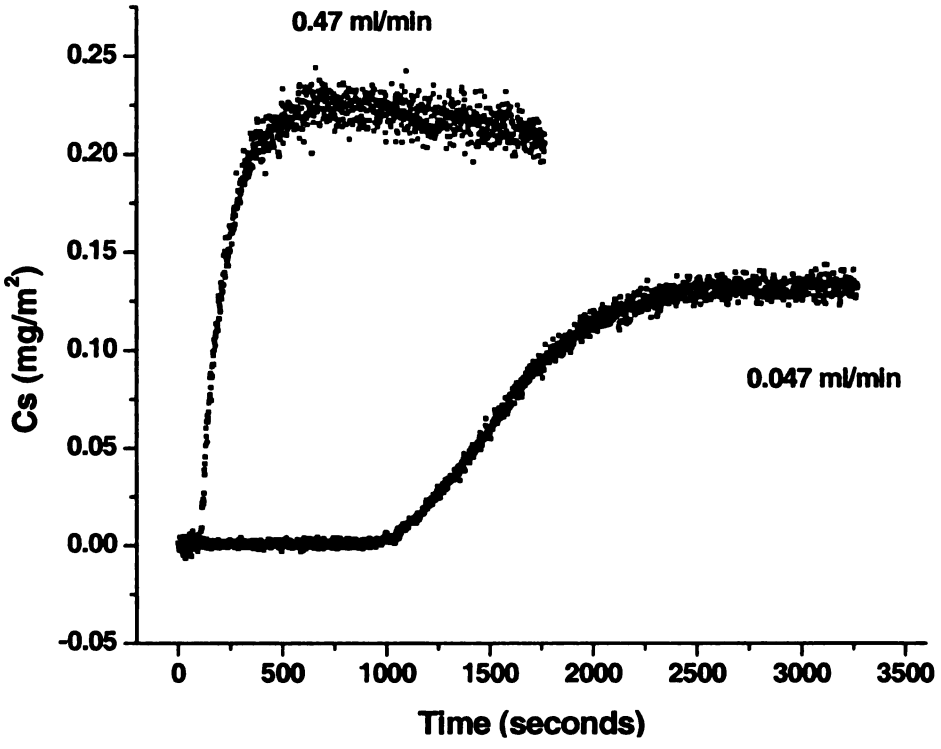

Figure 3.8: Adsorption of BSA-FITC (0.2mg/ml) to octadecyltrichlorosilane self assembled monolayers at flow rates of 0.47 ml/min (γ=2.7 s^{-1}, top curve) and 0.047 ml/min (γ=0.27 s^{-1}, bottom curve).

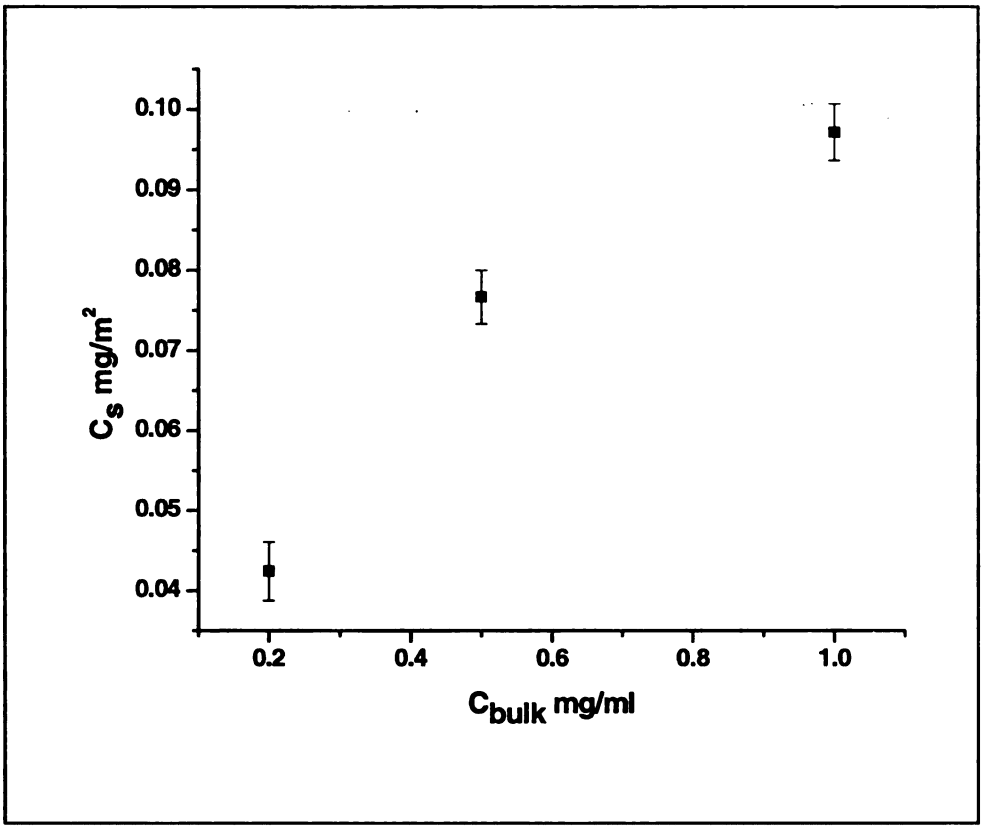

Figure 3.9: Sequential adsorption experiments at the oil-water interface: BSA-FITC at a concentration of 0.2, 0.5 and 1 mg/ml was sequentially introduced into the flow-cell and in each case, interfacial coverages were computed using the calibration protocol.

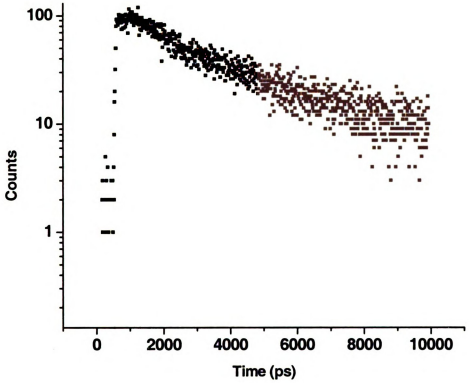

Figure 3.10: Typical fluorescence decay profiles obtained for BSA-FITC adsorbing to the oil-water interface at a concentration of 1 mg/ml using 2-photon TCSPC.

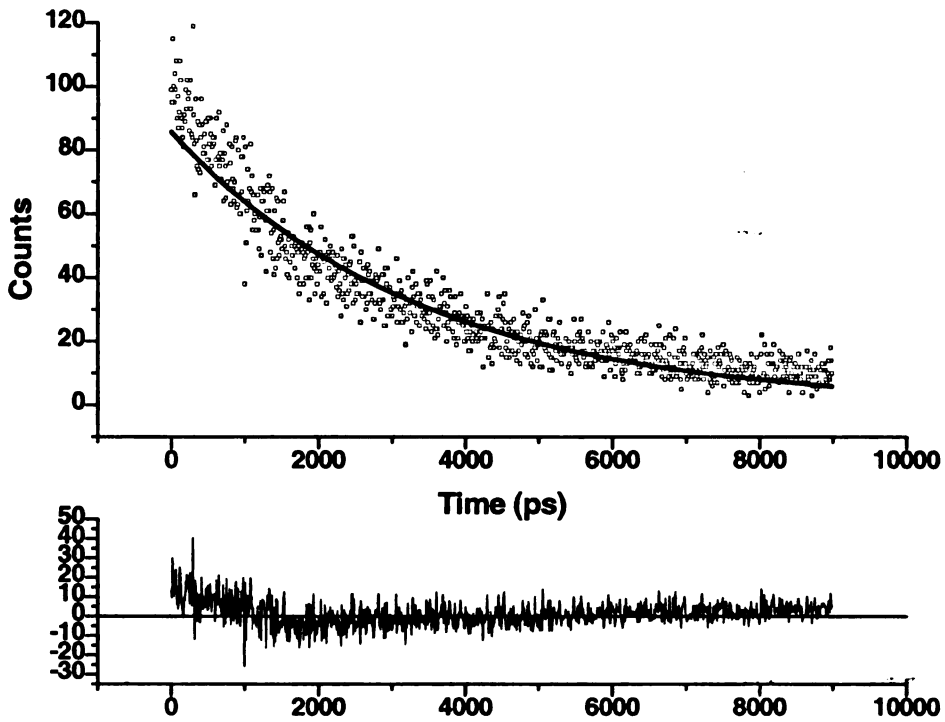

Figure 3.11: Single exponential fit to fluorescence decay profile for BSA-FITC (1 mg/ml) adsorbed at the oil-water interface.

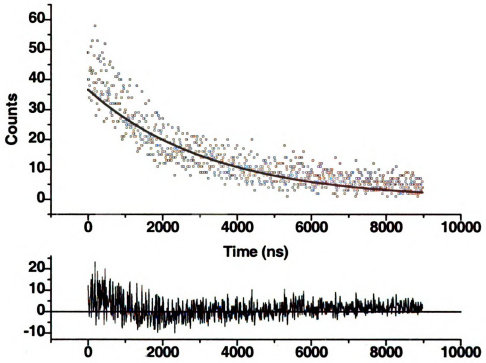

Figure 3.12: Single exponential fit to fluorescence decay profiles for BSA-FITC (1mg/ml) in phosphate buffer.

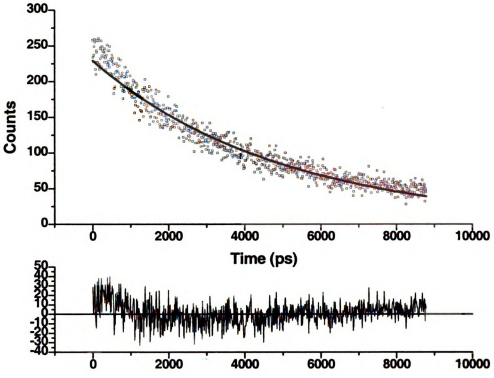

Figure 3.13: Single exponential fit to decay profiles of unbound FITC (0.15mg/ml) in phosphate buffer.

Table 3.1: Comparison of initial adsorption rates obtained using the photobleaching model with that predicted by the Leveque equation.

i	Shear rate γ (s^{-1})	t_c (s)	Initial adsorption rate $\frac{d\Gamma}{dt}$ (mg m^{-2} s^{-1})		$R=\frac{(d\Gamma/dt)_i}{(d\Gamma/dt)_2}$	
			photoblea-ching	Leveque	photobleac--hing	Leveque
1	0.13	940	4.65e-6	0.026	0.17	0.8
2	0.27	580	2.67e-5	0.032	1	1
3	0.54	360	2.74e-5	0.041	1.03	1.28

Table 3.2: Results of fitting of the fluorescence decay to the single exponential model given by Equation (3.16).

Molecule	Location	**No.**	α_1	τ_1 (ns)	χ^2_{red}
BSA-FITC **adsorbed from 1 mg/ml solution**	Oil-water Interface	1	85.73	3.38	1.34
		2	57.18	3.36	1.26
BSA-FITC **1 mg/ml**	Bulk solution (buffer)	1	34.86	3.36	1.26
		2	36.69	3.27	1.29
FITC **0.15 mg/ml**	Bulk solution (buffer)	1	229.13	4.96	1.22

Table 3.3: Results of fitting of fluorescence decay to multi-exponential model given by Equation (3.17).

Molecule	Location	No.	α_1	α_2	τ_1(ns)	τ_2 (ns)	χ^2_{red}
BSA-FITC adsorbed from 1 mg/ml solution	**Oil-water Interface**	1	53.81	47.8	1.35	4.98	1.11
		2	40.7	28.32	1.38	5.45	1.05
BSA-FITC 1 mg/ml	**Bulk solution (buffer)**	1	36.26	4.37	2.11	38.03	1.115
		2	30.04	14.28	36.69	1.51	6.29
FITC 0.2 mg/ml	**Bulk solution (buffer)**	1	130.7	119.42	2.31	8.40	0.98

4 3-D ARRAYS OF LIPID BILAYERS ON POLYELECTROLYTES MULTILAYERS

4.1 ABSTRACT

This paper presents novel and robust methods to produce 3-D arrays of lipid bilayers on polyelectrolyte multilayer surfaces. Such arrays may be useful for high-throughput screening of compounds that interact with cell membranes, and for applications in biosensors and biocatalysis. Liposomes composed of 1,2-Dioleoyl-sn-Glycero-3-Phosphocholine (DOPC) and 1,2-Dioleoyl-sn-Glycero-3-Phosphate (Monosodium Salt) (DOPA) were found to adsorb preferentially on poly(dimethyldiallylammonium chloride) (PDAC) and poly(allylamine hydrochloride) (PAH). Liposome adsorption on sulfonated poly(styrene) (SPS) surfaces was minimal due to electrostatic repulsion between the negatively charged liposomes and the SPS coated surface. Surfaces coated with poly(ethylene glycol) (m-dPEG acid) also resisted liposome adsorption. These results allowed us to create arrays of lipid bilayers by exposing PDAC, PAH and m-dPEG patterned substrates to DOPA/DOPC vesicles of various compositions. The patterned substrates were created by stamping PDAC/PAH on SPS multilayers and m-dPEG acid on PDAC multilayers, respectively. Total internal reflection fluorescence microscopy (TIRFM), fluorescence recovery after pattern photobleaching (FRAPP) and fluorescence microscopy were used to characterize the resulting interfaces and to check the feasibility of the desired approach.

4.2 Introduction

Cell membranes are complex moieties composed of lipids, with membrane proteins and other biomacromolecules interposed between them. They represent one of the major structural components of biological cells. Systems that can mimic biological cell membranes and their functionality have great potential for applications such as biosensors and can also provide a platform for fundamental investigations of biomolecular behavior[95-99]. To mimic biological cell membranes, supported bilayer lipid membranes (sBLMs) have been formed on glass, silica surfaces and unfunctionalized metal surfaces[95-113]. Such BLMs enabled researchers to probe lipid properties such as phase transition, lateral diffusion, permeation and lipid protein interactions [114]. However, there were some limitations associated with these supported membranes: (1) there was no cushion between the substrate and the lipid bilayer to provide space for the hydrophilic moieties of the membrane proteins and to give lateral mobility to the membrane components, (2) they were fragile, and (3) no ionic reservoirs were present on either side of the bilayer, a typical characteristic of cell membranes.

To overcome these drawbacks and allow transmembrane molecular transport, the use of hydrophilic cushions (on which lipid bilayers are deposited) is becoming popular. Such cushions have consisted of hydrogels, polymeric tethers or polymer films and polyelectrolytes[22,115-130]. Polyelectrolytes offer the following advantages as cushions[122,131-133]: (1) they are robust and easy to fabricate, (2) they can be deposited on many surfaces, (3) they can provide a reservoir for electron mediators and cofactors for sensor applications and (4) their porosity and flexibility may allow the protein to exist in its natural conformation inside the lipid bilayer. Lipid bilayers composed of negatively

charged lipids like 1,2-Dioleoyl-*sn*-Glycero-3-Phosphate (Monosodium Salt) (DOPA) and 1,2-Dimyristoyl-*sn*-Glycero-3-[Phospho-*rac*-(1-glycerol)] (Sodium Salt) (DMPG) with other zwitterionic lipids have already been shown to form on poly(allylamine hydrochloride) (PAH) and poly(ethyleneimine) (PEI) coated substrates. These studies[122] indicate that lipid coverages increase and diffusion coefficients decrease on increasing the quantity of charged lipids. In another approach, polyelectrolyte multilayers were adsorbed on melamine formaldehyde latex particles, which were soluble at low pH, resulting in the formation of thin polyelectrolyte shells upon dissolving the core. Lipid bilayers were then formed on the empty shells by exposing them to charged vesicles and the properties of this new model system as an artificial cell were then evaluated[134].

Arrays of lipid bilayers have also been fabricated and characterized on glass surfaces[128,135-138]. A patterned polydimethyl siloxane (PDMS) stamp was brought into contact with a supported lipid bilayer formed on a glass slide for a short time and then removed. Approximately 90% of the lipids in areas in contact with the stamp were transferred to the stamp surface, resulting in an array of patches of lipid bilayers separated from one another by regions of bare glass. The same group showed that a bilayer can be preassembled directly onto oxidized PDMS surfaces and then transferred intact onto a glass slide. Bilayer patches in the resulting arrays were found to be fully fluid and stable under water. To date, this methodology can only be applied to glass surfaces. Thus, techniques that can extend the approach to other surfaces and address the previously described limitations of sBLMs are of interest.

The approach described in this chapter, is based on the ionic layer by layer assembly technique introduced by Decher[139], microcontact printing by Whitesides[140] and

the polymer-on-polymer stamping process (POPS) developed by Hammond[141,142]. Layer by layer assembly can be used to deposit polyelectrolyte multilayers (PEMs) on most substrates. PEMs are thin films[139] formed by electrostatic interactions between oppositely charged polyelectrolyte species to create alternating layers of sequentially adsorbed ions. PEMs are effective and economical approaches to depositing ultrathin organized films whose uses have included functional polymers[143], colloids[144,145], biomaterials[146] and selective electroless metal deposition[147]. Microcontact printing (μCP) is a soft lithographic technique used in physics, chemistry, materials science and biology to transfer patterned thin organic films to surfaces with sub-micron resolution. Unlike other fabrication methods that merely provide topographic contrast between the feature and the background, μCP also allows chemical contrast to be achieved via selection of an appropriate ink. Microcontact printing offers advantages over conventional photolithographic techniques because it is simple to perform and is not diffraction-limited. This technique has been used to make patterns of various small and large molecules on metals and silicon substrates[148-150] as well as to deposit proteins, biological cells[151-153] and polyelectrolyte aggregates.[154] Polymer on polymer stamping is an approach that combines LBL assembly technique and microcontact printing to generate alternating regions of different chemical functionalities on a surface by using graft polymers, diblock copolymers or polyelectrolytes as ink.[141,142]

In this chapter, we present a new approach for generating arrays of 3-D lipid bilayers and liposomes on polyelectrolytes. The height of these arrays can be precisely controlled depending on the number of polyelectrolyte layers used to form the PEMs. The arrays offer potential advantages over previous approaches and provide solutions to some

of the limitations discussed earlier. They also have excellent potential as biomimetic interfaces for high-throughput screening of compounds that interact with cell membranes, and for probing, and possibly controlling interactions between living cells and synthetic membranes. Arrays of lipid bilayers were created by exposing poly(dimethyldiallylammonium chloride) PDAC patterns, polyethylene glycol (m-dPEG acid) patterns and poly(allylamine hydrochloride) (PAH) patterns on PEMs to liposomes of various compositions. Total internal reflection fluorescence microscopy (TIRFM) was used to monitor liposome adsorption and desorption to the PEMs. Fluorescence recovery after pattern photobleaching (FRAPP) and fluorescence microscopy were used to characterize the resulting interfaces. The fabrication of the 3-D array patterns and quartz crystal microbalance studies was conducted by Neeraj Kohli while TIRFM adsorption studies and FRAPP characterization studies were conducted by the author of this dissertation. All results obtained are reported for completeness.

4.3 Experimental section

4.3.1 Materials

Sulfonated poly(styrene) (SPS) (M_w~70,000), poly(allylamine hydrochloride) (PAH) (M_w~50,000) and poly(diallyldimethyl ammonium chloride) (PDAC) (M_w~100,000) were obtained from Sigma. 1,2-Dioleoyl-*sn*-Glycero-3-Phosphate (Monosodium Salt) (DOPA), 1,2-Dioleoyl-*sn*-Glycero-3-Phosphocholine (DOPC) and 1-Palmitoyl-2-[6-[(7-nitro-2-1,3-benzoxadiazol-4-yl)amino]hexanoyl]-*sn*-Glycero-3-Phosphocholine(16:0-06:0 NBD PC) were purchased from Avanti Polar Lipids. 1-tetradecanethiol, 4-(2-hydroxyethyl)piperazine-1-ethanesulfonic acid sodium salt

(HEPES) was obtained from Fluka. The m-dPEG molecule was purchased from Quanta Biodesign. Sylgard 184 silicone elastomer kit (Essex Brownell) was used to prepare the PDMS stamps used for microcontact printing. Structures of PDAC, SPS and m-dPEG are shown in Figure 4.1. The fluorosilanes were purchased from Aldrich Chemical. Ultrapure water (18.2MΩ) was supplied by a Nanopure-UV four-stage purifier (Barnstead International); the purifier was equipped with a UV source and a final 0.2 μm filter.

4.3.2 Preparation of stamps:

An elastomeric stamp was made by curing poly(dimethylsiloxane) (PDMS) on a microfabricated silicon master, which acts as a mold, to allow the surface topology of the stamp to form a negative replica of the master. The poly(dimethylsiloxane) (PDMS) stamps were made by pouring a 10:1 solution of elastomer and initiator over a prepared silicon master. The silicon master was pretreated with fluorosilanes to facilitate the removal of the PDMS stamps from the silicon masters. The mixture was allowed to cure overnight at 60 °C. The masters were prepared in the Microsystems Technology Lab at MIT and consisted of features (parallel lines and circles) from 1 to 10 μm.

4.3.3 Preparation of liposomes:

Small unilamellar vesicles were prepared by mixing appropriate amounts of DOPC/DOPA with 1% NBD-PC in chloroform. This mixture was then dried under nitrogen and care was taken to ensure that the lipids form a thin cake like film on the walls of the test tube. The residual chloroform was then removed under high vacuum. The lipids were then reconstituted in either HEPES, pH 7.4 (0.1M NaCl) or 18.2 MΩ water. The resulting liposome solution was then sonicated until they became clear inside

an ice bath using a Bransonic tip sonicator or bath sonicator. In some of the initial experiments, vesicles were made by extruding the reconstituted lipids through a mini-extruder.

4.3.4 Preparation of arrays:

Figure 4.2 and Figure 4.3 show two different schemes used to prepare arrays of lipid bilayers. **Scheme 1:** (Figure 4.2) A PDMS stamp was dipped in a 250mM solution of PDAC (or 200mM solution of PAH) in 75/25 ethanol-water mixture for about 20 minutes. The stamp was then washed with ethanol, dried under nitrogen and brought into contact with a glass slide that was coated with PDAC/SPS multilayers, with SPS forming the uppermost layer. The stamp was removed after 15 min and the resulting PDAC (or PAH) patterns were then rinsed with water to remove unbound or loosely bound PDAC. The slide was then exposed to DOPC/DOPA liposomes of varying compositions, and imaged using a microscope with attached camera.

Scheme 2: (Figure 4.3) A PDMS stamp was dipped in a 100μM solution of m-dPEG acid in 75/25 ethanol-water mixture for 30 minutes.[155] The stamp was then washed, dried under nitrogen and brought into contact with the glass slide coated with PDAC/SPS multilayers with PDAC as the topmost layer. The stamp was removed after 20 minutes and the resulting PEG patterns were then rinsed with water to remove excess PEG.

All TIRFM and FRAPP characterizations were done on non-patterned slides (i.e. slides having a uniform top layer).

4.3.5 Total internal reflection microscopy:

The experimental setup and the flow cell has been described previously[5] as well as in chapter 2 (Figure 2.1) . All fluorescence measurements were made using the photon counter. As in the case of experiments described in Chapter 2 and 3, the optical chopper was used to prevent unintended photobleaching of fluorophores during all adsorption experiments. The only modification to the experimental procedure described in Chapter 2, was that the data was sampled continuously, rather than intermittently, since we did not observe significant photobleaching by the monitoring beam at the incident laser intensities chosen for these experiments. A 500 nm long-pass band filter was used to separate the excitation and emission intensities. The photon counter was triggered by an output reference voltage from the chopper, so that data collection only occurs during periods when the flow cell is illuminated by the laser beam. For TIRFM experiments, the flow cell was initially filled with buffer. Subsequently, liposome solution was introduced into the flow cell at a controlled flow rate for 10-12 minutes. The infusion was then halted and adsorption was allowed to continue for 1 hour, followed by a buffer wash (for desorption or TIRF-FRAP experiments).

4.3.6 Fluorescence recovery after photobleaching (TIRF-FRAP):

A system of optical flats[5] enables us to easily switch between a low intensity monitoring beam for observation of surface dynamics and a high intensity beam for conducting fluorescence recovery after photobleaching (FRAP) experiments in TIRF mode (Figure 2.1). After liposome adsorption was complete, TIRF-FRAP experiments were conducted by application of one to three bleach pulses followed by monitoring of the fluorescence recovery. Experiments conducted in the TIRF-FRAP protocol utilize

spot diameters significantly greater than 50 μm and are used to characterize systems with faster diffusivities. Molecules with lower diffusivities are more accurately characterized by fluorescence recovery after pattern photobleaching (discussed later) in which the characteristic length scale for diffusion is much smaller than in TIRF-FRAP experimentation.

X-Y stage calibrations: In TIR mode, the area illuminated by the laser beam waist at the interface is typically characterized by an elliptical spot. The accurate characterization of the dimensions of this spot is not a trivial undertaking due to the location of the beam waist. Thus, classical methods that employ translation of the beam across a knife edge in order to determine spot diameters cannot be applied here. Spot diameters were estimated by photobleaching a spot and translating the stage in the X and Y planes across the bleach spot[5](Refer to Figure 5.3 and Figure 5.4 in Appendix.).

4.3.7 Fluorescence recovery after pattern photobleaching (FRAPP):

The experimental configuration used for FRAPP has been depicted in Figure 4.4. Stripe patterns were imposed on the substrate by directing the 488 nm laser beam (expanded through a 5X beam expander (Edmund optics, Barrington NJ) through a 50 or 100 line per inch Ronchi ruling (Edmund optics, Barrington,NJ) placed in a real image plane. Placing a ruling in a back image plane, results in projection of a sharply focused pattern of alternating dark and bright fringes on the substrate in the sample plane. This back real image plane is located near the epi-port of the Axiovert 135M microscope, coincident with the field iris diaphragm of a fluorescence light illuminator (Zeiss)

[5] A complete description of this method and stage calibration charts is presented in Appendix C

mounted through the epi-port. The fluorescent light illuminator has a lens that projects the beam through a Zeiss filter cube (Ex: 450-490/DM: 510/Em: 515-565), and a 32X Zeiss objective on to the substrate. For focusing the objective, a fluorescent coating was brushed onto a glass slide using a yellow fluorescent marker (Sanford). The objective position was then adjusted till the fringes appeared in sharp focus. The fringe spacing was estimated by using a reticule containing 10 lines per centimeter in the eyepiece. The glass slide was then replaced by the sample slide. Prior to initiating photobleaching, minute adjustments were made to the objective focus knob to bring the fringes into sharp focus.

Beam alignment was checked at the start of each experiment and objective focusing was performed prior to initiation of every FRAPP experiment. For FRAPP experiments, it is crucial that the monitoring beams and the photobleaching beams be precisely coincident. Checking that the beams coincided was accomplished with the following steps. (1) The monitoring and photobleaching beams were projected on to a screen some distance away from the vibration isolation table, and beam recombination was checked.(2) Occasionally, as an additional check for recombination, once the laser beam was directed through the Ronchi ruling so that fringe pattern was formed on the fluorescently coated glass slide, a CCD camera or the microscope oculars was used to re-confirm that the beams recombined by observing the overlaying of the faint monitoring fringes over the photobleaching fringes[6] [156]. For all experiments, the monitoring beam intensity ranged from 1μW to 5μW. For photobleaching, the beam intensity required was approximately 0.5W. Additional neutral density filters (NDF) were required to attenuate

---

[6] Precautionary note:- Laser safety glasses must be used during alignment, especially when viewing the sample through the oculars.)

the monitoring beam to the desired level. The use of additional NDFs causes significant deviation in the path of the monitoring beam, so checking for recombination is especially crucial. A high bleaching intensity is required to obtain a sufficient bleach depth within a reasonable time. Typical bleach times varied from 350ms to 1 second. An aperture placed in the image plane in front of the PMT or CCD camera was used to restrict the observation area. Thus, the illuminated area was approximately 200 μm, while the observed area was 150 μm. Stripe periodicity in the sample plane was approximately 12.5 μm. A typical fringe pattern obtained using this configuration is shown in Figure 4.5.

For FRAPP experiments, liposome adsorption on the polyelectrolyte coated substrates was initiated by directly introducing the liposome solution at a flow rate of 0.34 ml/min for approximately 10-12 minutes using the syringe pump. The infusion was then halted and adsorption was allowed to continue for approximately 45 minutes. The flow cell was subsequently flushed with 4-5 flow cell volumes of buffer in order to remove the fluorescently labeled liposomes in the bulk solution.

4.4 Theory and Data Analyses for Fluorescence recovery after pattern photobleaching

FRAP is a technique that is commonly used to obtain estimates of translational (lateral) mobilities of proteins or lipids. There are two principal variants of this method. The first involves using a focused laser beam to create a small spot. This is known as spot photobleaching and can be effected using epi- illumination as well as using TIRFM. In the second method (FRAPP), a laser beam is passed through a Ronchi ruling placed in a back image plane to create a pattern of alternating dark and bright stripes of well defined

periodicity over a broadly illuminated area. The principle advantage of FRAPP over spot photobleaching lies in the well defined characteristics of the pattern obtained in the sample plane. For spot photobleaching, the recovery kinetics and shape depend very strongly on the shape of the focused spot at the interface. The precise shape of the spot is difficult to discern as the beam travels through several optics in order to form the spot. As a result there is considerable uncertainty in measurements of diffusion coefficient especially for non-ideal samples. In contrast the well defined periodicity of the stripe pattern produced in the sample plane offers two distinct advantages: (i) It allows us to measure slow as well as fast diffusion coefficients (10^{-10} cm^2/s to 10^{-7} cm^2/s), as the stripe periodicity can easily be varied and (ii) It allows us to examine samples where multiple populations with different mobilities coexist, using models that describe such populations. Other variants of FRAPP involve creation of the stripe pattern using the intersection of two beams either in the sample plane (using TIRF illumination) or in a back image plane (using EPI illumination). The advantage of using TIRFM-FRAPP over EPI-FRAPP is that due to the surface selectivity of TIRFM, a buffer wash to eliminate bulk fluorophores is not necessary. The trade-off is the complexity in the experimental configuration.

4.4.1 Theory

A complete mathematical analysis of fluorescence recovery after pattern photobleaching has been presented by Starr and Thompson[157]. A brief description of this analysis is presented below. Consider a sample of mobile fluorescent lipids with diffusion coefficient *D*. The fluorescence emission from such a sample can be described as:

$$F(t) = Q\int_{-\infty}^{\infty}\int_{-\infty}^{\infty} I(x,y)C(x,y,t)dxdy \tag{4.1}$$

where Q is a proportionality constant that incorporates factors such as fluorophore quantum yield and the instrument constant , $I(x,y)$ is the monitoring beam intensity and $C(x,y,t)$ is the concentration of unbleached molecules as a function of position and time. The equation that describes the intensity profile for a Gaussian-shaped laser beam intersected by a Ronchi ruling placed in a back image plane is given by

$$I(x,y) = \frac{I_o}{2}\exp\left[-\frac{2(x^2+y^2)}{s^2}\right].\left[1+\sum_{n\,odd} c_n \cos(nkx)\right] \tag{4.2}$$

Here, I_0 is the intensity at the origin, s is the $1/e^2$ radius of the expanded beam, k is the spatial frequency of the pattern, superimposed on the sample plane, defined by:

$$k = \frac{2\pi}{a} \;; c_n = \frac{4}{n\pi}(-1)^{\left(\frac{n-1}{2}\right)} \tag{4.3}$$

and a is the spatial period of the stripe pattern. The concentration profile of diffusing fluorophores is,

$$C(x,y,t) = \frac{1}{4\pi Dt}\int_{-\infty}^{\infty}\int_{-\infty}^{\infty} C(x',y',0).\exp\left[-\frac{(x-x')^2+(y-y')^2}{4Dt}\right]dx'dy' \tag{4.4}$$

The initial concentration of unbleached fluorophores in the sample is given by:

$$C(x,y,0) = C\exp[-KI(x,y)] \tag{4.5}$$

where C is the total fluorophore concentration and K is a constant that incorporates the bleach pulse duration, quantum yield and absorptivity of the fluorophores.

After developing Equation (4.1) using Equations (4.2), (4.3), (4.4) and (4.5), for cases where the stripe periodicity is small compared to the illuminated area, the following specific instances can be considered:

4.4.1.1 Samples containing a single diffusive population:

For bilayer systems containing fluorophores with a single diffusion coefficient, the fluorescence pattern photobleaching recovery profile $\phi(t)$ is given by[158]

$$\phi(t) = \phi(0) + \frac{\mu}{2}[1-\phi(0)].\left[1-\left(\frac{8}{\pi^2}\right).\left\{\exp\left(-\frac{4\pi^2 Dt}{a^2}\right)+\frac{1}{9}\exp\left(-\frac{36\pi^2 Dt}{a^2}\right)\right\}\right] \quad (4.6)$$

for $t \geq 0$, where $\phi(t)$ is the ratio of the postbleach fluorescence ($t>0$, after the bleach pulse) to the prebleach fluorescence $\phi(t<0)$,μ represents the fraction of the fluorophores present that are mobile and a and D have already been defined previously. This analysis neglects rapidly decaying (higher order) terms.

4.4.1.2 Samples containing multiple diffusive populations ($n \geq 1$)

For samples containing populations with multiple diffusion coefficients and an immobile fraction, the recovery profile can be characterized by[159],

$$\phi(t) = \phi(0) + \frac{1}{2}[1-\phi(0)].\left[\sum_{i=1}^{n}\mu_i\left(1-\left(\frac{8}{\pi^2}\right).\left\{\exp\left(-\frac{4\pi^2 D_i t}{a^2}\right)+\frac{1}{9}\exp\left(-\frac{36\pi^2 D_i t}{a^2}\right)\right\}\right)\right] \quad (4.7)$$

where μ_i is the fraction of the fluorescence recovery from mobile fluorophores with diffusion coefficient D_i.

4.4.2 Data Analyses and curve fitting

Data fitting was accomplished using OriginPro 7.5 (OriginLab Corporation, Northampton MA) which uses the Levenberg-Marquardt algorithm for non-linear least squares fitting. The post-bleach fluorescence emission intensity was normalized against the pre-bleach fluorescence emission intensity (t<0). All data sets were fitted to the models given above by weighting datasets with the Poisson error and an F-test of comparison was conducted to determine whether the model using higher parameters provided a statistically significant improvement in the goodness of the fit. This F-statistics was defined as:

$$F = \frac{(\chi_1^2 - \chi_2^2)(N-5)}{2\chi_2^2} \tag{4.8}$$

where χ_1^2 and χ_2^2 are the chi-squared goodness-of-fit statistics for the models described by Equations (4.6) and (4.7) respectively. If this F statistic exceeds 3.0, the fit using the model with more parameters is considered as a significant improvement[159,160].

Equations (4.6) and (4.7) describe profiles where the recovery of fluorescence from diffusing fluorophores comes from diffusion between the illuminated and non-illuminated stripes. This model does not account for the possibility of recovery

originating from diffusion between the illuminated region and outside the illuminated region[157].

4.5 Results and Discussions

4.5.1 TIRFM Adsorption experiments:

The curves in Figure 4.6 depict adsorption of fluorescently tagged liposomes composed of varying amounts of DOPA and DOPC on PEMs with either PDAC or SPS as the top layer. In Figure 4.6, curves A and B depict adsorption of negatively charged liposomes composed of 90% DOPC / 10% DOPA to PEMs with positively charged PDAC and negatively charged SPS as the top layers respectively. The higher intensities obtained in curve A indicate that the liposomes adsorbed onto PDAC preferentially to SPS (curve B) presumably due to electrostatic interactions. To investigate the role of liposome charge on subsequent adsorption, we conducted adsorption experiments with liposomes composed of 80% DOPC and 20% DOPA on PEMs (curves C and D) with PDAC and SPS as the top layer respectively. (Note: Curves C and D were experiments conducted with a separate batch of liposomes from those used to obtain curves A and B. Due to batch to batch variability in liposome characteristics and small changes in labeling ratios, etc., we are cautious about directly comparing the fluorescence emission data obtained from different batches.) The higher concentration of negatively charged lipids in the liposomes further increased the adsorption selectivity for PDAC suggesting that adsorption of liposomes on PEMs is significantly influenced by strong electrostatic interactions between the charged lipids and polyelectrolytes. The increasing fluorescence intensities even after 1 hour for curve C may suggest that multilayer deposition occurs on

increasing the amounts of DOPA in the liposomes. For the remainder of the studies in this chapter, liposomes composed of 10% DOPA and 90% DOPC were used, to minimize the likelihood of multilayer deposition.

To determine the reversibility of liposome adsorption to PDAC/SPS PEMs the flow cell was flushed with 3-4 volumes of liposome-free buffer. This wash resulted in the removal of significant amounts of liposomes adsorbed to PEMs with SPS as the top layer (Figure 4.7). In comparison, the binding of liposomes to PEMs with PDAC as the top layer is relatively strong and a buffer wash resulted in a smaller reduction in total fluorescence (Figure 4.8, top curve and Figure 4.9b, top curve). Since the evanescent wave decays rapidly with distance from the interface, only a small contribution to the total fluorescence comes from illumination of fluorophores in the bulk solution. Therefore, while the buffer wash experiments may reflect, in part, depletion of liposomes in the bulk liquid, it is much more likely that the results suggest that lipid binding to PDAC is stronger than to SPS.

Liposome adsorption on m-dPEG tailored surfaces was also studied. The ability of PEG to resist biomolecular adsorption has been well established in the literature[161]. In Figure 4.8, the upper curve depicts liposome adsorption onto PEMs with PDAC as the top layer, while the bottom curve depicts liposome adsorption on m-dPEG acid layers. Thus the m-dPEG layer resists liposome adsorption. In such experiments, buffer wash steps are more crucial as it allows us to further examine whether the liposomes that do adsorb are loosely or tightly bound. The results of Figure 4.8 have been re-plotted in Figure 4.9b, to show the liposome desorption more clearly. Figure 4.9b shows profiles for experiments in which a buffer wash was initiated after approximately 45 minutes of

liposome adsorption. At t=0 min, liposome adsorption to PDAC (top curve) and m-dPEG (bottom curve) PEMs was halted by introducing liposome-free buffer and only the desorption profiles are shown. In each curve the fluorescence intensity has been normalized against the corresponding fluorescence value obtained prior to initiation of the buffer wash in each experiment. There is a 70% decrease in the fluorescence emission intensity for the m-dPEG case as compared to a 10% decrease in the case of PDAC. A similar TIRFM study where the adsorption/desorption of liposomes on slides coated with lipid monolayers is monitored, has been reported in the literature[162]. That study indicated that the kinetics of liposome adsorption and desorption were strongly dependent on the solution ionic strength and the lipid concentration in solution. Much research has been conducted to determine the mechanism of PEG resistance to adsorption of biomolecules and many theories have been proposed to explain the resistive ability of PEG molecules. While the mechanism for biomolecular resistance is not completely clear, it appears to stem either from steric exclusions between the biomolecule and the PEG chain[163,164] or from long range electrostatic repulsions[165].

We have observed that in case of liposome adsorption onto multilayers with SPS and PEG as the top layer, in spite of electrostatic or steric repulsions, some liposome adsorption does occur. In Figure 4.9a, although the rate of liposome adsorption to the m-dPEG surface is much diminished in comparison to that for PDAC, no saturation of fluorescence is detected, and the signal would appear to continue increasing if the experiment had not been terminated at 45 minutes. Thus, the additional step of flushing the flow-cell with liposome-free buffer results in removal of large amounts of loosely

bound liposomes and is an important step during formation of BLM arrays. This was confirmed with fluorescence micrographs which have been discussed in the next section.

It is also interesting to note the shapes of the adsorption curves obtained for the different PEM surfaces. For example in Figure 4.9a for adsorption to m-dPEG PEMs, a sharp break in the adsorption profile occurs at approximately 400 seconds, at which point there is a change in the adsorption rate, but no apparent saturation. In the case of PDAC (Figure 4.8), after this break, the fluorescence saturates indicating no additional vesicular adsorption. Some researchers propose that this characteristic break indicates the point at which a single bilayer is formed[162]. Beyond this point, any further increase in fluorescence can be construed as occurring due to the reversible adsorption of vesicles to the bilayers. Thus multiple breaks can be attributed to the formation of multilayers. It is interesting then, to note, that in the case of liposome adsorption to m-dPEG, a second layer of vesicles appears to adsorb in spite of the electrostatic repulsions between the negatively charged bilayer and vesicles.

It should also be noted that direct comparison of fluorescence emission intensities in the experiments described in this section, requires the assumption that the quantum yield of the dye is unaffected by its proximity to the charged polyelectrolyte surface. While we have not measured fluorophore lifetimes to confirm this, Nollert and coworkers measured the lifetime of NBD-PE in a POPC BLM on glass and found it to be comparable to its value in a vesicle[166].

4.5.2 Arrays of lipid bilayers:

Two different schemes were used to fabricate arrays of lipid bilayers using methods detailed in Section 4.3. Figure 4.10a and Figure 4.10b show the resulting fluorescent images of the line and circular patterns respectively. Images in this dissertation are presented in color. Consistent with the adsorption results, as indicated by the fluorescent features of the line and circular arrays and the clean background regions, liposomes bind preferentially to PDAC features and negligibly to the SPS background. Similar fluoresence results were obtained when we stamped a weak polyelectrolyte PAH instead of a strong polyelectrolyte PDAC on SPS. Figure 4.10c shows the resulting fluoresence image. It can be clearly seen that the liposomes adsorb preferentially on PAH in comparison to SPS as the lines are well defined. The fluorescence micrographs clearly indicate that the system is homogeneous with the exception of few bright spots which may be due to crystalline dye.

In another approach m-dPEG acid was stamped on a glass slide coated with multilayers with PDAC being the topmost layer. The m-dPEG acid molecule has a carboxylic acid group on one end; therefore at a pH above the pK_a of the carboxylic group it has a negative charge and can therefore be stamped on PDAC, resulting in patterns of m-dPEG acid on PDAC[155]. As discussed earlier, m-dPEG acid also resists liposome adsorption. Arrays of lipid bilayers could be created in this case by exposing m-dPEG acid patterns to liposome solution. Liposome adsorption occurred only on the exposed PDAC while m-dPEG acid patterns resisted their adsorption. Figure 4.11a and Figure 4.11b show the obtained line and circular patterns. In this case liposomes bound to the background pattern rather than the circular or line features. Thus the fluorescent

patterns seen in Figure 4.11 are a negative replica of those seen in Figure 4.10. The ability to make either the positive or negative image of the stamp adds to the versatility of this method.

4.5.3 TIRF spot photobleaching:

Figure 4.12 depicts TIRF-FRAP data for bilayers formed on PDAC PEMs. For this particular experiment, the beam waist was characterized as an elliptical profile 166 μm along the major axis and 70 μm along the minor axis (Refer Appendix C, Figure 5.4). This can be roughly approximated to a circular spot of 108 μm diameter. We observed no fluorescence recovery after application of the bleach pulse. Over long durations, the fluorescence signal appears to drop due to photobleaching by the monitoring beam (Figure 4.12a). We also conducted recovery experiments, where the recovery was intermittently monitored over longer time scales in order to prevent photobleaching effects by the monitoring beam (Figure 4.12b). We observed no significant fluorescence recovery under these conditions.

For bleach spots with length scales in the region of 50-100 microns, recovery profiles in a reasonable short time duration (<1000s) can be obtained for lipid bilayers with higher diffusivities (10^{-7} cm^2/s). However for bilayers with diffusivities in the region of 10^{-9}- 10^{-10} cm^2/s, characteristic recovery times are significantly larger, and hence FRAPP is more accurate for interrogating lipid diffusion in BLMs with lower diffusion coefficients. We did not obtain significant recoveries on PDAC surfaces using conventional TIRF photobleaching; diffusivities for these bilayers appeared to be considerably lower and hence we used FRAPP to obtain estimates of these values.

4.5.4 Fluorescence recovery after pattern photobleaching:

FRAPP was used to determine if the adsorbed liposomes remain intact on the surface or fused together to form a bilayer. Models used to describe recoveries for species containing one or more mobile fractions were used to fit the data (Equations (4.6) and (4.7))[158,159]. Both recoveries on PAH and PDAC were better described by the two mobile-species model which is shown to provide a statistically better fit than the one-mobile species model. Figure 4.13 and Figure 4.14 show typical recovery curves for lipids deposited on PDAC and PAH respectively. The mobilities and diffusion coefficients for populations on PDAC have been summarized in Table 4.1 (one mobile species) and Table 4.2 (two-mobile species) while the mobilities and diffusion coefficients obtained for bilayers on PAH, have been summarized in Table 4.3 (one-mobile species) and Table 4.4 (two-mobile species).

Although the data are well represented by the two-mobile species model, it is still unclear whether there is an actual underlying physical basis for the presence of two diffusing components. If the data above is indeed described more accurately by a two component model, there are two principal hypotheses which could explain the presence of two distinct populations with different mobilities. (i) Since bilayer deposition occurs through liposome adsorption to the PEM surface, the dye (NBD-PC) is present both in the lower as well as the upper leaflet of the lipid bilayer. The bottom leaflet is more strongly bound to the PEM cushion with PDAC or PAH as the topmost layer on account of favorable electrostatic interactions between the charged lipids and the surface. If so, diffusion in the lower leaflet would be slower than the upper leaflet. However, in that case, assuming a random distribution of dye molecules across the two leaflets (since they

are randomly distributed in the liposomes), one would expect to obtain equal amplitudes for the two mobile fractions, which does not hold true (Refer Table 4.2 and Table 4.4) (ii) There may be phase separation in the lipid bilayer due to the immiscibility of the two lipids. The dye is thus located in two distinct regions, a more viscous (lower mobility) region and a less viscous (higher mobility region). However for our lipid system, the phase transition temperature of both lipids is below -8 °C (obtained from Avanti Lipids), and the lipids (DOPC and DOPA) can be considered to be miscible. Also, fits from the two-mobile species model show considerable variation in the parameters from one spot on the sample to another for bilayers on PDAC as well as PAH (Table 4.2 and Table 4.4). In addition, the error associated with the fit parameters is large. The fits obtained using the single mobile-species model are much more consistent. In light of these observations, even though the two-mobile species model offers a superior fit, we chose to characterize the sample as a system containing a single population of mobile fluorophores in addition to an immobile fraction.

The results summarized in Table 4.1 and Table 4.3 indicate that bilayers formed on PAH have higher mobile fractions (>0.65) than those formed on PDAC substrates (<0.37). Therefore, a substantial fraction of lipids deposited on PDAC are immobile. Since FRAPP measures long range diffusion much greater than the diameter of a liposome (20-100 nm), this suggests that some of the adsorbed liposomes remain unruptured. Nollert and coworkers[166] have proposed two possibilities that occur when liposomes adsorb to surfaces. In one scenario, liposomes adsorb unruptured, as supported vesicles (which represent the immobile fraction). In the other case, they adsorb, fuse and spread to form sBLMs. It is also possible that lipids present in the bilayer or liposomes

may exist in different phases that have varying degrees of mobility. Thus, lipids in phases of low mobility could also contribute to the immobile fraction. While FRAPP can provide indirect evidence about the presence of multiple populations, it is difficult to use this technique to distinguish between an intact liposome and an immobile lipid phase.

We expected higher mobile fractions for bilayers formed on PDAC, because it is a strong polyelectrolyte that we expect should facilitate liposome rupture and bilayer formation more then a weak polyelectrolyte such as PAH. However we observed higher mobile fractions on PAH in comparison to PDAC. The following theories may explain this observation: (i) An examination of the PDAC and PAH molecules indicates that the charge on PDAC is shared by more atoms than PAH. This may influence the interaction of the liposome with the PDAC PEM in a way that reduces inhibits rupture (ii) Jenkins and coworkers[167] have proposed on the basis of experimental observations that the interactions of vesicles with a hydrophilic/hydrophobic boundary causes rupture and bilayer formation. A recent theoretical analysis[168] predicted that a heterogeneous surface (i.e. surface having both hydrophobic and hydrophilic moieties) is more likely to facilitate bilayer formation than a completely hydrophilic surface. While both PDAC and PAH have hydrophilic groups and hydrophobic backbones, it is possible that the bulky side chain on PDAC, reduces accessibility of the liposome to the hydrophobic backbone. Thus, PAH exhibits greater hydrophobicity than PDAC which may explain the higher mobile fractions. It is also possible that differences in the extent of swelling of the PDAC and PAH PEMs can influence liposome rupture.

The diffusion coefficients obtained in this study are comparable to those reported for bilayers containing SOPS and POPC deposited on PDAC/SPS multilayers (2×10^{-9}

cm^2/s)[169,170]. The diffusion coefficients obtained in this study are lower than values reported in the literature the literature for DMPC:DOPA (10:1) bilayers deposited on PSS/PAH multilayers[131]. The average diffusion coefficient for bilayers on PDAC was 0.072±0.03 $\mu m^2/s$, while bilayers on PAH exhibited a diffusion coefficient of 0.0565 ± 0.009 $\mu m^2/s$. One possible explanation for this trend is the location of the dye molecule with respect to the bilayer. In our study, NBD was attached to one of the hydrophobic tails of phosphocholine; therefore, its location in the interior of the bilayer may make it less mobile. For example, diffusion coefficients for lipids have been reported to be four times greater if the NBD molecule is attached to the head-group than to the tail of the phosphocholine molecule[131]. Moreover, other groups generally use dye molecules only in the upper leaflet and, as a result, they measure the diffusion coefficient only of the upper leaflet. The upper leaflet would be less influenced by the underlying substrate and would be expected to exhibit a higher diffusion coefficient than the bottom leaflet.

Studies of liposome adsorption and rupture on PDAC and PAH PEMs have also been conducted using QCM. The results obtained in these studies are consistent with trends reported using FRAPP and can be found in APPENDIX D: Quartz crystal microbalance studies.

4.6 Conclusions

3-D arrays of liposomes and BLMs have been fabricated on PEMs. Such arrays have potential applications in biosensors, biocatalysis and devices that may use high throughput screening. TIRFM and fluorescence microscopy results suggested that liposomes composed of DOPA and DOPC adsorbed strongly on PDAC and PAH

surfaces, but weakly on SPS. Poly(ethylene glycol) (m-dPEG) coated surfaces resisted liposome adsorption. These results allowed us to create micro arrays of lipid bilayers. Lipid diffusion coefficients for lipids deposited on PDAC and PAH were in the range of 10^{-9} cm^2/s. FRAPP results suggest that a higher fraction of liposomes rupture to form bilayers on PAH surfaces than on PDAC, where a significant percentage of the adsorbed lipids are essentially immobile.

The mechanism of liposome rupture and bilayer formation is not fully understood. However, nanoscale surface heterogeneity is known to facilitate liposome rupture. Thus, the ability to tune the characteristics of the interface using different kinds of polyelectrolytes may help to elucidate the underlying mechanisms for bilayer formation and also allow BLM formation to be controlled.

4.7 Recommendations for future work

One possible study for examining liposome rupture and bilayer formation on these charged surfaces involves making epi-FRAPP measurements on liposomes that adsorb to the PEMs in the presence of an electric field. The presence of the electric field can alter the conformation of the charged PEMs thereby altering the surface characteristics which in turn may influence liposome rupture. This study will allow us to probe the underlying mechanisms for liposome rupture and bilayer formation, and will also allow us to tune the characteristics of the surface to optimize it for deposition of BLMs. Another interesting method to study vesicular fusion and rupture is using Fluorescence Resonant Energy Transfer (FRET). FRET is the radiationless transfer of energy from a donor molecule to an acceptor molecule. The amount of energy transfer is dependent on the

extent of overlap between the emission spectrum of the donor and the absorption spectrum of the acceptor. This rate of energy transfer varies inversely with the 6^{th} power of the distance between the donor and the acceptor[80]. FRET has been used for studying the mechanism of initial rupture of liposomes using single vesicle fluorescence assays[171]. It would be useful to probe the mechanism of liposome rupture on the highly charged polyelectrolyte substrates using such assays.

It will also be helpful to characterize liposome adsorption under a multitude of flow rates and ionic strengths to examine the shape of the adsorption profile, since the ionic strength of the solution will have a strong influence on the structure of the highly charged polylectrolytes. In addition, this study will allow us to examine the phenomenon of multibilayer formation. In fact, we have already attempted to fabricate 3-D structures composed of alternating layers of lipid-bilayers and polyelectrolytes in our flow-cell, by making sequential introductions of liposomes and polyelectrolytes and monitoring the fluorescence emission.

Another rapidly emerging thrust of research is in the area of lipid rafts. Lipid rafts are assemblies of lipids and proteins that can agglomerate to form ordered structures. These rafts are rich in cholesterol and sphingolipids and are considerably more viscous than the rest of the cell membrane. It is believed that a number of important biomolecules such as ion-channels or G-protein coupled receptors are localized within these rafts. We have already commented on the possibility of the presence of different phases in the lipid system used in our study. Since the ultimate goal of this project is to develop viable biomimetic interfaces, incorporating rafts and studying their formation is a natural progression of this research. In addition to more rigorous characterization of such

systems with FRAPP, studies using two-photon spectroscopy will allow us to probe phase separation at interfaces[89].

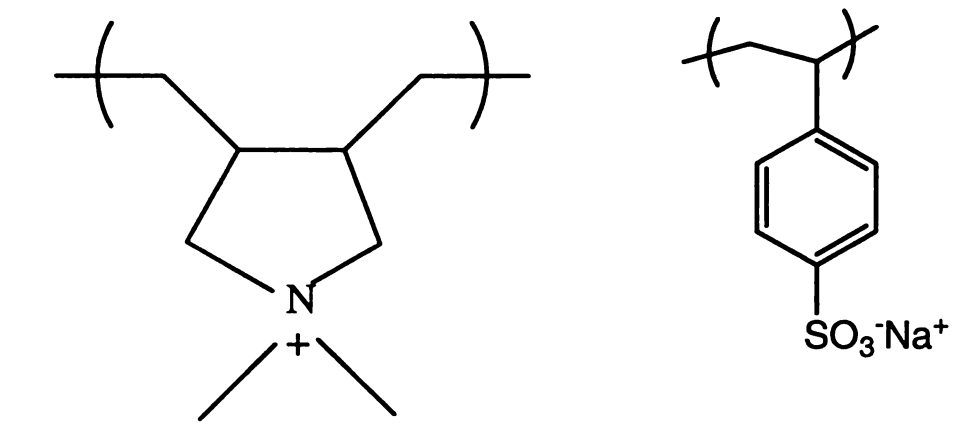

a

PDAC **SPS**

PAH

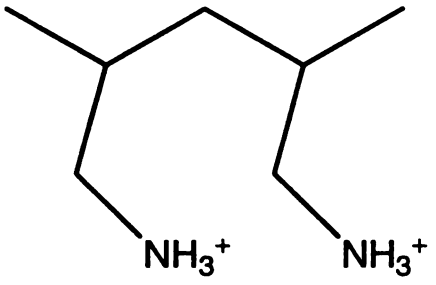

b

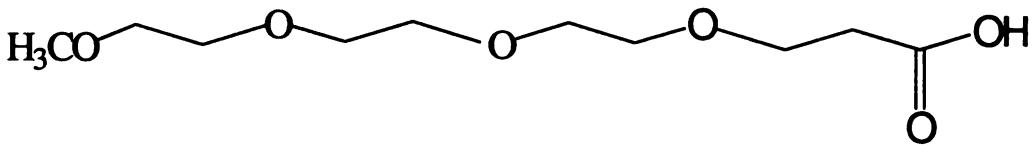

Figure 4.1: Structures for a) common polyelectrolytes and b) m d-PEG.

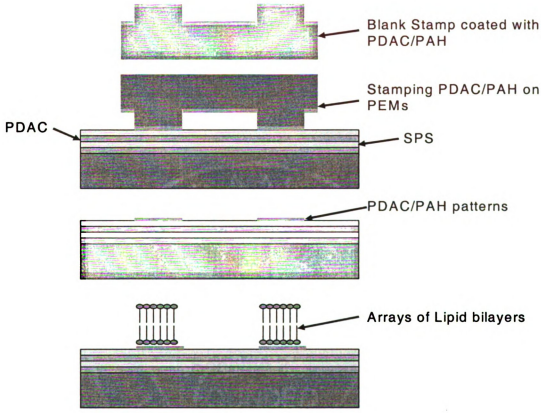

Scheme 1

Figure 4.2: Illustration showing creation of arrays of lipid bilayers on PEMs with PDAC or PAH as the topmost layer.

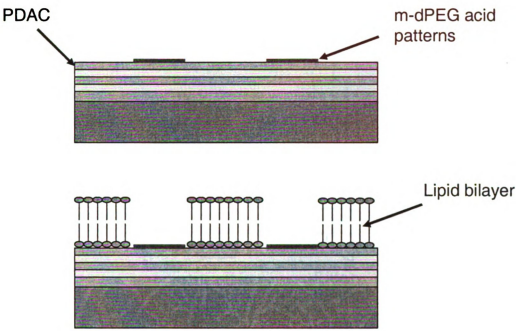

Scheme 2

Figure 4.3: Illustration showing formation of lipid bilayers on PEMs with m-dPEG acid as the uppermost layer.

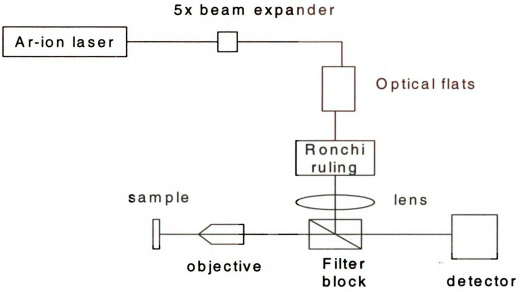

Figure 4.4: Experimental set-up for Fluorescence recovery after pattern photobleaching using EPI-illumination.

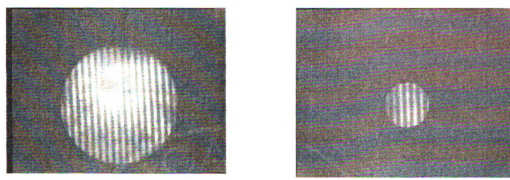

Figure 4.5: a) Fringe pattern in illuminated region obtained using 100 lines per inch ruling. b) Observation area restricted by placing an aperture in the camera/PMT image plane.

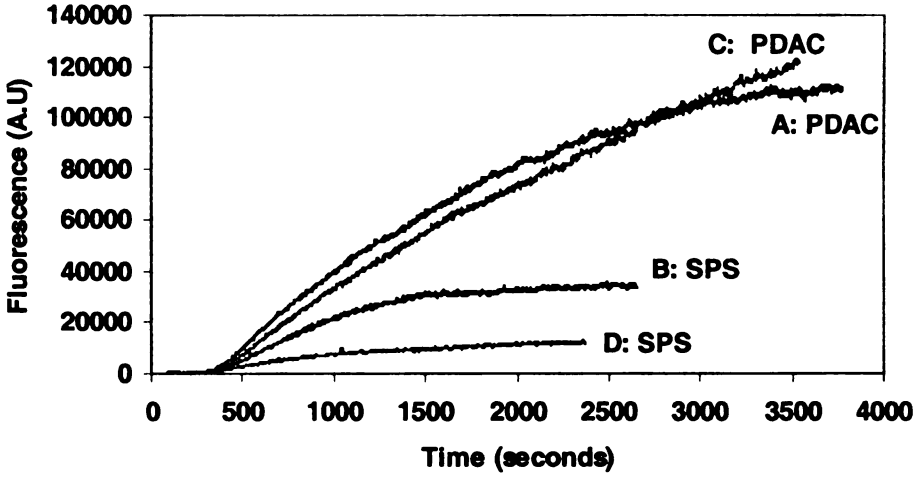

Figure 4.6: Adsorption curves of (A) liposomes (10%DOPA, 90% DOPC) on PDAC. (B) Liposomes (10%DOPA, 90% DOPC) on SPS. (C) Liposomes (20%DOPA, 80% DOPC) on PDAC. (D) Liposomes (20%DOPA, 80% DOPC) on SPS.

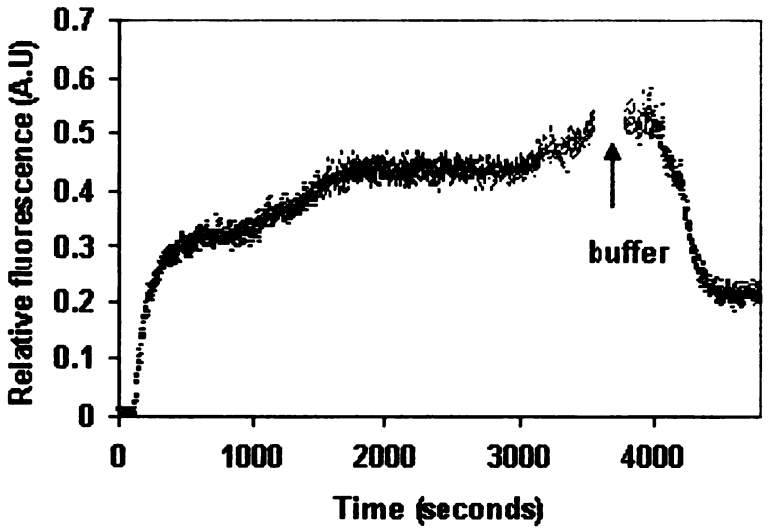

Figure 4.7: Shear induced desorption of liposomes from PDAC/SPS PEMs with SPS as the topmost layer. Binding of liposomes to these surfaces is relatively loose and a large fraction is removed upon introduction of buffer solution at a flow rate of 0.34 ml/min.

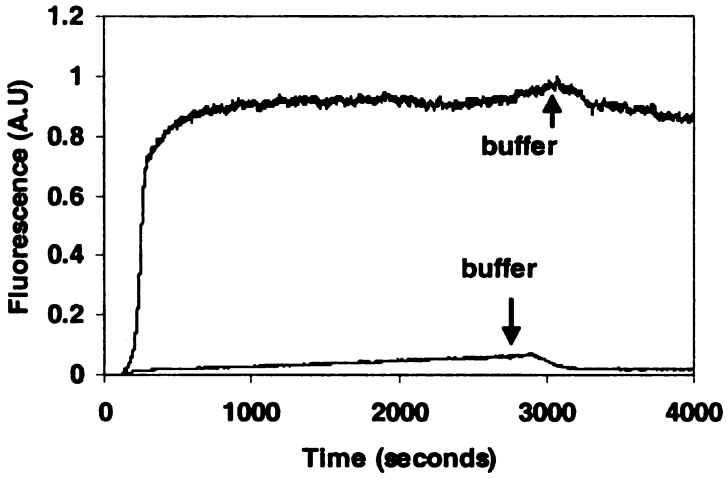

Figure 4.8: Adsorption curves of liposomes (10%DOPA, 90% DOPC) on glass slide coated with PEMs with PDAC (upper curve) and m-dPEG acid (lower curve) being the topmost layer. As can be seen, the lower fluorescence intensitites obtained are indicative of the ability of PEG to resist liposome adsorption.

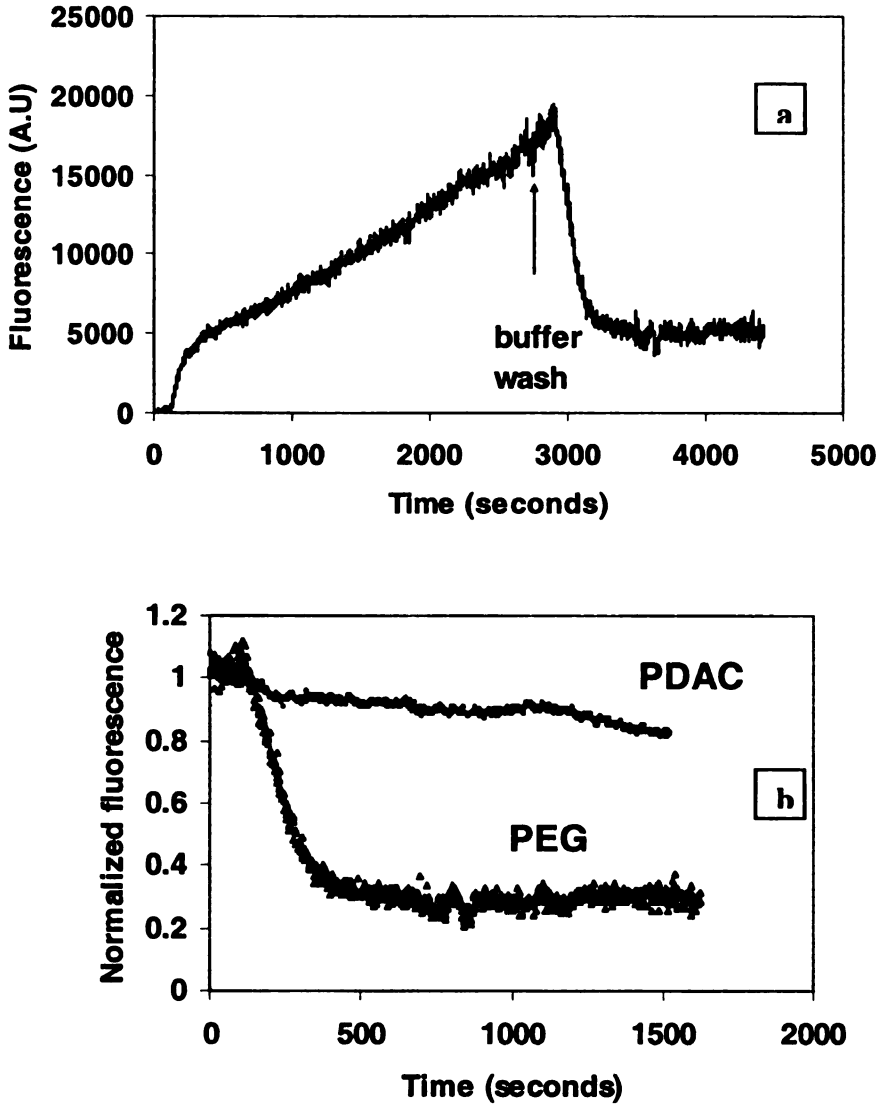

Figure 4.9: a) Adsorption of liposomes (10%DOPA, 90% DOPC) on a glass slide coated with PEMs with m-dPEG acid being the topmost layer. b) Buffer-wash experiments to study liposome desorption from PEMs. The top and bottom curves depict desorption of liposomes from PEMs with PDAC and m-dPEG as the top layer, respectively. At t=0, adsorption of liposomes (which have adsorbed for at least 45 minutes) is halted by introducing liposome-free buffer. In each curve, the fluorescence intensity has been normalized by the corresponding fluorescence value obtained prior to initiation of the buffer wash in each case.

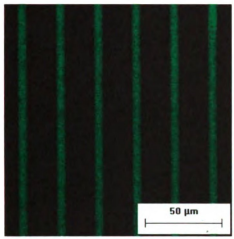

(a)

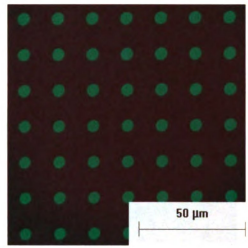

(b)

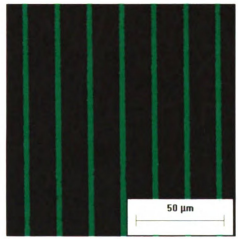

(c)

Figure 4.10: Fluoresence images showing (a) line patterns on a PDAC patterned substrate (b) circular patterns on a PDAC patterned substrate (c) line patterns on a PAH patterned substrate.

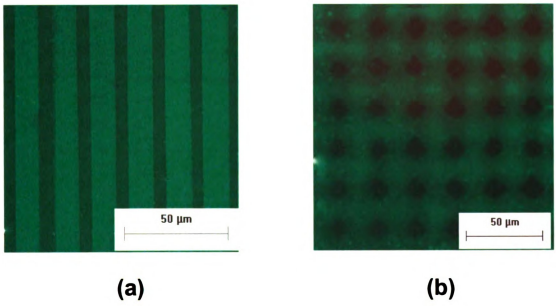

Figure 4.11: Fluorescence images showing (a) line patterns on a m-dPEG acid patterned substrate (b) circular patterns on a m-dPEG patterned substrate.

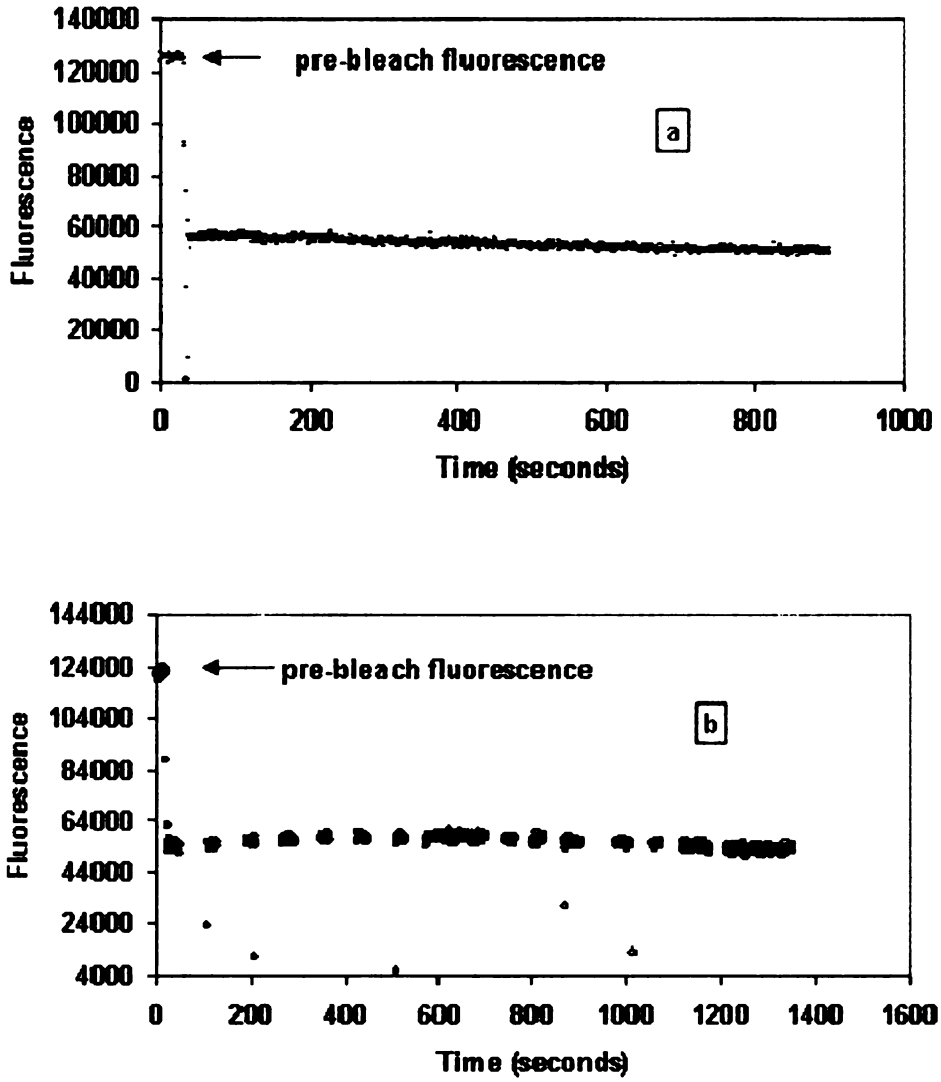

Figure 4.12: a) TIRF-FRAP data for DOPA/DOPC liposomes adsorbed on PEMs with PDAC as the top layer. b) TIRF-FRAP data under conditions of intermittent monitoring to prevent monitoring beam induced photobleaching over longer time scales.

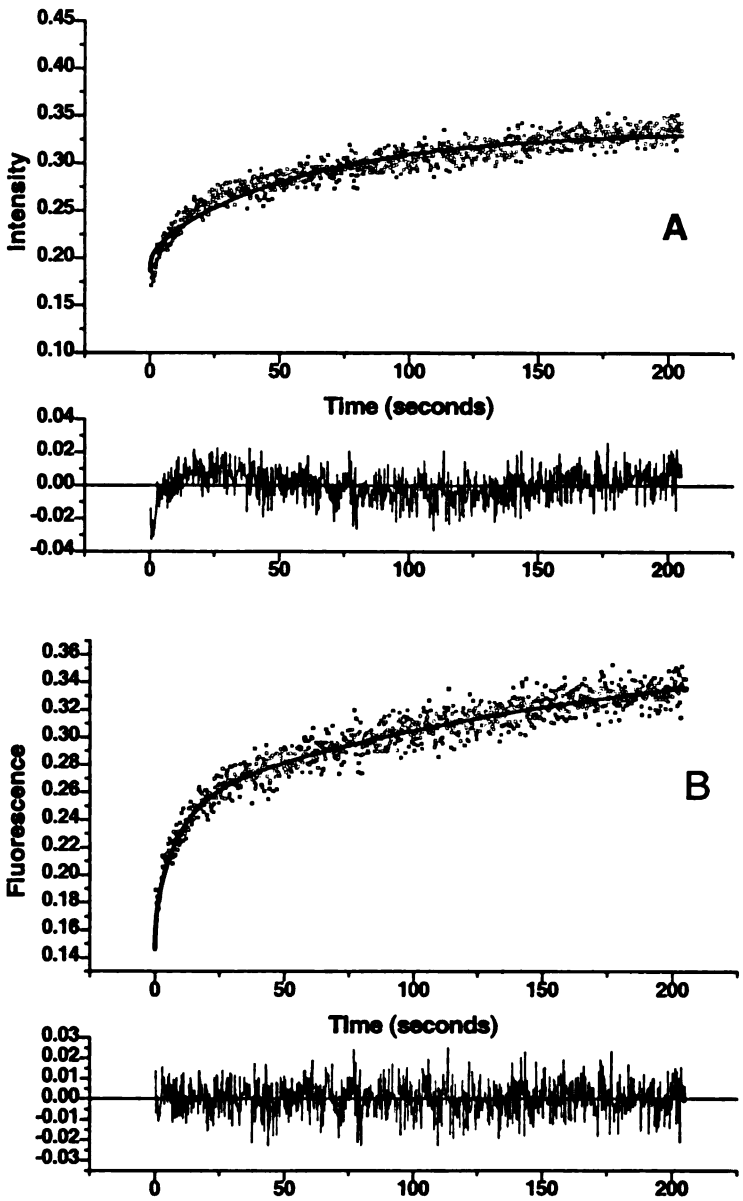

Figure 4.13: Fluoresence recovery after pattern photobleaching (EPI-FRAPP) profiles on PDAC. The solid line in the plate A represent fits to the recovery data set with a model[159] that describes the sample as containing containing a single mobile and immobile fraction, while in plate B the solid line is the fit to a model describing a sample with two mobile populations (with different mobilities) and an immobile fraction. Average values obtained with these models are summarized in Table 4.1 and Table 4.2. Also shown below each fit is a plot of the residuals vs. time as an indication of the goodness of fit.

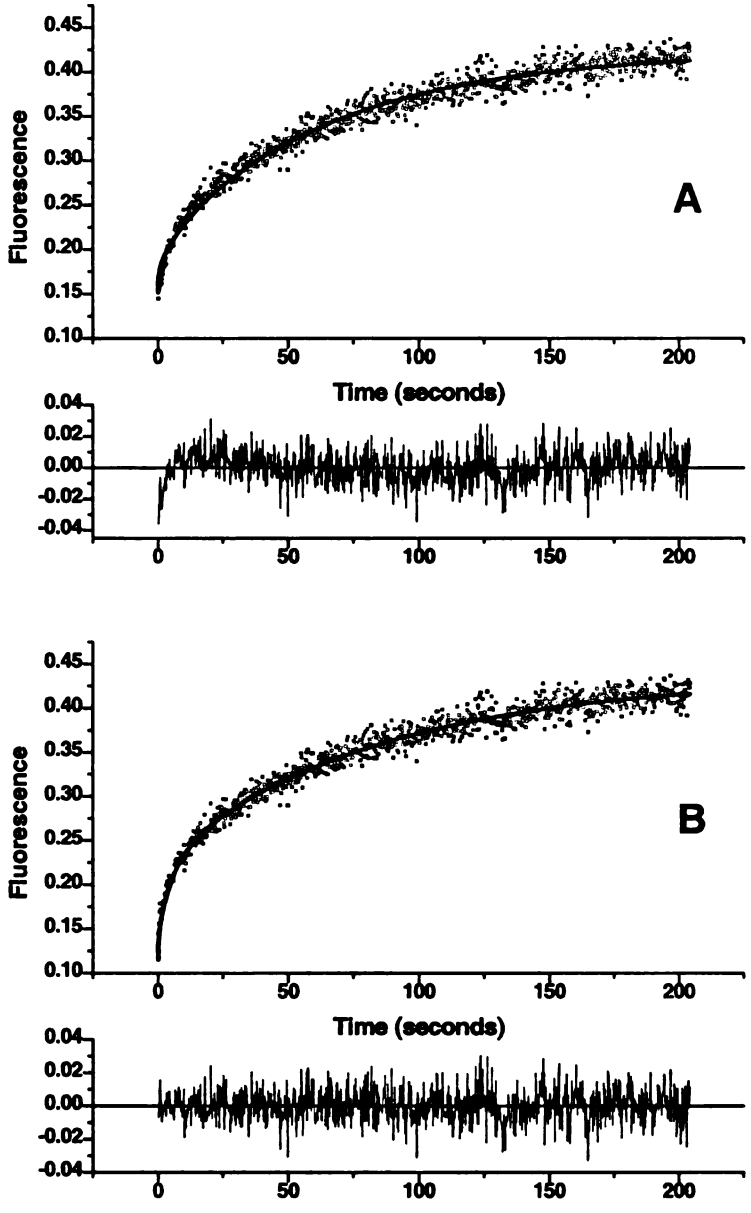

Figure 4.14: Fluoresence recovery after pattern photobleaching (EPI-FRAPP) profiles on PAH. The solid line in the plate A represent fits to the recovery data set with a model[159] that describes the sample as containing containing a single mobile and immobile fraction, while in plate B the solid line is the fit to a model describing a sample with two mobile populations (with different mobilities) and an immobile fraction. Average values obtained with these models are summarized in Table 4.3 and Table 4.4. Also shown below each fit is a plot of the residuals vs. time as an indication of the goodness of fit.

Table 4.1: Summary of model parameters obtained from fit of BLM recovery on PDAC to Equation (4.6) (single mobile-species model)

	parameter	1	2	3	Average
PDAC	f_o	0.187	0.31	0.325	
	m	0.363	0.096	0.201	0.22±0.13
	D (10^8 cm^2/s)	0.062	0.108	0.0465	0.072±0.03

Table 4.2: Fit parameters for lipid bilayer formed on substrates topped with PDAC, using the two mobile-species model given by (4.7). f_o represents the unbleached fraction (at t=0), and m_1, m_2 and D_1, D_2 are the mobile fractions and their corresponding diffusion coefficients respectively.

	Parameter	1	2	3
Substrate PDAC	f_o	0.14611	0.28191	0.28546
	m_1	0.18469	0.10216	0.13883
	m_2	0.35847	0.07429	0.2276
	D_1 ($10^8 cm^2/s$)	0.44962	1.86424	1.01905
	D_2(($10^8 cm^2/s$)	0.02094	0.06672	0.01802
	F-statistic	210	13.16	46.37

Table 4.3: Summary of model parameters obtained from fit of BLM recovery on PAH to Equation (4.6) (single mobile-species model)

	parameter	1	2	3	4	Average
PAH	f_o	0.15213	0.16429	0.28392	0.25053	
	m	0.63635	0.66456	0.65787	0.74132	0.67±0.05
	D (10^8 cm^2/s)	0.06066	0.06491	0.05634	0.0444	0.06±0.009

Table 4.4: Summary of model parameters obtained from fit of BLM recovery on PAH to Equation (4.7) (two mobile-species model).

	Parameter	1	2	3	4
Substrate PAH	f_o	0.11526	0.14067	0.24257	0.21486
	m_1	0.13961	0.09044	0.13076	0.16178
	m_2	0.58087	0.6402	0.62934	0.72163
	D_1 ($10^8 cm^2/s$)	0.75737	0.88423	2.25164	0.47875
	D_2(($10^8 cm^2/s$)	0.04773	0.05385	0.04789	0.02906
	F-statistic	114.3622	7.71	6.49	71

5 APPENDICES

5.1 Appendix A: Labview flowsheets

5.1.1 Labview flowsheets for TIRFM experiments conducted in analog mode

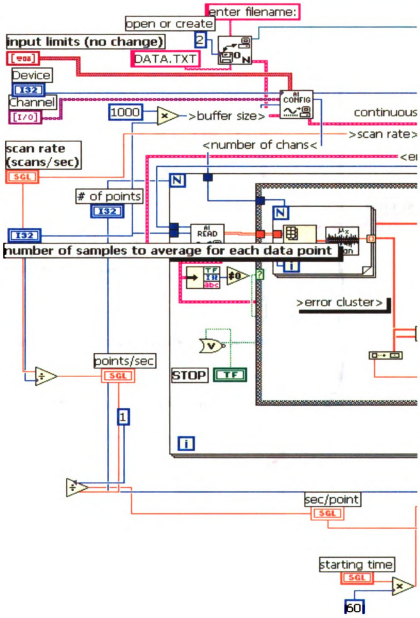

Figure 5.1: Labview flow sheets for TIRF data acquisition in analog mode. The flow sheet is continued on the next page.

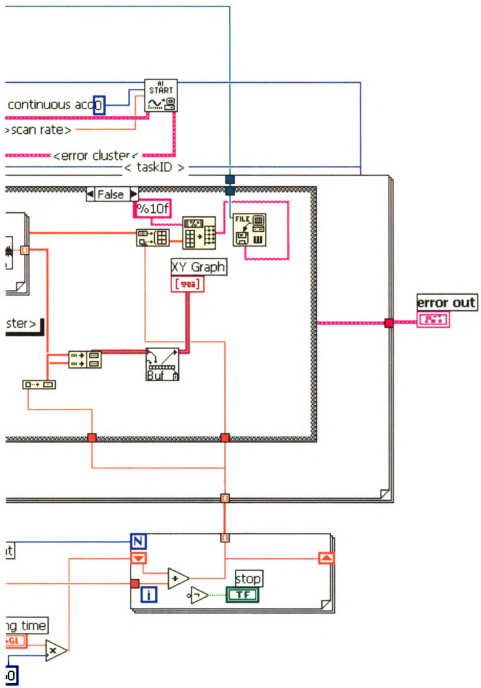

Figure 5.1 (continued): This flow sheet has been continued from the previous page

5.1.2 Labview flow sheets for photon counting

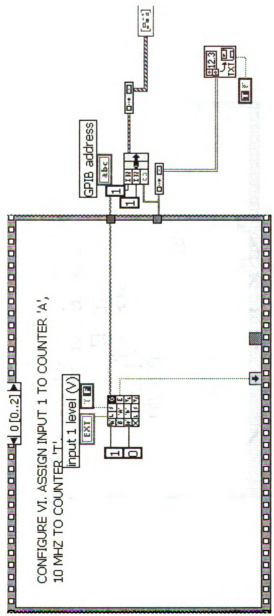

Figure 5.2: Flow sheets for computer interfacing with SR400 photon counter. These flow sheets have been continued on the succeeding pages. These flowsheets have been derived from Labview templates obtained from National Instruments, Austin, TX

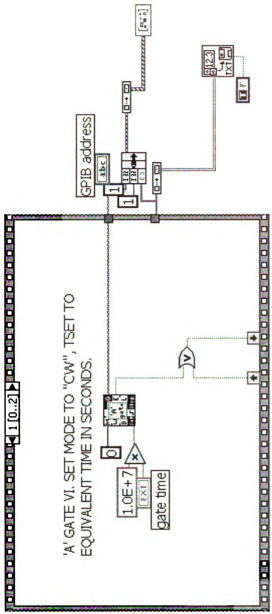

Figure 5.2(continued): This figure has been continued from the previous page and depicts subroutines for operating the SR400 photon counter

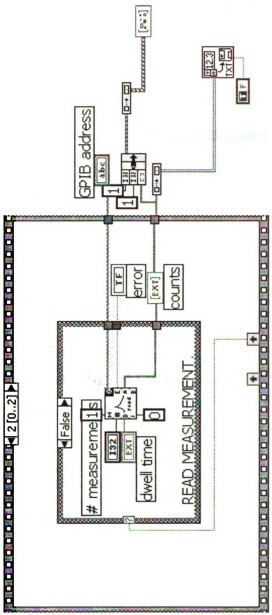

Figure 5.2 (continued): This flow sheet has been continued from the previous page and depicts subroutines for operating the SR400 photon-counter

5.2 Appendix B: Matlab programs for filtering and averaging analog measurements

5.2.1 Filtering program

This Matlab program discriminates the signal from the background

```
function p = test(data)
delete 'r:\colloid-surface-science\output.txt'
max_val = 0;
min_val = data(1,1);

for i=1:length(data)
    if (data(i,1)>max_val)
        max_val=data(i,1);
    end
    if (data(i,1)<min_val)
        min_val=data(i,1);
    end
end

threshold = (0.72) * (max_val-min_val) + min_val;
counter=1;
finaldata(1, 1) = 0;
finaldata(1, 2) = 0;

for i=1:length(data);
    if (data(i,1)>threshold)
        finaldata(counter, 1) = data(i,1);
        finaldata(counter, 2) = data(i,2);
        counter = counter+1;
    end
end

p=finaldata;

%mean and std. dev.%

m=mean(p,1)
average=m(1)
s=std(p,1)
stdev=s(1)

counter=1;
endgame(1, 1) = 0;
endgame(1, 2) = 0;

for i=1:length(p);
    diff=p(i,1)-average;
    absolute=abs(diff);
    if (absolute<stdev)
        endgame(counter, 1) = p(i,1);
        endgame(counter, 2) = p(i,2);
```

```
        counter = counter+1;
    end
end
save 'r:\colloid-surface-science\output.txt' endgame -ASCII;
p=endgame;
```

5.2.2 Averaging Script

Matlab program for averaging TIRFM fluorescence data obtained in analog mode

```
c=1;
b=1;
g=size(A,1)/8;
p=floor(g)+1
while b<p
 sum=0;
 d=c+7;
 for j=c:d
  sum=sum+A(j);
 end
 avg(1,b)=sum/8;
 c=c+8;
 b=b+1;
end;
n=avg';
delete 'r:\colloid-surface-science\my_data.txt'
save my_data.txt n -ASCII
```

5.3 Appendix C: Protocol for estimation of spot diameters for TIRF-photobleaching

Estimation of bleach spot diameters was determined using the following procedures.

Calibration of the actual speed of the stage translation: The speed of translation of the stage in the X-coordinate was determined as follows: Two scratch marks were made at a precise distance from each other in a microscope slide. The objective was then centered and focused on one of the marks. The motion of the stage was then actuated and a stopwatch and reticule in the eyepiece was used to determine the amount of time required for the second scratch to appear in the field of view. Using this procedure, a stage speed calibration chart was generated for different motor settings. This procedure was repeated for speed calibrations in the Y- coordinate. These charts are shown in Figure 5.3.

Determination of beam waist profile: After adsorption of fluorescently labeled liposomes was completed and the flow cell was rinsed with buffer, a bleach pulse was applied. Translation of the stage in the X and Y directions across the spot was then performed and the fluorescence signal was monitored. The bleached area in each scan was detected as a momentary drop in the fluorescence. Figure 5.4 shows the fluorescence collected during such a scan. Since the speed of translation of the stage is known and the duration of the fluorescence drop can be measured, the spot diameters can be easily

calculated. This procedure provides a reasonable accurate estimate of the elliptical spot dimensions.

For these methods, the assumption is made that the lateral diffusivities of the lipids in the bilayer are considerably slower than the duration of time taken for the stage to traverse the length of the dimension of the bleach spot. This was confirmed in TIRF-FRAP experiments where essentially no recovery was observed after photobleaching for bilayers formed on PDAC substrates.

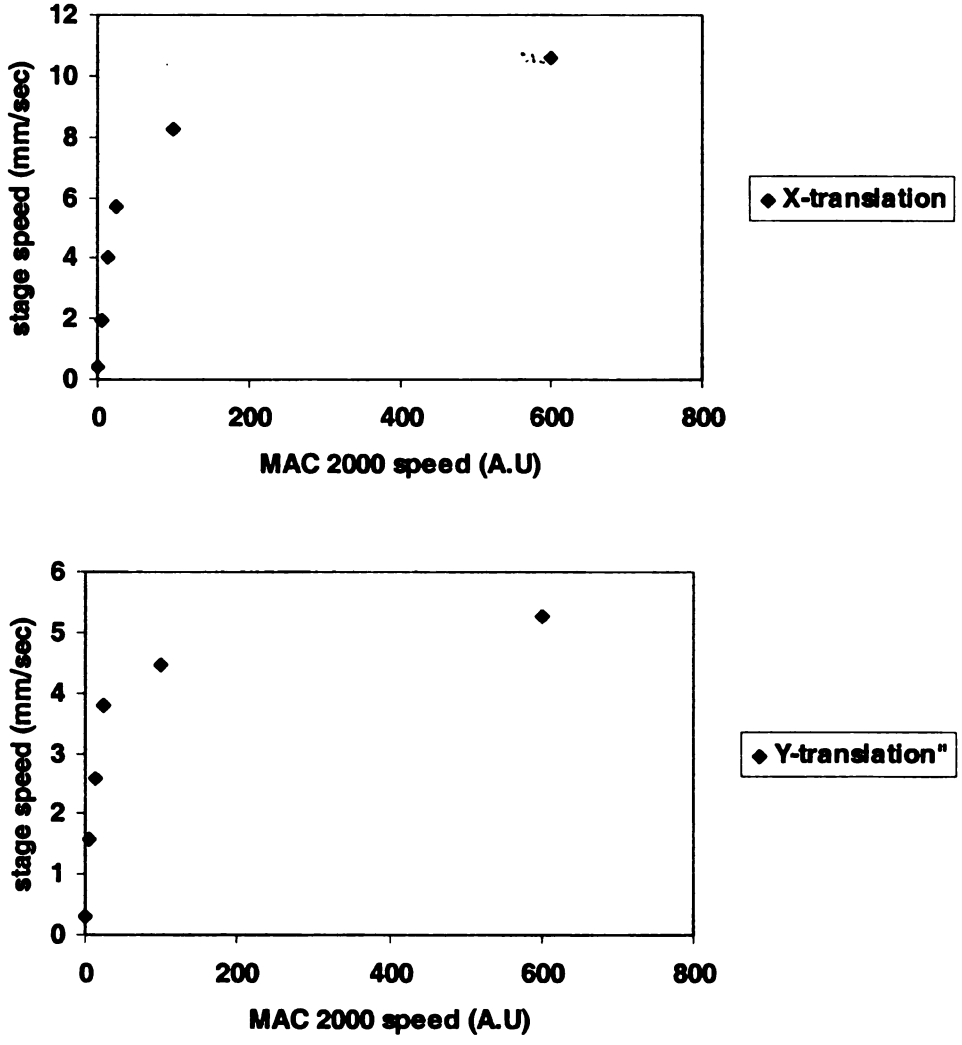

Figure 5.3: Stage speed calibrations displaying speed (in arbitrary units) against actual speed for both X- and Y motion controllers.

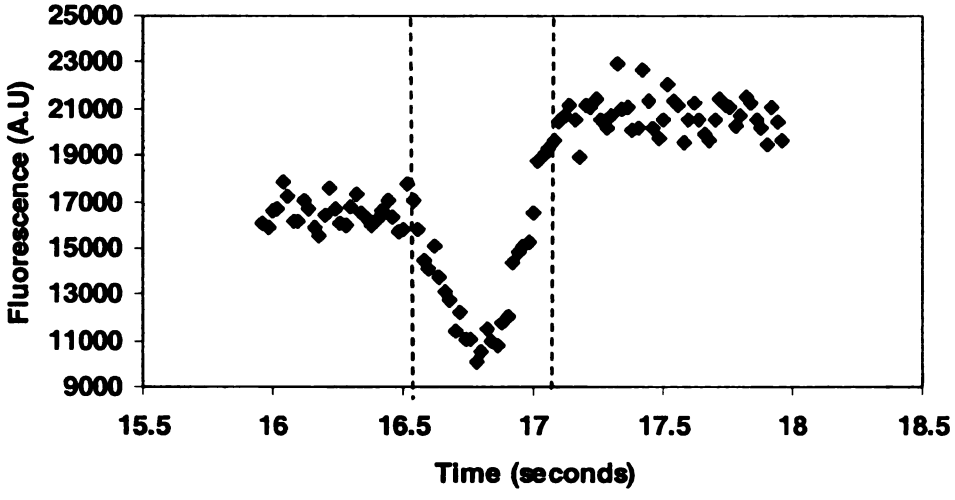

Figure 5.4: Estimating the dimensions of the elliptical spot. This picture shows a typical scan in the x-coordinate. A spot is bleached and the specimen is translated in the x-direction across the bleached spot. The data between the dotted lines represents the duration during the scan when the objective collects light from the bleached area of the sample.

5.4 APPENDIX D: Quartz crystal microbalance studies

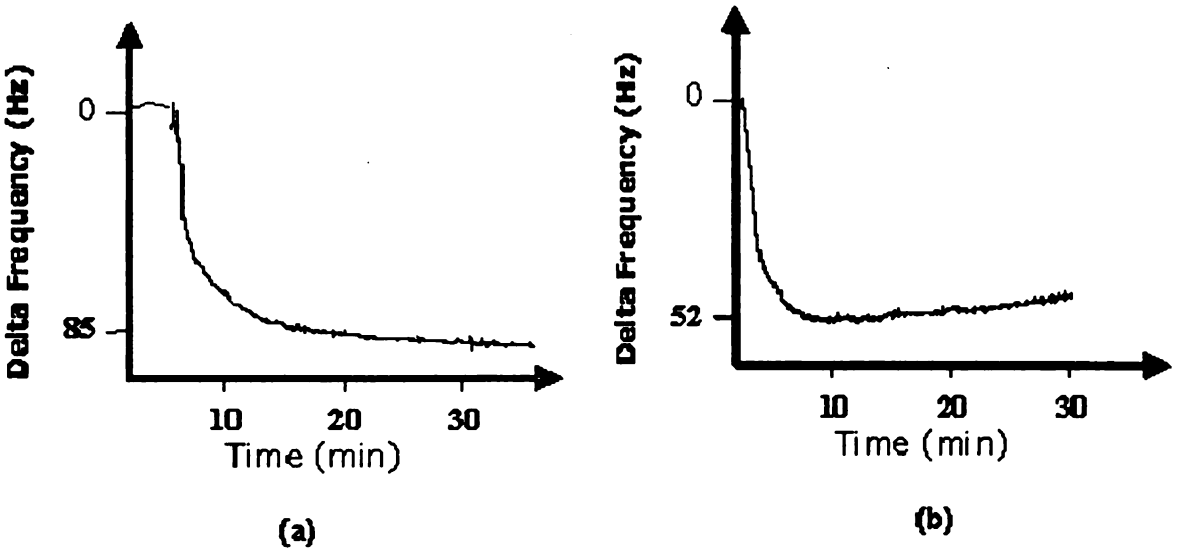

Figure 5.5: Adsorption of liposomes as studied by QCM on (a) PDAC (b) PAH. Note the presence of two distinct phases for adsorption on PAH (suggesting vesicle adsorption and rupture), in contrast with the presence of one phase for PDAC (suggesting vesicle adsorption without rupture).

LIST OF REFERENCES

(1) Volkov, A. G. "Redox reactions at liquid hydrocarbon/water interfaces: Biophysical aspects", *Electrochimica Acta* **1998**, *44*, 139-153.

(2) Arai, K.; Ohsawa, M.; Kusu, F.; Takamura, K. "Drug Ion Transfer across on Oil-Water Interface and Pharmacological Activity", *Bioelectrochem. Bioenerg.* **1993**, *31*, 65-76.

(3) Mackie, A. R.; Gunning, A. P.; Wilde, P. J.; Morris, V. J. "Orogenic displacement of protein from the oil/water interface", *Langmuir* **2000**, *16*, 2242-2247.

(4) Bowers, J.; Zarbakhsh, A.; Webster, J. R. P.; Hutchings, L. R.; Richards, R. W. "Neutron reflectivity studies at liquid-liquid interfaces: Methodology and analysis", *Langmuir* **2001**, *17*, 140-145.

(5) Gajraj, A.; Ofoli, R. Y. "Quantitative technique for investigating macromolecular adsorption and interactions at the liquid-liquid interface", *Langmuir* **2000**, *16*, 4279-4285.

(6) Gajraj, A.; Ofoli, R. Y. "Effect of extrinsic fluorescent labels on diffusion and adsorption kinetics of proteins at the liquid-liquid interface", *Langmuir* **2000**, *16*, 8085-8094.

(7) Naujok, R. R.; Paul, H. J.; Corn, R. M. "Optical second harmonic generation studies of azobenzene surfactant adsorption and photochemistry at the water/1,2-dichloroethane interface", *J Phys Chem-Us* **1996**, *100*, 10497-10507.

(8) Sauer, B. B.; Chen, Y. L.; Zografi, G.; Yu, H. "Static and Dynamic Interfacial-Tensions of a Phospholipid Monolayer at the Oil-Water Interface - Dipalmitoylphosphatidylcholine at Heptane Water", *Langmuir* **1986**, *2*, 683-685.

(9) Graham, D. E.; Chatergoon, L.; Phillips, M. C. "Technique for Measuring Interfacial Concentrations of Surfactants at Oil-Water Interface", *J Phys E Sci Instrum* **1975**, *8*, 696-699.

(10) Ando, J.; Albelda, S. M.; Levine, E. M. "Culture of Human Adult Endothelial-Cells on Liquid-Liquid Interfaces - a New Approach to the Study of Cell-Matrix Interactions", *In Vitro Cellular & Developmental Biology* **1991**, *27*, 525-532.

(11) Han, M.; Sethuraman, A.; Kane, R. S.; Belfort, G. "Nanometer-scale roughness having little effect on the amount or structure of adsorbed protein", *Langmuir* **2003**, *19*, 9868-9872.

(12) Wertz, C. F.; Santore, M. M. "Adsorption and relaxation kinetics of albumin and fibrinogen on hydrophobic surfaces: Single-species and competitive behavior", *Langmuir* **1999**, *15*, 8884-8894.

(13) Calonder, C.; Tie, Y.; Van Tassel, P. R. "History dependence of protein adsorption kinetics", *Proc. Natl. Acad. Sci. U. S. A.* **2001**, *98*, 10664-10669.

(14) Hlady, V.; Reinecke, D. R.; Andrade, J. D. "Fluorescence of Adsorbed Protein Layers .1. Quantitation of Total Internal-Reflection Fluorescence", *J. Colloid Interface Sci.* **1986**, *111*, 555-569.

(15) Sengupta, T.; Damodaran, S. "A new methodology for studying protein adsorption at oil-water interfaces", *J. Colloid Interface Sci.* **1998**, *206*, 407-415.

(16) Zimmermann, R. M.; Schmidt, C. F.; Gaub, H. E. "Absolute Quantities and Equilibrium Kinetics of Macromolecular Adsorption Measured by Fluorescence Photobleaching in Total Internal-Reflection", *J. Colloid Interface Sci.* **1990**, *139*, 268-280.

(17) Cornell, B. A.; BraachMaksvytis, V. L. B.; King, L. G.; Osman, P. D. J.; Raguse, B.; Wieczorek, L.; Pace, R. J. "A biosensor that uses ion-channel switches", *Nature* **1997**, *387*, 580-583.

(18) Palmisano, F.; Centonze, D.; Guerrieri, A.; Zambonin, P. G. "An Interference-Free Biosensor Based on Glucose-Oxidase Electrochemically Immobilized in a Nonconducting Poly(Pyrrole) Film for Continuous Subcutaneous Monitoring of Glucose through Microdialysis Sampling", *Biosens. Bioelectron.* **1993**, *8*, 393-399.

(19) Ikeda, T.; Matsushita, F.; Senda, M. "Amperometric Fructose Sensor Based on Direct Bioelectrocatalysis", *Biosens. Bioelectron.* **1991**, *6*, 299-304.

(20) Chew, T. L.; Wolf, W. A.; Gallagher, P. J.; Matsumura, F.; Chisholm, R. L. "A fluorescent resonant energy transfer-based biosensor reveals transient and regional myosin light chain kinase activation in lamella and cleavage furrows", *J. Cell Biol.* **2002**, *156*, 543-553.

(21) Wang, B. Q.; Li, B.; Deng, Q.; Dong, S. J. "Amperometric glucose biosensor based on sol-gel organic-inorganic hybrid material", *Analytical Chemistry* **1998**, *70*, 3170-3174.

(22) Raguse, B.; Braach-Maksvytis, V.; Cornell, B. A.; King, L. G.; Osman, P. D. J.; Pace, R. J.; Wieczorek, L. "Tethered lipid bilayer membranes: Formation and ionic reservoir characterization", *Langmuir* **1998**, *14*, 648-659.

(23) Sackmann, E.; Tanaka, M. "Supported membranes on soft polymer cushions: fabrication, characterization and applications", *Trends in Biotechnology* **2000**, *18*, 58-64.

(24) Cunningham, J. J.; Nikolovski, J.; Linderman, J. J.; Mooney, D. J. "Quantification of fibronectin adsorption to silicone-rubber cell culture substrates", *Biotechniques* **2002**, *32*, 876-887.

(25) McFarland, C. D.; Thomas, C. H.; DeFilippis, C.; Steele, J. G.; Healy, K. E. "Protein adsorption and cell attachment to patterned surfaces", *J. Biomed. Mater. Res.* **2000**, *49*, 200-210.

(26) Whittle, J. D.; Bullett, N. A.; Short, R. D.; Douglas, C. W. I.; Hollander, A. P.; Davies, J. "Adsorption of vitronectin, collagen and immunoglobulin-G to plasma polymer surfaces by enzyme linked immunosorbent assay (ELISA)", *J. Mater. Chem.* **2002**, *12*, 2726-2732.

(27) MacDonald, D. E.; Markovic, B.; Allen, M.; Somasundaran, P.; Boskey, A. L. "Surface analysis of human plasma fibronectin adsorbed to commercially pure titanium materials", *J. Biomed. Mater. Res.* **1998**, *41*, 120-130.

(28) Hynes, R. *Fibronectins*; Springer: New York, 1990.

(29) Williams, E. C.; Janmey, P. A.; Ferry, J. D.; Mosher, D. F. "Conformational States of Fibronectin - Effects of Ph, Ionic- Strength, and Collagen Binding", *J. Biol. Chem.* **1982**, *257*, 4973-4978.

(30) Koteliansky, V. E.; Bejanian, M. V.; Smirnov, V. N. "Electron-Microscopy Study of Fibronectin Structure", *FEBS Lett.* **1980**, *120*, 283-286.

(31) Koteliansky, V. E.; Glukhova, M. A.; Bejanian, M. V.; Smirnov, V. N.; Filimonov, V. V.; Zalite, O. M.; Venyaminov, S. Y. "A Study of the Structure of Fibronectin", *Eur. J. Biochem.* **1981**, *119*, 619-624.

(32) Engel, J.; Odermatt, E.; Engel, A.; Madri, J. A.; Furthmayr, H.; Rohde, H.; Timpl, R. "Shapes, Domain Organizations and Flexibility of Laminin and Fibronectin, 2 Multifunctional Proteins of the Extracellular- Matrix", *J. Mol. Biol.* **1981**, *150*, 97-120.

(33) Erickson, H. P.; Carrell, N.; McDonagh, J. "Fibronectin Molecule Visualized in Electron-Microscopy - a Long, Thin, Flexible Strand", *J. Cell Biol.* **1981**, *91*, 673-678.

(34) Paynter, R. W.; Ratner, B. D.; Horbett, T. A.; Thomas, H. R. "Xps Studies on the Organization of Adsorbed Protein Films on Fluoropolymers", *J. Colloid Interface Sci.* **1984**, *101*, 233-245.

(35) Lai, C. S.; Wolff, C. E.; Novello, D.; Griffone, L.; Cuniberti, C.; Molina, F.; Rocco, M. "Solution Structure of Human Plasma Fibronectin under Different Solvent Conditions - Fluorescence Energy-Transfer, Circular- Dichroism and Light-Scattering-Studies", *J. Mol. Biol.* **1993**, *230*, 625-640.

(36) Wolff, C.; Lai, C. S. "Fluorescence Energy-Transfer Detects Changes in Fibronectin Structure Upon Surface Binding", *Arch. Biochem. Biophys.* **1989**, *268*, 536-545.

(37) Bergkvist, M.; Carlsson, J.; Oscarsson, S. "Surface-dependent conformations of human plasma fibronectin adsorbed to silica, mica, and hydrophobic surfaces, studied with use of Atomic Force Microscopy", *Journal of Biomedical Materials Research Part A* **2003**, *64A*, 349-356.

(38) Sagvolden, G.; Giaever, I.; Pettersen, E. O.; Feder, J. "Cell adhesion force microscopy", *Proc. Natl. Acad. Sci. U. S. A.* **1999**, *96*, 471-476.

(39) Jonsson, U.; Ivarsson, B.; Lundstrom, I.; Berghem, L. "Adsorption Behavior of Fibronectin on Well-Characterized Silica Surfaces", *J. Colloid Interface Sci.* **1982**, *90*, 148-163.

(40) Cheng, Y. L.; Darst, S. A.; Robertson, C. R. "Bovine Serum-Albumin Adsorption and Desorption Rates on Solid- Surfaces with Varying Surface-Properties", *J. Colloid Interface Sci.* **1987**, *118*, 212-223.

(41) Lassen, B.; Malmsten, M. "Competitive protein adsorption studied with TIRF and ellipsometry", *J. Colloid Interface Sci.* **1996**, *179*, 470-477.

(42) Sengupta, T.; Damodaran, S. "Role of dispersion interactions in the adsorption of proteins at oil-water and air-water interfaces", *Langmuir* **1998**, *14*, 6457-6469.

(43) Kim, D. T.; Blanch, H. W.; Radke, C. J. "Direct imaging of lysozyme adsorption onto mica by atomic force microscopy", *Langmuir* **2002**, *18*, 5841-5850.

(44) Beverung, C. J.; Radke, C. J.; Blanch, H. W. "Protein adsorption at the oil/water interface: characterization of adsorption kinetics by dynamic interfacial tension measurements", *Biophys. Chem.* **1999**, *81*, 59-80.

(45) Dickinson, E. "Adsorbed protein layers at fluid interfaces: interactions, structure and surface rheology", *Colloid Surf. B-Biointerfaces* **1999**, *15*, 161-176.

(46) Giaever, I.; Keese, C. R. "Behavior of Cells at Fluid Interfaces", *Proceedings of the National Academy of Sciences of the United States of America-Biological Sciences* **1983**, *80*, 219-222.

(47) Keese, C. R.; Giaever, I. "Cell-Growth on Liquid Interfaces - Role of Surface-Active Compounds", *Proceedings of the National Academy of Sciences of the United States of America-Biological Sciences* **1983**, *80*, 5622-5626.

(48) Koenig, A. L.; Gambillara, V.; Grainger, D. W. "Correlating fibronectin adsorption with endothelial cell adhesion and signaling on polymer substrates", *Journal of Biomedical Materials Research Part A* **2003**, *64A*, 20-37.

(49) Technical Documentation,Chemicon International.

(50) "Amine-Reactive Probes", *Molecular Probes, Eugene, OR* **2003**.

(51) "Albumin product information sheet", *Sigma-Aldrich, St. Louis MO.*

(52) Jeon, S. I.; Lee, J. H.; Andrade, J. D.; Degennes, P. G. "Protein Surface Interactions in the Presence of Polyethylene Oxide .1. Simplified Theory", *J. Colloid Interface Sci.* **1991**, *142*, 149-158.

(53) Jeon, S. I.; Andrade, J. D. "Protein Surface Interactions in the Presence of Polyethylene Oxide .2. Effect of Protein Size", *J. Colloid Interface Sci.* **1991**, *142*, 159-166.

(54) Andrade, J. D.; Hlady, V.; Jeon, S. I. In *Hydrophilic Polymers*, 1996; Vol. 248, pp 51-59.

(55) Gajraj, A. "A novel total internal reflection fluorescence (TIRF) technique for investigating macromolecular adsorption and interactions at the liquid-liquid interface", *PhD thesis, Michigan State University* **1999**.

(56) Lok, B. K.; Cheng, Y. L.; Robertson, C. R. "Protein Adsorption on Crosslinked Polydimethylsiloxane Using Total Internal-Reflection Fluorescence", *J. Colloid Interface Sci.* **1983**, *91*, 104-116.

(57) Johnson, K. J.; Sage, H.; Briscoe, G.; Erickson, H. P. "The compact conformation of fibronectin is determined by intramolecular ionic interactions", *J. Biol. Chem.* **1999**, *274*, 15473-15479.

(58) Michael, K. E.; Vernekar, V. N.; Keselowsky, B. G.; Carson Meredith, J.; Latour, R. A.; Garcý´, A. J. "Adsorption-induced conformational changes in Fibronectin due to interactions with well-defined surface chemistries", *Langmuir* **2003**, *19*, 8033-8040.

(59) Malmsten, M.; Lassen, B. "Competitive Adsorption at Hydrophobic Surfaces from Binary Protein Systems", *Journal of Colloid and Interface Science* **1994**, *166*, 490-498.

(60) 2nd edition ed.; Putnam, F. W., Ed.; Academic Press, New York, 1975; Vol. 1, pp 133-181.

(61) Green, R. J.; Davies, M. C.; Roberts, C. J.; Tendler, S. J. B. "Competitive protein adsorption as observed by surface plasmon resonance", *Biomaterials* **1999**, *20*, 385-391.

(62) Vroman, L.; Adams, A. In *Proteins at Interfaces: Physiochemical and Biochemical Studies*, 1987, pp 154-164.

(63) Fang, F.; Szleifer, I. "Kinetics and thermodynamics of protein adsorption: A generalized molecular theoretical approach", *Biophys. J.* **2001**, *80*, 2568-2589.

(64) Sanocki VA "Cell culture at the liquid-liquid interface: effects of fluorocarbon layer thickness on cell growth", *M.S. thesis, Michigan State University* **2004**.

(65) Zhang, H. L.; Bremmell, K.; Kumar, S.; Smart, R. S. C. "Vitronectin adsorption on surfaces visualized by tapping mode atomic force microscopy", *Journal of Biomedical Materials Research Part A* **2004**, *68A*, 479-488.

(66) Voet, D.; Voet, J. G. *Biochemistry*; 2nd ed.; J. Wiley & Sons: New York, 1995.

(67) Green, R. J.; Su, T. J.; Lu, J. R.; Webster, J.; Penfold, J. "Competitive adsorption of lysozyme and C12E5 at the air/liquid interface", *Phys. Chem. Chem. Phys.* **2000**, *2*, 5222-5229.

(68) Robeson, J. L.; Tilton, R. D. "Spontaneous reconfiguration of adsorbed lysozyme layers observed by total internal reflection fluorescence with a pH-sensitive fluorophore", *Langmuir* **1996**, *12*, 6104-6113.

(69) Choi, E. J.; Foster, M. D.; Daly, S.; Tilton, R.; Przybycien, T.; Majkrzak, C. F.; Witte, P.; Menzel, H. "Effect of flow on human serum albumin adsorption to self-assembled monolayers of varying packing density", *Langmuir* **2003**, *19*, 5464-5474.

(70) Fragneto, G.; Su, T. J.; Lu, J. R.; Thomas, R. K.; Rennie, A. R. "Adsorption of proteins from aqueous solutions on hydrophobic surfaces studied by neutron reflection", *Phys. Chem. Chem. Phys.* **2000**, *2*, 5214-5221.

(71) Marsh, R. J.; Jones, R. A. L.; Sferrazza, M. "Adsorption and displacement of a globular protein on hydrophilic and hydrophobic surfaces", *Colloid Surf. B-Biointerfaces* **2002**, *23*, 31-42.

(72) Rodahl, M.; Hook, F.; Krozer, A.; Brzezinski, P.; Kasemo, B. "Quartz-Crystal Microbalance Setup for Frequency and Q-Factor Measurements in Gaseous and Liquid Environments", *Rev Sci Instrum* **1995**, *66*, 3924-3930.

(73) Kidoaki, S.; Matsuda, T. "Mechanistic aspects of protein/material interactions probed by atomic force microscopy", *Colloid Surf. B-Biointerfaces* **2002**, *23*, 153-163.

(74) Richter, R. P.; Brisson, A. "Characterization of lipid bilayers and protein assemblies supported on rough surfaces by atomic force microscopy", *Langmuir* **2003**, *19*, 1632-1640.

(75) Rebar, V. A.; Santore, M. M. "History-dependent isotherms and TIRF calibrations for homopolymer adsorption", *Macromolecules* **1996**, *29*, 6262-6272.

(76) Reichert, W. M.; Rockhold, S.; Van Wagenen, R. A.; Andrade, J. D. In *Interfacial Aspects of biomedical polymers*; Plenum Press: New York, 1984; Vol. 2.

(77) Crosby, G. A.; Demas, J. N.; Callis, J. B. "Absolute Quantum Efficiencies", *J Res Nbs C Eng Inst* **1972**, *A 76*, 561-577.

(78) Magde, D.; Wong, R.; Seybold, P. G. "Fluorescence quantum yields and their relation to lifetimes of rhodamine 6G and fluorescein in nine solvents: Improved absolute standards for quantum yields", *Photochem Photobiol* **2002**, *75*, 327-334.

(79) Brannon, J. H.; Magde, D. "Absolute Quantum Yield Determination by Thermal Blooming - Fluorescein", *J Phys Chem-Us* **1978**, *82*, 705-709.

(80) Lakowicz, J. R. *Principles of fluorescence spectroscopy*; Plenum Press: New York, 1983.

(81) Strickler, S. J.; Berg, R. A. "Relationship between Absorption Intensity and Fluorescence lifetime of molecules", *Journal of Chemical Physics* **1962**, *37*, 814-822.

(82) Lakowicz, J. R. "Radiative decay engineering: Biophysical and biomedical applications", *Anal Biochem* **2001**, *298*, 1-24.

(83) Rao, A.; Dhinojwala, A. "Two-photon fluorescence technique to study polymer adsorption at the toluene-water interface", *Langmuir* **2003**, *19*, 8813-8817.

(84) Denk, W.; Svoboda, K. "Photon upmanship: Why multiphoton imaging is more than a gimmick", *Neuron* **1997**, *18*, 351-357.

(85) Xu, C.; Webb, W. W. "Measurement of two-photon excitation cross sections of molecular fluorophores with data from 690 to 1050 nm", *Journal of the Optical Society of America B-Optical Physics* **1996**, *13*, 481-491.

(86) Dunaevsky, A.; Tashiro, A.; Majewska, A.; Mason, C.; Yuste, R. "Developmental regulation of spine motility in the mammalian central nervous system", *Proc. Natl. Acad. Sci. U. S. A.* **1999**, *96*, 13438-13443.

(87) Miller, M. J.; Wei, S. H.; Parker, I.; Cahalan, M. D. "Two-photon imaging of lymphocyte motility and antigen response in intact lymph node", *Science* **2002**, *296*, 1869-1873.

(88) Konig, K. "Multiphoton microscopy in life sciences", *Journal of Microscopy-Oxford* **2000**, *200*, 83-104.

(89) Dietrich, C.; Bagatolli, L. A.; Volovyk, Z. N.; Thompson, N. L.; Levi, M.; Jacobson, K.; Gratton, E. "Lipid rafts reconstituted in model membranes", *Biophys. J.* **2001**, *80*, 1417-1428.

(90) Grinvald, A.; Steinberg, I. Z. "Analysis of Fluorescence Decay Kinetics by Method of Least-Squares", *Anal Biochem* **1974**, *59*, 583-598.

(91) Beaglehole, D.; Lawson, F.; Harper, G.; Hossain, M. "Tryptophan, tryptophan-leucine, and BSA adsorption at an oil-water interface", *J. Colloid Interface Sci.* **1997**, *192*, 266-268.

(92) Butler, S. M.; Tracy, M. A.; Tilton, R. D. "Adsorption of serum albumin to thin films of poly(lactide-co-glycolide)", *J Control Release* **1999**, *58*, 335-347.

(93) Lakowicz, J. R.; Malicka, J.; D'Auria, S.; Gryczynski, I. "Release of the self-quenching of fluorescence near silver metallic surfaces", *Anal Biochem* **2003**, *320*, 13-20.

(94) Kelepouris, L.; Blanchard, G. J. "Dynamics of 7-azatryptophan and tryptophan derivatives in micellar media. The role of ionic charge and substituent structure", *J. Phys. Chem. B* **2003**, *107*, 1079-1087.

(95) Heysel, S.; Vogel, H.; Sanger, M.; Sigrist, H. "Covalent Attachment of Functionalized Lipid Bilayers to Planar Wave-Guides for Measuring Protein-Binding to Biomimetic Membranes", *Protein Science* **1995**, *4*, 2532-2544.

(96) McConnell, H. M.; Watts, T. H.; Weis, R. M.; Brian, A. A. "Supported Planar Membranes in Studies of Cell-Cell Recognition in the Immune-System", *Biochimica Et Biophysica Acta* **1986**, *864*, 95-106.

(97) Nikolelis, D. P.; Siontorou, C. G.; Krull, U. J.; Katrivanos, P. L. "Ammonium ion minisensors from self-assembled bilayer lipid membranes using Gramicidin as an ionophore. Modulation of ammonium selectivity by platelet-activating factor", *Analytical Chemistry* **1996**, *68*, 1735-1741.

(98) Seifert, K.; Fendler, K.; Bamberg, E. "Charge Transport by Ion Translocating Membrane-Proteins on Solid Supported Membranes", *Biophysical Journal* **1993**, *64*, 384-391.

(99) Stelzle, M.; Sackmann, E. "Sensitive Detection of Protein Adsorption to Supported Lipid Bilayers by Frequency-Dependent Capacitance Measurements and Microelectrophoresis", *Biochimica Et Biophysica Acta* **1989**, *981*, 135-142.

(100) Favero, G.; D'Annibale, A.; Campanella, L.; Santucci, R.; Ferri, T. "Membrane supported bilayer lipid membranes array: preparation, stability and ion-channel insertion", *Analytica Chimica Acta* **2002**, *460*, 23-34.

(101) Furuike, S.; Hirokawa, J.; Yamada, S.; Yamazaki, M. "Atomic force microscopy studies of interaction of the 20S proteasome with supported lipid bilayers", *Biochimica Et Biophysica Acta-Biomembranes* **2003**, *1615*, 1-6.

(102) Glasmastar, K.; Larsson, C.; Hook, F.; Kasemo, B. "Protein adsorption on supported phospholipid bilayers", *Journal of Colloid and Interface Science* **2002**, *246*, 40-47.

(103) Graneli, A.; Rydstrom, J.; Kasemo, B.; Hook, F. "Formation of supported lipid bilayer membranes on SiO2 from proteoliposomes containing transmembrane proteins", *Langmuir* **2003**, *19*, 842-850.

(104) Groves, J. T.; Mahal, L. K.; Bertozzi, C. R. "Control of cell adhesion and growth with micropatterned supported lipid membranes", *Langmuir* **2001**, *17*, 5129-5133.

(105) Lahiri, J.; Kalal, P.; Frutos, A. G.; Jonas, S. T.; Schaeffler, R. "Method for fabricating supported bilayer lipid membranes on gold", *Langmuir* **2000**, *16*, 7805-7810.

(106) Ohlsson, P. A.; Tjarnhage, T.; Herbai, E.; Lofas, S.; Puu, G. "Liposome and Proteoliposome Fusion onto Solid Substrates, Studied Using Atomic-Force Microscopy, Quartz-Crystal Microbalance and Surface-Plasmon Resonance - Biological-Activities of Incorporated Components", *Bioelectrochemistry and Bioenergetics* **1995**, *38*, 137-148.

(107) Tien, H. T.; Barish, R. H.; Gu, L. Q.; Ottova, A. L. "Supported bilayer lipid membranes as ion and molecular probes", *Analytical Sciences* **1998**, *14*, 3-18.

(108) Tien, H. T.; Ottova, A. L. "Supported planar lipid bilayers (s-BLMs) as electrochemical biosensors", *Electrochimica Acta* **1998**, *43*, 3587-3610.

(109) Ariga, K.; Okahata, Y. "Polymerized Monolayers of Single-Chain, Double-Chain, and Triple-Chain Silane Amphiphiles and Permeation Control through the Monolayer-Immobilized Porous-Glass Plate in an Aqueous-Solution", *J. Am. Chem. Soc.* **1989**, *111*, 5618-5622.

(110) Fare, T. L. "Electrical Characterization of Dipalmitoylphosphatidylethanolamine and Cadmium Stearate Films on Platinum Surfaces in Aqueous-Solutions", *Langmuir* **1990**, *6*, 1172-1179.

(111) Plant, A. L. "Self-Assembled Phospholipid Alkanethiol Biomimetic Bilayers on Gold", *Langmuir* **1993**, *9*, 2764-2767.

(112) Plant, A. L.; Gueguetchkeri, M.; Yap, W. "Supported Phospholipid/Alkanethiol Biomimetic Membranes - Insulating Properties", *Biophys. J.* **1994**, *67*, 1126-1133.

(113) Stenger, D. A.; Fare, T. L.; Cribbs, D. H.; Rustin, K. M. "Voltage Modulation of a Gated Ion Channel Admittance in Platinum-Supported Lipid Bilayers", *Biosensors and Bioelectronics* **1992**, *7*, 11-20.

(114) Hoppe, W.; Lohmann, W. *Biophysics*; Springer-Verlag: Berlin, 1983.

(115) Beddow, J. A.; Peterson, I. R.; Heptinstall, J.; Walton, D. J. "Electrochemical characterisation of the diffusion of a biomolecule through a hydrogel", *Journal of Electroanalytical Chemistry* **2003**, *544*, 107-112.

(116) Cornell, B. A.; Krishna, G.; Osman, P. D.; Pace, R. D.; Wieczorek, L. "Tethered-bilayer lipid membranes as a support for membrane-active peptides", *Biochemical Society Transactions* **2001**, *29*, 613-617.

(117) Fortig, A.; Jordan, R.; Graf, K.; Schiavon, G.; Purrucker, O.; Tanaka, M. "Solid-supported biomimetic membranes with tailored lipopolymer tethers", *Macromolecular Symposia* **2004**, *210*, 329-338.

(118) Jin, T.; Pennefather, P.; Lee, P. I. "Lipobeads: A hydrogel anchored lipid vesicle system", *Febs Letters* **1996**, *397*, 70-74.

(119) Krishna, G.; Schulte, J.; Cornell, B. A.; Pace, R.; Wieczorek, L.; Osman, P. D. "Tethered bilayer membranes containing ionic reservoirs: The interfacial capacitance", *Langmuir* **2001**, *17*, 4858-4866.

(120) Krysinski, P.; Zebrowska, A.; Michota, A.; Bukowska, J.; Becucci, L.; Moncelli, M. R. "Tethered mono- and bilayer lipid membranes on Au and Hg", *Langmuir* **2001**, *17*, 3852-3857.

(121) Krysinski, P.; Zebrowska, A.; Palys, B.; Lotowski, Z. "Spectroscopic and electrochemical studies of bilayer lipid membranes tethered to the surface of gold", *Journal of the Electrochemical Society* **2002**, *149*, E189-E194.

(122) Kugler, R.; Knoll, W. "Polyelectrolyte-supported lipid membranes", *Bioelectrochemistry* **2002**, *56*, 175-178.

(123) Melzak, K. A.; Gizeli, E. "A silicate gel for promoting deposition of lipid bilayers", *Journal of Colloid and Interface Science* **2002**, *246*, 21-28.

(124) Moncelli, M. R.; Becucci, L.; Schiller, S. M. "Tethered bilayer lipid membranes self-assembled on mercury electrodes", *Bioelectrochemistry* **2004**, *63*, 161-167.

(125) Munro, J. C.; Frank, C. W. "Adsorption of lipid-functionalized poly(ethylene glycol) to gold surfaces as a cushion for polymer-supported lipid bilayers", *Langmuir* **2004**, *20*, 3339-3349.

(126) Naumann, R.; Schiller, S. M.; Giess, F.; Grohe, B.; Hartman, K. B.; Karcher, I.; Koper, I.; Lubben, J.; Vasilev, K.; Knoll, W. "Tethered lipid Bilayers on ultraflat gold surfaces", *Langmuir* **2003**, *19*, 5435-5443.

(127) Naumann, R.; Walz, D.; Schiller, S. M.; Knoll, W. "Kinetics of valinomycin-mediated K+ ion transport through tethered bilayer lipid membranes", *Journal of Electroanalytical Chemistry* **2003**, *550*, 241-252.

(128) Proux-Delrouyre, V.; Elie, C.; Laval, J. M.; Moiroux, J.; Bourdillon, C. "Formation of tethered and streptavidin-supported lipid bilayers on a microporous electrode for the reconstitution of membranes of large surface area", *Langmuir* **2002**, *18*, 3263-3272.

(129) Sinner, E. K.; Knoll, W. "Functional tethered membranes", *Current Opinion in Chemical Biology* **2001**, *5*, 705-711.

(130) Wagner, M. L.; Tamm, L. K. "Tethered polymer-supported planar lipid bilayers for reconstitution of integral membrane proteins: Silane-polyethyleneglycol-lipid as a cushion and covalent linker", *Biophysical Journal* **2000**, *79*, 1400-1414.

(131) Cassier, T.; Sinner, A.; Offenhauser, A.; Mohwald, H. "Homogeneity, electrical resistivity and lateral diffusion of lipid bilayers coupled to polyelectrolyte multilayers", *Colloids and Biointerfaces* **1999**, *15*, 215-225.

(132) Perez-Salas, U. A.; Faucher, K. M.; Majkrzak, C. F.; Berk, N. F.; Krueger, S.; Chaikof, E. L. "Characterization of a biomimetic polymeric lipid bilayer by phase sensitive neutron reflectometry", *Langmuir* **2003**, *19*, 7688-7694.

(133) Moya, S.; Richter, W.; Leporatti, S.; Baumler, H.; Donath, E. "Freeze-Fracture Electron Microscopy of Lipid Membranes on Colloidal Polyelectrolyte Multilayer Coated Supports", *Biomacromolecules* **2003**, *4*, 808-814.

(134) Tiourina, O. P.; Radtchenko, I.; Sukhorukov, S. B.; Mohwald, H. "Artificial cell based on lipid hollow polyelectrolyte microcapsules: Channel reconstruction and membrane potential measurement", *Journal of Membrane Biology* **2002**, *190*, 9-16.

(135) Hovis, J. S.; Boxer, S. G. "Patterning barriers to lateral diffusion in supported lipid bilayer membranes by blotting and stamping", *Langmuir* **2000**, *16*, 894-897.

(136) Kam, L.; Boxer, S. G. "Cell adhesion to protein-micropatterned-supported lipid bilayer membranes", *Journal of Biomedical Materials Research* **2001**, *55*, 487-495.

(137) Kung, L. A.; Kam, L.; Hovis, J. S.; Boxer, S. G. "Patterning hybrid surfaces of proteins and supported lipid bilayers", *Langmuir* **2000**, *16*, 6773-6776.

(138) Saccani, J.; Castano, S.; Desbat, B.; Blaudez, D. "A phospholipid bilayer supported under a polymerized Langmuir film", *Biophysical Journal* **2003**, *85*, 3781-3787.

(139) Decher, G.; Hong, J. D. "Buildup of ultrathin multilayer films by a self-assembly process .2. Consecutive adsorption of anionic and cationic bipolar amphiphiles and polyelectrolytes on charged surfaces", *Ber Bunsen-Ges.* **1991**, *95*, 1430-1434.

(140) Kumar, A.; Whitesides, G. M. "Features of Gold Having Micrometer to Centimeter Dimensions Can Be Formed through a Combination of Stamping with an Elastomeric Stamp and an Alkanethiol Ink Followed by Chemical Etching", *Appl. Phys. Lett.* **1993**, *63*, 2002-2004.

(141) Jiang, X.; Hammond, P. T. "Selective deposition in layer-by-layer assembly: Functional graft copolymers as molecular templates", *Langmuir* **2000**, *16*, 8501-8509.

(142) Jiang, X.; Zheng, H.; Shoshna, G.; Hammond, P. T. "Polymer-on-polymer stamping: Universal approaches to chemically patterned surfaces", *Langmuir* **2002**, *18*, 2607-2615.

(143) Fou, A. C.; Rubner, M. F. "Molecular-Level Processing of Conjugated Polymers .2. Layer-by-Layer Manipulation of in-Situ Polymerized P-Type Doped Conducting Polymers", *Macromolecules* **1995**, *28*, 7115-7120.

(144) Lee, I.; Zheng, H.; Rubner, M. F.; Hammond, P. T. "Controlled cluster size in patterned particle arrays via directed adsorption on confined surfaces", *Advanced Materials* **2002**, *14*, 572-577.

(145) Zheng, H.; Lee, I.; Rubner, M. F.; Hammond, P. T. "Two component particle arrays on patterned polyelectrolyte multilayer templates", *Adv. Mater* **2002**, *14*, 569-572.

(146) Lvov, Y.; Ariga, K.; Ichinose, I.; Kunitake, T. "Assembly of Multicomponent Protein Films by Means of Electrostatic Layer-by-Layer Adsorption", *J. Am. Chem. Soc.* **1995**, *117*, 6117-6123.

(147) Lee, I.; Hammond, P. T.; Rubner, M. F. "Selective electroless nickel plating of particle arrays on polyelectrolyte multilayers", *Chemistry of Materials* **2003**, *15*, 4583-4589.

(148) St. John, P. M.; Craighead, H. G. "Microcontact printing and pattern transfer using trichlorosilanes on oxide substrates", *Appl. Phys. Lett.* **1996**, *68*, 1022-1024.

(149) Xia, Y.; Kim, E.; Mrksich, M.; Whitesides, G. M. "Microcontact printing of alkanethiols on copper and its application in microfabrication", *Chem. Mater.* **1996**, *8*, 601-603.

(150) Yang, X. M.; Tryk, D. A.; Hasimoto, K.; Fujishima, A. "Surface enhanced Raman imaging of a patterned self-assembled monolayer formed by microcontact printing on a silver film", *Appl. Phys. Lett.* **1996**, *69*, 4020-4022.

(151) Berg, M. C.; Yang, S. Y.; Hammond, P. T.; Rubner, M. F. "Controlling mammalian cell interactions on patterned polyelectrolyte multilayer surfaces", *Langmuir* **2004**, *20*, 1362-1368.

(152) Kim, H.; Doh, J.; Irvine, D. J.; Cohen, R. E.; Hammond, P. T. "Large area two-dimensional B cell arrays for sensing and cell-sorting applications", *Biomacromolecules* **2004**, *5*, 822-827.

(153) Yang, S. Y.; Mendelsohn, J. D.; Rubner, M. F. "New class of ultrathin, highly cell-adhesion-resistant polyelectrolyte multilayers with micropatterning capabilities", *Biomacromolecules* **2003**, *4*, 987-994.

(154) Lee, I.; Ahn, J.; Hendericks, T.; Rubner, M. F.; Hammond, P. T. "Patterned and controlled polyelectrolyte fractal growth and aggregations", *Langmuir* **2004**, *20*, 2478-2483.

(155) Kidambi, S.; Chan, C.; Lee, I. "Selective depositions on polyelectrolyte multilayers: Self-assembled monolayers of m-dpeg acid as molecular template", *J. Am. Chem. Soc.* **2004**, *126*, 4697-4703.

(156) Robeson, J. L. "Application of total internal reflection fluorescence to probe surface diffusion and orientation of adsorbed protiens."**1995**

(157) Starr, T. E.; Thompson, N. L. "Fluorescence pattern photobleaching recovery for samples with multi-component diffusion", *Biophys. Chem.* **2002**, *97*, 29-44.

(158) Smith, B. A.; McConnell, H. M. "Determination of Molecular-Motion in Membranes Using Periodic Pattern Photobleaching", *Proc. Natl. Acad. Sci. U. S. A.* **1978**, *75*, 2759-2763.

(159) Wright, L. L.; Palmer, A. G.; Thompson, N. L. "Inhomogeneous Translational Diffusion of Monoclonal-Antibodies on Phospholipid Langmuir-Blodgett Films", *Biophys. J.* **1988**, *54*, 463-470.

(160) Ameloot, M.; Hendrickx, H. "Criteria for Model Evaluation in the Case of Deconvolution Calculations", *Journal of Chemical Physics* **1982**, *76*, 4419-4432.

(161) Zhu, B.; Eurell, T.; Gunawan, R.; Leckband, D. "Chain-length dependence of the protein and cell resistance of oligo(ethylene glycol)-terminated self-assembled monolayers on gold", *J. Biomed. Mater. Res.* **2001**, *56*, 406-416.

(162) Kalb, E.; Frey, S.; Tamm, L. K. "Formation of Supported Planar Bilayers by Fusion of Vesicles to Supported Phospholipid Monolayers", *Biochimica Et Biophysica Acta* **1992**, *1103*, 307-316.

(163) Harris, J. M. *Poly(ethylene glycol) chemistry : biotechnical and biomedical applications*; Plenum Press: New York, 1992.

(164) Harris, J. M.; Zalipsky, S.; American Chemical Society. Division of Polymer Chemistry.; American Chemical Society. Meeting *Poly(ethylene glycol) : chemistry and biological applications*; American Chemical Society: Washington, DC, 1997.

(165) Feldman, K.; Hahner, G.; Spencer, N. D.; Harder, P.; Grunze, M. "Probing resistance to protein adsorption of oligo(ethylene glycol)-terminated self-assembled monolayers by scanning force microscopy", *Journal of the American Chemical Society* **1999**, *121*, 10134-10141.

(166) Nollert, P.; Kiefer, H.; Jahnig, F. "Lipid Vesicle Adsorption Versus Formation of Planar Bilayers on Solid-Surfaces", *Biophys. J.* **1995**, *69*, 1447-1455.

(167) Jenkins, A. T. A.; Bushby, R. J.; Evans, S. D.; Knoll, W.; Offenhausser, A.; Ogier, S. D. "Lipid vesicle fusion on mu CP patterned self-assembled monolayers: Effect of pattern geometry on bilayer formation", *Langmuir* **2002**, *18*, 3176-3180.

(168) Efremov, A.; Mauro, J. C.; Raghavan, S. "Macroscopic model of phospholipid vesicle spreading and rupture", *Langmuir* **2004**, *20*, 5724-5731.

(169) Zhang, L. Q.; Longo, M. L.; Stroeve, P. "Mobile phospholipid bilayers on a polyion/alkylthiol layer pair", *Langmuir* **2000**, *16*, 5093-5099.

(170) Ma, C.; Srinivasan, M. P.; Waring, A. J.; Lehrer, R. I.; Longo, M. L.; Stroeve, P. "Supported lipid bilayers lifted from the substrate by layer-by-layer polyion cushions on self-assembled monolayers", *Colloid Surf. B-Biointerfaces* **2003**, *28*, 319-329.

(171) Johnson, J. M.; Ha, T.; Chu, S.; Boxer, S. G. "Early steps of supported bilayer formation probed by single vesicle fluorescence assays", *Biophys. J.* **2002**, *83*, 3371-3379.

MICHIGAN STATE UNIVERSITY LIBRARIES
3 1293 02736 4631